Port-city
Universities
League

The 12th International Seminar of Port-city Universities League

"Green Technology and Sustainable Development for Port Cities: Challenges and Solutions"

Proceedings

Ho Chi Minh City University of Technology, Vietnam

on October 16-17, 2018

Y N U
PRESS

ISSN 2434-4133

Table of Contents

Appendix

Academic Collaboration among PUL Network Through the Experience of HydroAsia Program

Prof. Gyewoon CHOI Ph. D. and Prof. Jong-Hwa SHIN Ph. D.
Incheon National University, Republic of Korea

Abstract

In this paper, the academic collaboration approach among PUL network is suggested based upon the experience of HydroAsia program, which was established in 2007 with a global Asian vision to promote the key concepts, methodologies, tools and good practices which are essential for a sustainable water management. The program is focusing to the collaboration for graduate students and capacity building related to the real water issues in the Asian countries.

HydroAsia program is a unique opportunity to develop professional skills and knowledge in the field of hydroinformatics and collaborative engineering. The provided program is focusing in the perfect real solutions in which several approaches can be implemented in order to assess the flood and to elaborate engineering solutions. Every year HydroAsia program welcomes over 50 participants from more than 15 different countries with the support by experienced instructors. The international atmosphere among participants provides a unique opportunity to develop teamwork and communication skills, and at the same time to create a first professional network at the international level.

The program can be categorized in two phases, which are online activities and face-to-face meeting. The online activities provide to the participants with the possibility to work based upon a full collaborative environment, available technical data, and modelling tools provided by the industrial partners of HydroAsia program. In the face-to-face meeting, team projects, which are given as water issues in the real watershed by the hosting university, are conducted through leading by team leaders as well as advices from experienced instructors. The field trip and the effort for technical data collection from the related agencies can be the good experiences for the graduate students.

In the paper, step-by-step approaches for academic collaboration among PUL network are presented and the deep discussion can be continued during the whole

2018 PUL conference period for better implementation.

Introduction

The HydroAsia program was initiated with the purpose to share and exchange the ideas and experiences related to water issues among graduate students in Asian countries. Especially, this program focused on the understanding and solution approaches of real water issues in the given watershed through conducting the team projects. The program was initiated through the collaboration between four universities, which are Incheon National University in Republic of Korea, Kyoto University in Japan, Tropical Marine Science Institute, National University of Singapore and University of Nice, Sopia-Antipolis, France. And, many other universities including Beijing University of technology in China, Tianjin University in China, and Asian Institute of technology in Thailand and so on were involved as the key collaborating institutions. The program is very closely linked with HydroEurope program, which is the collaborative program in the area of Hydroinformatics between European universities. The HydroAsia program is conducted with the joint effort from the public and private agencies such as K-water, Incheon Metropolitan city, DHI, etc. This program is open to all of graduate students in Asian countries.

The first HydroAsia program was initiated in 2007 with 12 student participants and 7 professors from four universities, which were Incheon National University, Kyoto University, Tropical Marine Science Institute, National University of Singapore, University of Nice, Sopia-Antipolis. The first HydroAsia was held at Incheon National University through the deep discussion between organizing committee during the summer vacation. The internet facilities including internet server was supported by University of Nice, Sopia-Antipolis and the technical support for the watershed was prepared by Incheon National University. The special lectures were prepared by the professors coming from four universities. Even though strong effort through joint collaboration between professors was given during the preparation process, several shortages and mistakes were indicated in conducting the first HydroAsia program. Many supplementations and inclusions in the next years' programs were given

through the evaluation and improvement processes. After initiating the first HydroAsia program in 2007, the more attention from the graduate students in Asian countries were given and 41 participants (31 students and 10 professors) in 2008 and 58 participants (45 students and 13 professors) in 2009 were attended in the second and third HydroAsia programs. The maximum participants during HydroAsia programs were increased until 96 (84 students and 12 professors) participants in 2015. The face-to-face meeting of Twelve HydroAsia program was held in August, 2018 with the participants of 56(43 students and 13 professors).

The participants in HydroAsia program indicate the positive opinion for the activities through the evaluation. Above all things, they give the emphasis in the experience for the complex water issues in the real watershed field. Also, instructors identified the advanced capacity building such as the approach to the real water problems with theoretical thinking after HydroAisia team projects. Also, they indicated additional advantages for making a good global network in the similar field and understanding the different culture and life environments.

Main Activities of HydroAsia Program

The program of HydroAsia is composed of online and face-to-face activities with placing the different emphases in the step-by-step processes. Because the students are coming from the different countries, the online activities are conducted in advance for the purposes of introduction of the program, team organization, comfortable communication between team members, and increasing the numerical knowledge related to the solution packages. The final results through team projects can be obtained through the face-to-face meeting and the results can be shared among participants in the final presentation.

Figure 1 indicates the flow chart for main activities of HydroAsia program.

The online meeting is started before 1 or 2 months of Face-to-face meeting. The specific focuses in the online meeting are given in the selection of team leaders, understanding HydroAsia program, selection of topic per each team and the personal role arrangement between team members and so on.

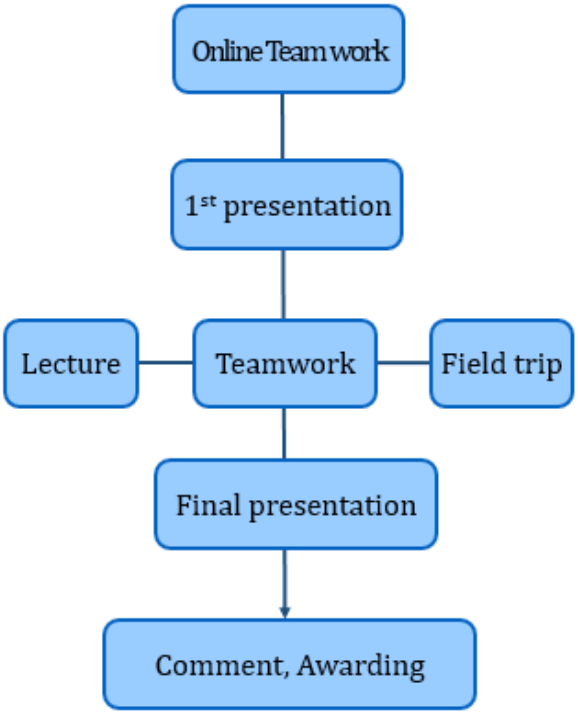

Figure 1 The flow chart for main activities of HydroAsia program

The team leaders are selected through the discussion between team members. The team members have an opportunity to know each other through attending an introductory online lecture and team communication meetings. They also share their knowledge and experiences about initial discussion for their concerning subjects and preparing the models and data. And then, they select a preliminary topic for the team project and distribute the role of each member in the team. They are continuing the communication through online team meetings once or twice per week using MSN masseger and SKYPE. The necessary information for technical approaches can be shared using HydroAsia website and their own internet devices.

Face-to-face meeting can be conducted through 5 different activities, which are 1st presentation during opening ceremony, lectures, Field trip, conducting team project and final presentation. In the first presentation, the backgrounds, objectives and approaching procedures for the team topics are presented with the comments from the instructors and participating students. The procedures for obtaining the results regarding to the given topics are given with the introduction of the selected software packages and/or models. The limitation for using or obtaining the real

data in the given watershed can be discussed through the open discussion between participants including instructors' comments. Lectures are conducted through the link with the projects by participated professors. The participants can open the eyes for the application on the real issues in different countries. They can also learn about the linkage between theory and practice for finding the problem solutions. At the same time, they can share the information related to participated professors through the open discussion just after the special lectures. Participants can share the experience about the real situation through visiting the target watershed. They can have the experience for obtaining the information and data through the field visit. Also, they want to visit for the specific area related for their projects, they can visit the important facilities and process, environmental conditions related to their projects. They can have the knowledge and linkage between the water quantity and water quality through field visit. They can find out the idea for the direct and indirect countermeasure for flood protection and drought damage reduction. Team projects are conducted with the supervision from one or two advisors. The advisors conduct their roles through open discussion between team members and answering for the specific questions from the participants. If team members proceed to the wrong direction, then supervisors can lead the team through the suggestion using their experiences or theoretical background. After finishing the team project during one week, they present their final results and conduct deep discussions between participants. Also, they are sharing the difficulties for simplifying the complicated phenomena in the real field. They can understand for the importance of the data accuracy and parameter values. The comments and suggestions from the supervisors and the other team members are very helpful to the participants. Fig.2 indicates the web-site of HydroAsia program. Participants can obtain the information for available data, several ideas and approaching methods for their tasks.

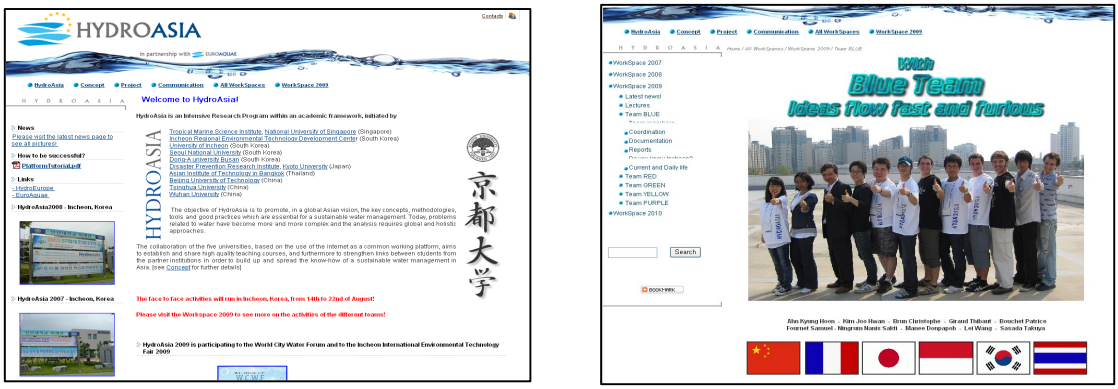

Fig. 2 Web-site of HydroAsia program

Experimental Watershed and Sharing the Results

Two different watersheds are used as the target study areas during HydroAsia program during 12 years. Incheon Gyo watershed was utilized as the experimental watershed except 2014 to 2017. During 2014 to 2017, Geum river watershed used as the experimental watershed. Table 1 indicates the comparison of the features between two different watersheds.

Table 1. Comparison of the features between two experimental watersheds

Period	2007~2013	2014~2017
Study Area	Incheon Gyo Watershed	Guem River
Issues	The extreme flood on 4th Aug 1997	The 4 rivers restoration Project
Object	To understand reasons of flooding and discuss recommendations for management of urban area	To analyze hydrological, hydraulic and water quality problems in study area
Topic	• Simulation of flooding in urban area to find countermeasures • Analysis on Tide effects and drainage system by changing pipe line	• 1D analysis in river from dam to sea • 2D analysis in specific area • Dredging and spur dyke
Software used for simulation	ArcGIS, SWMM, MOUSE, MIKE21	HEC-RAS, HEC-HMS, MIKE21

The Incheon Gyo watershed having the area of 34km^2 is very complicated

watershed which is located in the north-west direction at Incheon Metropolitan City, Republic of Korea. Originally, the watershed was seashore and was reclaimed until 1985, and then used as industrial and residential area. Because of the very mild slope in the lower part of the watershed, the flood can frequently be indicated in the flooding season having the high intensity of rainfall. The downstream boundary condition of sea water level is very important for outflow from the existing reservoir. The difference between high sea water level and low sea water level is around 9m. The reservoir operation using the pumps and reservoir volume is another important factor for flood simulation. The Fig. 3 indicates the schematic features of the watershed and an example of flow simulation result obtained by the participants during the HydroAsia program in the past years. Fig.4 indicates the example during the processing team projects.

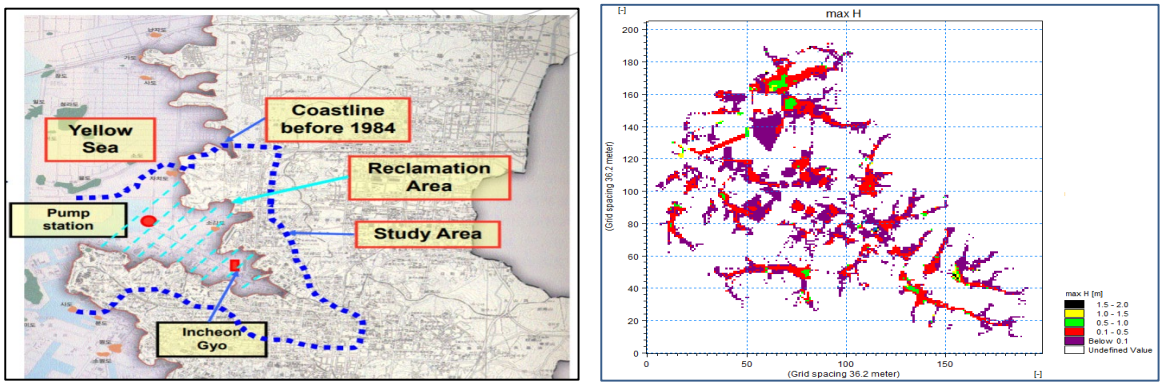

Fig.3 The schematic features of the watershed and a flow simulation result

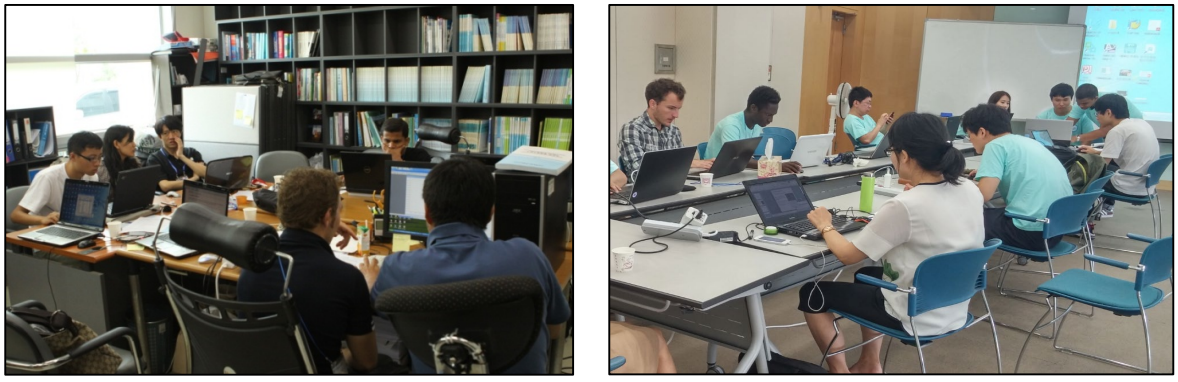

Fig. 4 The photographs during processing team projects

Suggestion for Collaboration among PUL Network

PUL aims to develop a global network among universities at port cities and exchange ideas and views about the culture related to ports in the world. It indicates not only the faculties and students, but also will be extended in the future collaboration including the citizens' activities and initiatives. Until now, PUL focuses about the information and research exchanges since established in 2006. PUL need to have more attractive activities through various joint efforts between member universities.

In the eleventh PUL meeting in last year, which was held at Incheon national University, two different suggestions were deeply discussed. The first suggestion is the joint research between member universities. And the second suggestion is related to student exchange and credit exchange program. However, the detail for those suggestions wasn't discussed among member universities.

In this paper, the collaboration approach which can easily be accepted by member universities is suggested through sharing the experience in the existing student collaboration. The student collaboration activities such as HydroAisa between member universities will be good initiatives for better collaboration between member universities. The subjects can be discussed through the selection of Task Force (TF) among member universities. Based upon the experience of HydroAsia program, the combination between the online meeting and face-to-face meeting can be well adopted for achieving fruitful results of the collaboration.

References

Choi, G. W., 2018, Introduction of HydroAsia, International Conference on Hydroinformatics, IWA.

PUL, 2017, International Collaboration Research Forum and PUL Working Level Meeting, The 11th Meeting of the Port-city Universities League(PUL),

HydrpAsia Web-site at https://www.hydroasia.org

Analysis of Calculation Methods of Piled Raft Foundations

Le Ba Vinh[1], Le Nguyen Anh Vu[2], To Le Huong[3]

1 Ho Chi Minh City University of Technology

2 Ho Chi Minh City University of Technology

3 Ho Chi Minh City University of Technology

268 Ly Thuong Kiet Street, Ward 14, District 10, Ho Chi Minh City, Viet Nam

Abstract: The piled raft foundations are widely used in the high rise buildings because its load bearing capacity and settlement are significantly improved as compared with the conventional pile foundations. In the design of piled-raft foundations, it is necessary to understand the real behavior of this foundation which depends on the interaction between the raft - piles - the surrounding soils. In this paper, the behaviors of piled raft foundations such as the settlement, the bending moment of raft, the load share between raft and piles,... are calculated and analyzed by the different analytical methods, and the numerical method by the PLAXIS 3D Foundation software. Based on these calculated results, the applicability of these calculation methods can be concluded.

Keywords: piled raft foundation, settlement, bending moment, pile's load share

Introduction

In case the raft foundations does not satisfy the design requirements, the piles were combined with the raft to improve the problems of load bearing capacity, settlement and the required thickness of raft. The piled raft foundation is a combination of three elements: piles, raft and soils. The behavior of the piled raft foundation mainly depends on the interaction between these elements of the foundation. Katzenbach et al. (2000) identified four types of interaction (soil and piles, piles and raft, soil and raft, pile and pile), and it is necessary to take into account the behavioral analysis of the piled raft foundations. There are many analytical methods for calculations of the piled raft foundation. This paper analyzes the applicability of these methods and the numerical method through a particular work.

Description of studied cases

In order to predict the behavior of piled raft foundation by different methods, Poulos has established a simple example with parameters as shown in Fig. 1. There were three cases of analysis as follows:

- Case A: Piled raft foundation with 15 piles and a total load of 12 MN.
- Case B: Piled raft foundation with 15 piles and total load of 15 MN.
- Case C: Piled raft foundation with 9 piles and a total load of 12 MN.

In each case, six methods of analysis were used:

1. Poulos-Davis Method (1980).
2. Randolph Method (1983).
3. Method of beam on the spring support, using the GASP program (Polous, 1991).
4. Method of plate on the spring support, using GARP program (Polous, 1994).

5. The finite element method by Ta and Small (1996).

6. The finite element method combined with boundary element method by Sinha (1996).

In this paper, we also use the Plaxis 3D Foundation software to analyze these cases, then the simulated results are compared with the results of six analytical mentioned above.

The simulation models by Plaxis 3D foundation are shown in Figure 2 and Figure 3.

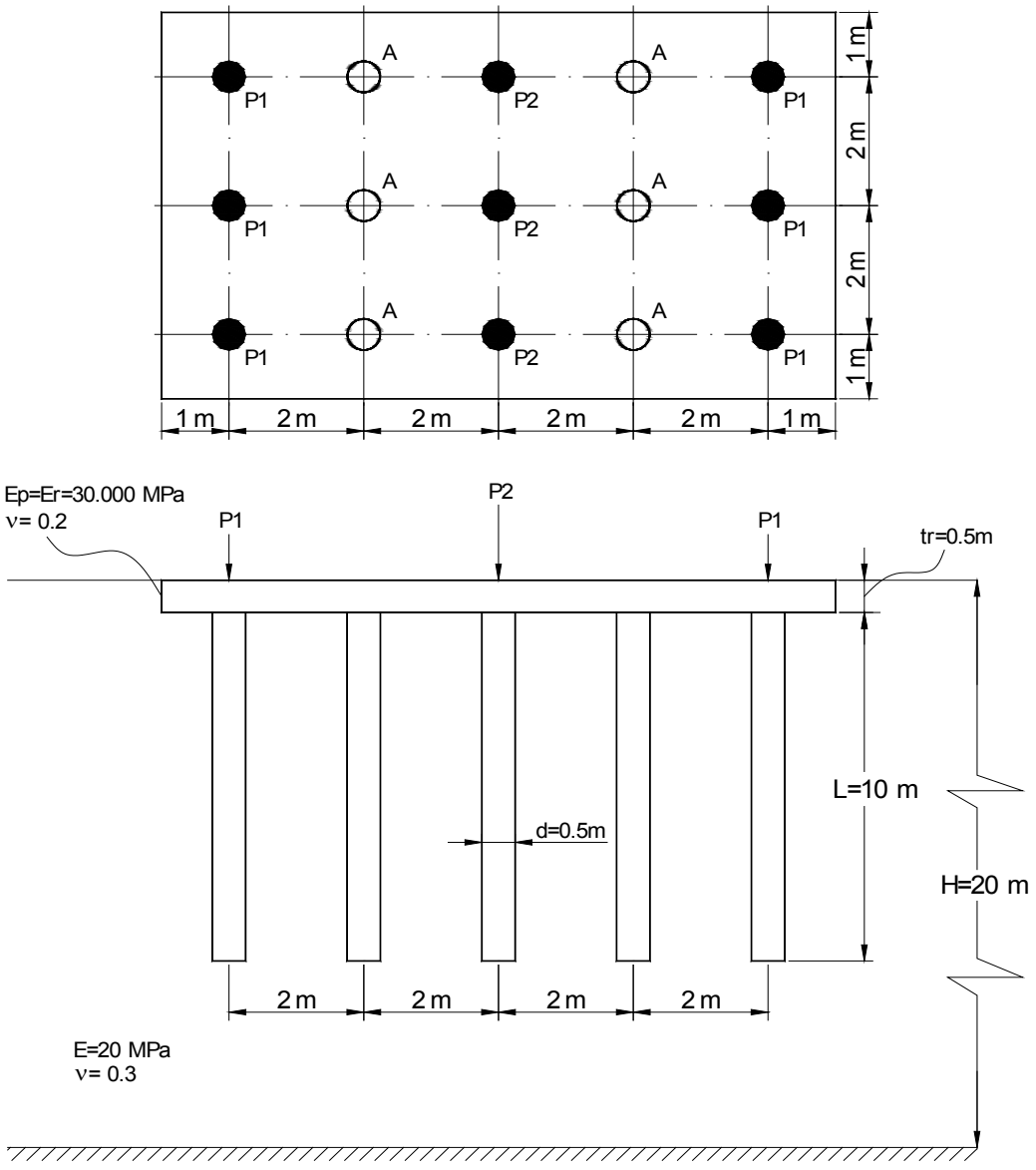

Figure 1. Model of analysis by different methods.

Note:

- P2 = 2P1
- With the 9 piles model, the piles are located at P1 and P2
- With the 15 piles model, the piles are located at P1, P2 and A.
- The load bearing capacity of the raft is 0.3 MPa.
- The load bearing capacity of each pile is 0.873 MN.

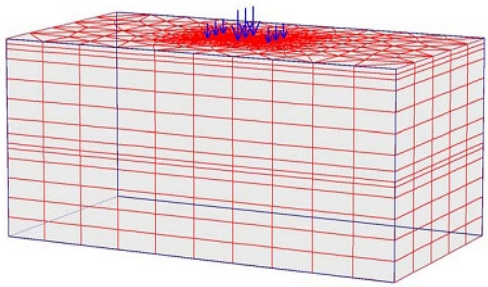

Figure 2. The overall model of simulation by Plaxis 3D Foundation.

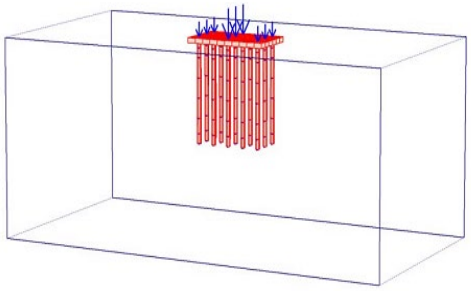

Figure 3. Piled raft foundation model by the Plaxis 3D Foundation.

Result of calculations

Fig. 6 to Fig. 8 show comparison of the mean settlement, maximum bending moment, differential setlement, and load share between the piles and the raft calculated by 7 methods for 3 cases mentioned above.

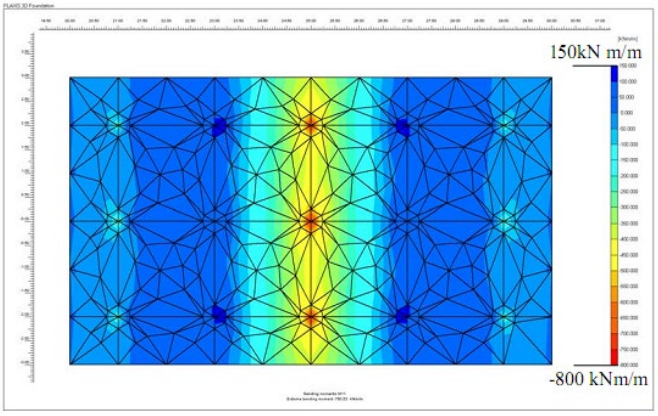

Figure 4. Bending moment of the raft, case A

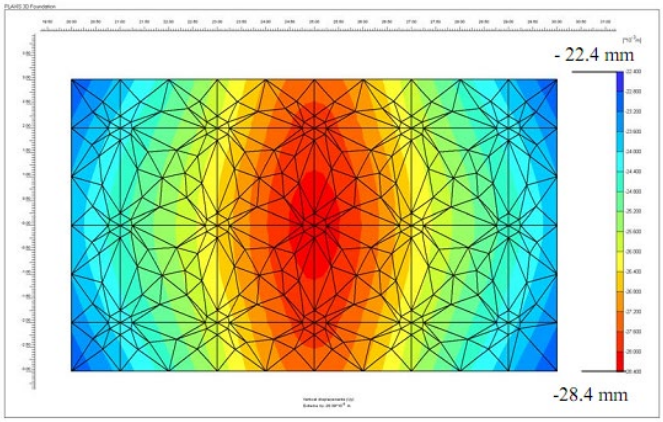

Figure 5. Settlement of the raft, case A

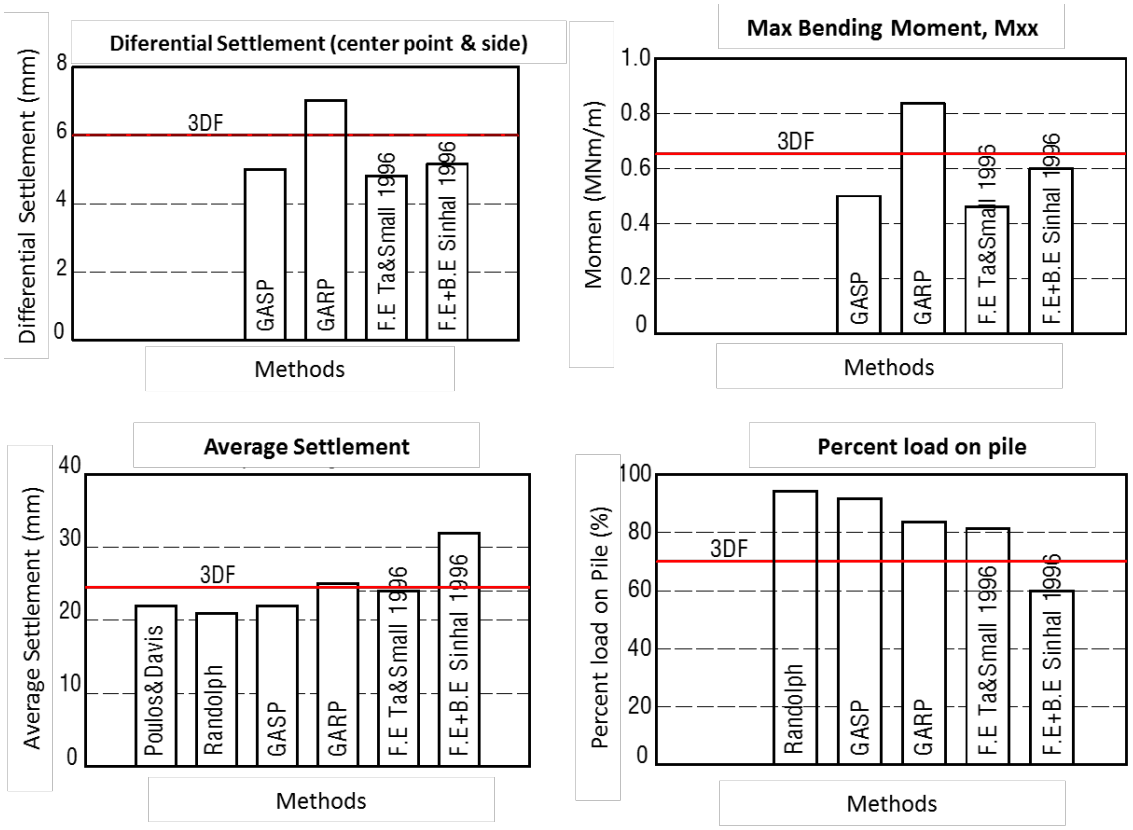

Figure 6. Calculated results by analytical methods, and Plaxis 3D Foundation (3DF), case A

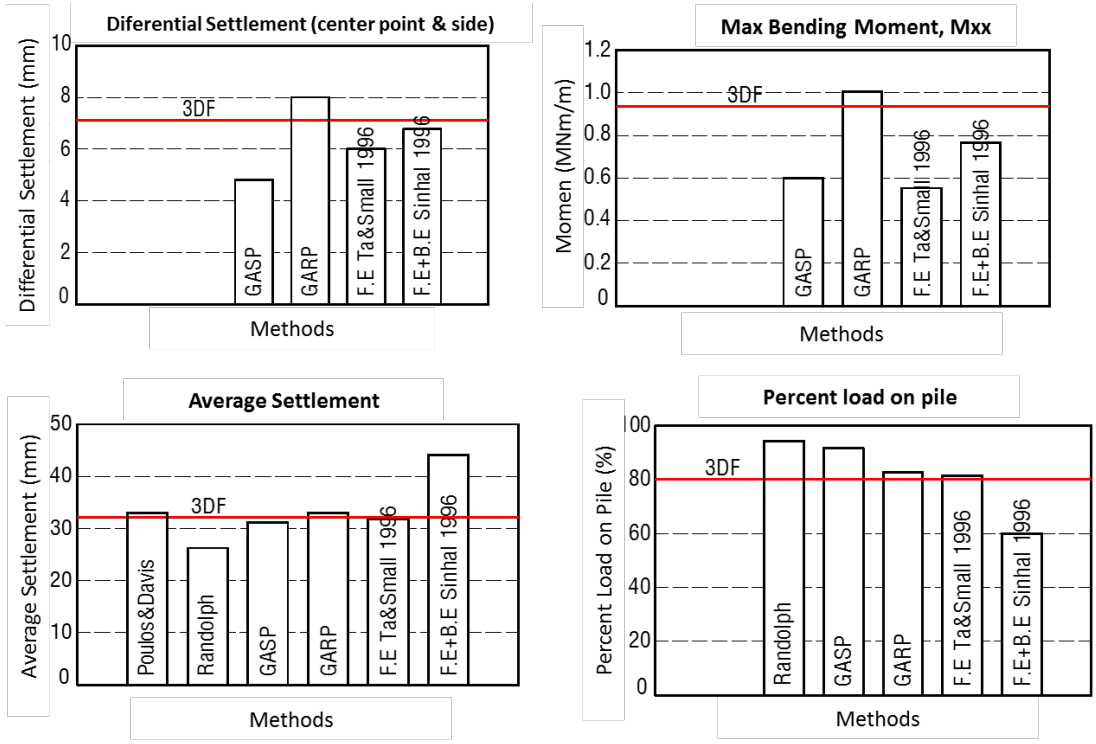

Figure 7. Calculated results by analytical methods, and Plaxis 3D Foundation (3DF), case B

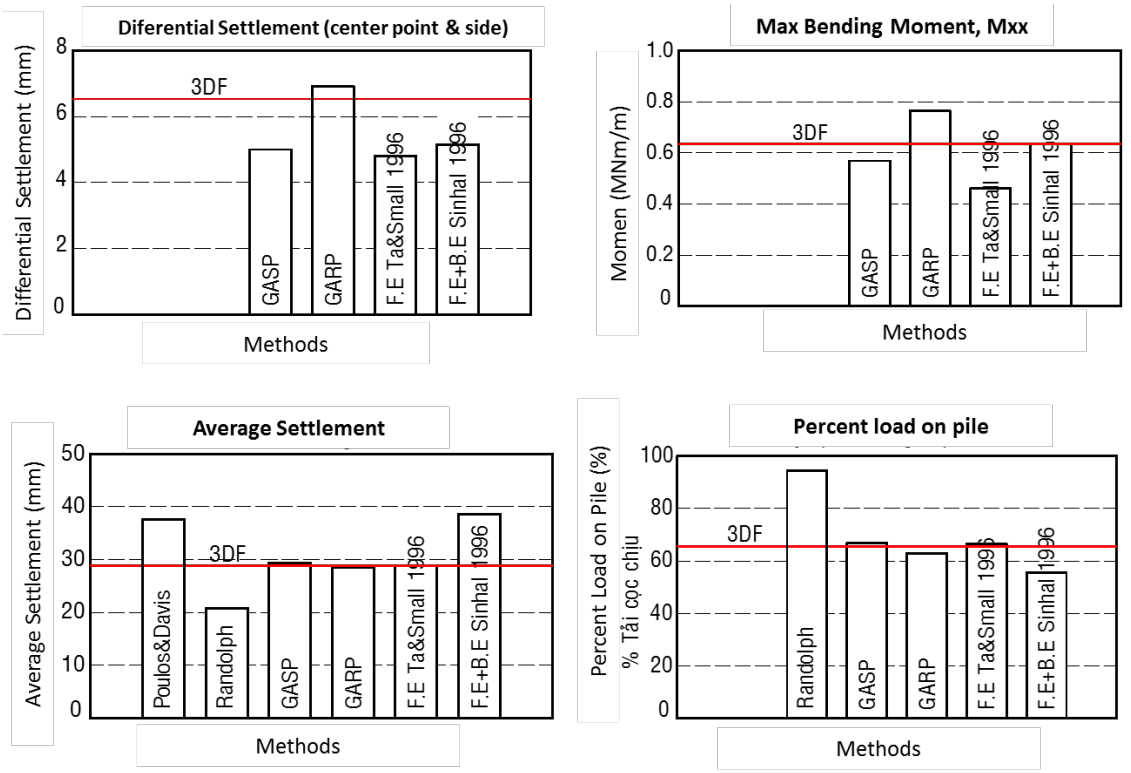

Figure 8. Calculated results by analytical methods, and Plaxis 3D Foundation (3DF), case C

Remarks and Conclusions

- The calculation method of Poulos and Davis results in a bigger settlement and load share between the piles and the raft.as compared with the results of other methods.
- The settlement calculated by GARP method and F.E. Ta and Small method have a smallest difference with the result simulated by Plaxis 3D Foundation.
- The maximum bending moment and differential setlement calculated by the GARP method are larger than the results predicted by the other methods and Plaxis 3D Foundation.
- The GARP method, F.E. Ta and Small' method, and Plaxis 3D Foundation gave the similar results of load share between the piles and the raft.
- The most suitable analytical method for calculating and analyzing the raft in the piled raft foundation is the GARP method.

References

Katzenbach, R., Arslan, U., and Moormann, C. (2000). "Piled raft foundations projects in Germany. Design applications of raft foundations."*Hemsley J. A., editor, Thomas Telford, London*, 323–392.

Poulos, H. G. & Davis, E. H. (1980). "Pile foundation analysis and design". *New York: Wiley*

Poulos, H. G. (1991) "Analysis of piled strip foundations. Computer Methods and Advances in Geomechanics",*Rotterdam*, 183-191

Poulos, H. G. (1994). "An approximate numerical analysis of pile-raft interaction". *Int. J. NAM Geomech. 18*, 73-92.

Randolph, M. F. (1994). "Design methods for pile groups and piled rafts."*State of the Art Rep., Proc.,*

13th ICSMFE, Vol. 5, 61–82.

Sinha, J. (1996). "Analysis of piles and piled rafts in swelling and shrinking soils". *PhD Thesis, Univ. of Sydney, Australia*.

Ta, L.D. & Small, J.C. (1996). "Analysis raft systems in layered soils". *Int J NAM Geomech. 2*, 57-72.

A Comparative Study on Selection Factors for Private and Public Sectors in Dry Ports – Focused on Xi'an Dry Port

Seung B. AHN 1**, Da ZUO** 2

1,2 Graduate School of Logistics, Incheon National University

119 Academy-ro, Yeonsu-gu, Incheon, 22012, Republic of Korea

E-mail: sbahn@inu.ac.kr

Abstract: As the economic development of Chinese coastal regions are approaching saturation, the Economic Development Centers need to be moved to inland regions. Chinese inland regions with vast territory and abundant resources have large population base and huge potential demands; bordering on many countries, foreign trade activities are frequent; moreover, logistics infrastructure of many inland regions has been gradually improved. In China, dry ports have been introduced for inland economy and the investment operation model can be divided in three types: landlord model, tool port model, and public service model. In Xi'an dry port (XITLP), the landlord model is adopted, which allows diverse PPP models to attract private investment. At present only a few PPP projects have succeeded with private investment and XITLP is facing with staggering and postponement. This paper aims to find the differences of perceptions between public sector and private sector through the comparative analysis of the factors on PPP projects. The data are obtained through the survey of public sector and private sector in 2017 and the analyses are: descriptive analysis, Cronbach's alpha, two sample t-test and factor analysis. There were significant differences in two sectors, especially on base costs and comprehensive service level.

Keywords: Dry port, Xi'an, XITLP, PPP, Comparative analysis

Introduction

In China, the inland region did not have such good opportunities to improve the economic development: in fact, there is a big economic gap between the inland and coastal cities. Chinese government found that the economic development is imbalance is became a big issue. Therefore, they focused on the infrastructure construction in inland and tried to build a traffic hub to drive economic development. With the trend of economic globalization, construction and development of inland dry ports are highly promoted by both the demands of development for worldwide costal ports as well as inland cities, and the objective needs of container intermodal development. In 2008, the Xi'an International Trade & Logistics Park (XITLP, thereafter) was formally established, with the objective of building China's first international land port, not along the river, off the coast and off the border: city-based dry port. As an integrated logistics park, it includes a new-build CFS, new-build CFS, a bonded logistics center, an international logistics zone, a domestic integrated logistics zone and a logistics cluster area. The administrative committee of XITLP has induced many project with the PPP model, but not much success. Thus, this

research aims to find the reason by analyzing the difference of the importance degree of factors between public sector and private sector.

Literature Review

Historically, dry ports have been used to enhance the competitive strength of the sea port as an inland terminal. Many researchers have defined dry ports one the most widely used one is that "The dry port concept is based on a seaport directly connected by rail with inland intermodal terminals where containers can be dealt with in the same way as if they were in a seaport." Dry port refers to a logistics center established in inland area which has service function of customs declaration, inspection declaration and insurance on bills of lading. Supervisory authorities, including customs, animal and plant quarantine bureau, commodity inspection bureau and health inspection authorities, are set up in dry ports to provide services for customs clearance (Bian, K. A., 2011). The dry port was built in the interior and supported by multimodal transport, it has a modern international logistics channel and platform with comprehensive service functions such as port supervision and port service, which is essentially a development form of coastal container port service extending inland (Wu, Shu, 2015).

Beresford, et al. (2012) and Xu, H. (2015) proposed that the development paths of Chinese dry ports show several differences, depending on their location. According to the paper, dry ports are classified in three types based on their location and function: 1) the seaport-based dry ports with a major function for pre-customs clearance, 2) city-based dry port, typically positioned within a larger logistics cluster which itself serves production and consumption, and 3) border dry ports, located in the border area/city, with the major function being as a transshipment center or custom clearance service. On the other hand, dry ports are classified according to distance from sea ports. Roso, V. et al. (2009), Woxenius, J. et al. (2004) and Wei, X. (2016) mainly classified into three categories: distant dry ports, midrange dry ports, close dry port, which has been adopted in many researches.

The investment operation model of a dry port can be identified through the works of Wu, S. (2015), Bichou, K. (2005) and Beresford, A. et al. (2012), which can be summarized as the following three categories: landlord, tool, and service port models. First, the landlord model describes a structure within which the port authority committee, as a governmental agency, unifies the port area facilities, port industry and other facilities land management, and has a great management autonomy and land use rights. The purpose is not for profit and not to participate in the market competition of port management, but to implement the government's management function to the port through the planning and construction. After the construction of the infrastructure, site and equipment, the port authority committee attracts the ports, railways, shipping, logistics and freight forwarding enterprises through the flexible PPP projects. The customs, quarantine and other

regulatory agencies are coordinated by the local government. Port enterprises participate in part of the business of dry port by providing technical supports, accredited representative offices or setting up corporation sole/co-partnership.

Secondly, the tool port model means that port authority not only provides infrastructure, also provide facilities and equipment to private operators, in other words, the port authority prepares a set of tools and provide to the private operator. The Stated-Owned Joint Venture are set up by port enterprise and port authority committee, as the main developer of the dry port, is responsible for the investment construction of the infrastructure, the site and the equipment of the dry port. After the completion of the construction of a dry port, the company will carry out the loading and unloading, warehousing, customs declaration, inspection and other services through recruitment of shipping companies, freight forwarders and logistics enterprises into the dry port. In both the landlord and tool model, the public sector owns and develops port infrastructure and lends to the private sector. In the tool model the public still owns the superstructure but may lend it to private companies for operation.

Thirdly, the service port model include two categories: public service and private service. The service port means that port authorities are responsible for all or most of construction of port facilities, participating in the harbor and port operation. In the service model, a port authority owns, maintains and develops both infrastructures and superstructures, operates all handling equipment and performs on its own all other commercial port functions. The main operation body is a social enterprise, which is responsible for the construction of the site, the purchase of equipment and the daily operation. It usually provides the service of the dry port.

The operation of PPP mode has three important features: partnership, sharing benefits and risks (Liu, W., 2015). Under the condition of China's diversified economic pattern, proposes definition suitable for China, clears the PPP's "partnership" and approaches to promoting PPP policies and mechanism innovation (Ye, X. and Xu, C., 2013). Under the new economic normality, institutional change, structural optimization and elements upgrading is the momentum of China's economic development. PPP mode can promote transforming government functions and is an effective way to give play to effect of market allocation of resources (Zhou, Z. et al., 2015).

In the operation field, there are some researches focusing on the investment mode, Wu, S. (2015), Bichou, K. (2005) and Beresford, A. et al. (2012) studied the investment operation mode and classified the types. As the result, several types of dry ports are adopted with different modes. There is a big difference among the modes in operating organizations and companies and operating methods, and each mode has own advantages and disadvantages. This research focuses on the XITLP, where the landlord model is adopted and the XITLP depends on the PPP projects to attract the private investment. However, there seems no specific research, showing how to establish a successful PPP project. Therefore, this study aims to compare the importance of factors between the

private and public sector.

Current Status of XITLP

Xi'an, the central city of western Chinese periods, plays an important role in the economic development strategy of China recently, as the originating point of the Silk Road Economic Belt (One Belt One Road). Xi'an is developing a modern, international, large-scale integrated inland port to meet the needs of transport, and promote the local economy. Xi'an International Trade & Logistics Park（XITLP is based on the existing railway, road and other transport means, cooperating with the coastal international port, forming a rallying and bonding point of sea-land combined transport in inland region. The XITLP not only possesses the basic functions of ordinary logistics park, but also has a variety of functions such as bonded areas, warehousing, customs, border inspection, commodity inspection, quarantine, foreign exchange banks, insurance companies, shipping market with shipping agents and other functions.

Table 1. The operation data of XITLP

Category	2014	2015	2016
Bulk cargo throughput of XITLP (Million tons)	589.02	637.49	776.83
Container throughput of XITLP (Million TEU)	10	11.6	13.2
Total gross revenue of XITLP (Million CNY)	45,700	58,850	83,000
Sales of logistics service (Million CNY)	19,800	26,000	37,050
Sales of circulation processing (Million CNY)	8,650	11,099	12,924
Total gross revenue of settled enterprise (Million CNY)	1,240,000	2,050,000	2850,000
Sales of logistics service (Million CNY)	299,240	493,300	683,300
Sales of circulation processing (Million CNY)	117,800	195,000	270,700
Annual investment of XITLP (Million CNY)	1,208,100	1,575,100	1,734,200
Number of management services of XITLP	1,000	1,350	1,800
Number of employed persons in settled enterprise	4,200	5,900	7,000

The logistics park in Xi’an international port area is located in the northeast of the main city of Xi’an, which is the center of the geographical geometry of China, and it has the highest standard of construction of Xi’an railway container center. In order to build the One Belt And One Road international multi-modal transport and trade logistics hub, China has already built several national logistics platforms and matching facilities in the logistics park, attracting a number of well-known logistics and trade enterprises at home and abroad. The park has 700,000m^2 of general warehouse (including bonded warehouse) (thereinto, 170,000$m^2$of general warehouse have been finished and 530,000$m^2$of it is in progress).

Xi'an Integrated Free Trade Zone is the first integrated free zone under closed operation in northwest China. Xi'an Railway Container Terminal, as one of 18 centers nationwide, is the core area of warehouse and logistics planned by Xi'an City and 7 km away from the Ring Expressway. Xi'an Cross-border Trade E-commerce Service Pilot has been approved by General Administration of Customs and built for operation. "Chang'an" International Regular train is an important international large channel to the west cooperated between Railway Corporation and the park. It first departed Xi'an Railway Container Terminal in November 2013. The annual cargo handling capacity is 130,000 TEU, with an annual growth of 20.3%. Xi'an International Inland Port Group has entered into an cooperative agreement with Germany TEL, HUPAC and TRSB so as to take advantage of transportation systems of the aforesaid three enterprises in Europe to rapidly distribute goods loaded in central Europe train from Xi'an to Hamburg (Germany) to Netherlands, France, Spain, Czech Republic, Italy, Finland and other countries. In respect to the Sea-rail transportation Channel, XITLP developed a combined transportation channel of international sea railway from Melbourne Port in Australia to Xi'an Port in 2015; and successfully developed a combined transportation channel of international sea railway from Littleton Port in New Zealand to Xi'an Port in 2016. XITLP has signed a cooperative agreement with 14 costal ports and nearby ports including Tianjin Port, Qingdao Port, Shanghai Port, Ningbo Port, Alataw Pass, Khorgos, Erenhor, Pingxiang in Guangxi and so on. It vigorously expands the combined channel of sea railways and land routes, provides a diversified logistics project for enterprises to choose, and becomes an important tongs and a strong support for constructions of new starting point of economic belt of provincial and municipal silk roads.

Methodology and Research Hypothesis

The variables used in this research are mainly obtained from the personal interviews conducted in Xi'an to the private owners of logistics companies, the officials of the government agencies, researchers on the logistics field. The variables adopted are explained in Table 2, to help the respondents to understand.

Table 2. Definition of Variables

Variables	Notes
Area Location	According to the distance to sea port, can define as the close dry port, midrange dry port and distant dry ports.
Warehousing Capacity	The size of the warehouse available space and the type of warehouse, need to meet various warehousing demand such as, bonded warehouse, general warehouse, cold chain warehouse, etc.
Transportation Condition	Different types of dry ports rely on different means of transportation, for

	convenience and diversity.
Loading/Unloading Capacity	Possibility to load/unload large quantities goods quickly, including containers and bulk cargoes
Base Cost	Cost of infrastructure construction and the cost of land acquisition by the main enterprise.
Operating Cost	Cost of the daily operation.
Service Charge	Expenses arising from the comprehensive service provided by the dry port such as the clearance, transport, storage, quarantine, etc.
Basic Service	Including the clearance, transport, storage, quarantine, international freight forwarding, etc.
Layout of Logistics Facilities Function	Integrated logistics facilities services: bonded area, container storage, multimodal transport, cross-border e-commerce, etc.
International Multimodal Transportation System	Different international multimodal transport routes to meet the needs of domestic import and export and cross-border transportation.
Informatization Level	Exchange and sharing of information between the dry port and its business partners.
Governmental Policy	Private capital can participate in the dry port PPP project through appropriate investment.
Investment and Financing System	Provision of a policy for non-public economic investors to participate in government projects, which include investment and financing methods without too many restrictions
Cooperation Model	Including the allocation of responsibilities and benefits, and the risk sharing. Existing cooperation models generally include BOT, BOO, BBT, and etc.

The methodology adopted in this research mainly focused on comparative analysis between two groups using statistical analysis. The reliability analysis is mainly used to determine whether the data collected by the questionnaire is correct when designing the survey with the Likert scale (Yoo, 2015; Li et al., 2005; Choi, 2008).

Factor analysis is to take advantage of the correlation between multiple variables and classify the various factors into the purpose. Factor analysis is the method of tying the high correlation to the common sub-element, using factor principal component analysis or common factor analysis to extract the factors. The T-test is the statistical analysis method used to compare the mean differences between two groups. It is mainly used to observe the differences existing in the importance of factors between two independent groups. In order to apply this method, it is necessary to assume that both groups are in normal distribution and are distributed in the same way.

In order to study the cognitive differences between the private sector and the public sector on the importance of each factor, the followings are the hypotheses set in the studye.

It is noteworthy that the hypothesis of this research is not based on the null hypothesis (H_o: $\mu_1 = \mu_2$, P>0.05), all of the following hypothesis are based on H_a ($\mu_1 \neq \mu_2$, $P \leq 0.05$)

- Ha: There are differences between the private sector and the public sector on the importance degree.

In order to determine the importance of the private sector and the public sector on the Infrastructure Condition, this study sets the hypothesis for four variables.

- H1: There are differences between the private sector and the public sector on the importance of Area Location
- H2: There are differences between the private sector and the public sector on the importance of Warehousing Capacity
- H3: There are differences between the private sector and the public sector on the importance of Transportation Condition
- H4: There are differences between the private sector and the public sector on the importance of Loading/Unloading Capacity

In order to determine the importance of the private sector and the public sector on Cost, this study sets the hypothesis for three variables.

- H5: There are differences between the private sector and the public sector on the importance of Base Cost
- H6: There are differences between the private sector and the public sector on the importance of Operating Cost
- H7: There are differences between the private sector and the public sector on the importance of Service Charge

In order to determine the importance of the private sector and the public sector on Comprehensive Service Level, this study sets the hypothesis for four variables.

- H8: There are differences between the private sector and the public sector on the importance of Basic Service.
- H9: There are differences between the private sector and the public sector on the importance of Layout of Logistics Facilities Function.
- H10: There are differences between the private sector and the public sector on the importance of International Multimodal Transportation System.
- H11: There are differences between the private sector and the public sector on the importance of Informatization Level.
- In order to determine the importance of the private sector and the public sector on Investment Climate, this study sets the hypothesis for three variables.
- H12: There are differences between the private sector and the public sector on the importance of Governmental Policy
- H13: There are differences between the private sector and the public sector on the importance of Investment and Financing System

- H14: There are differences between the private sector and the public sector on the importance of Cooperation Model

Empirical Analysis

The main subjects of this study are personnel of the private logistics enterprises in Xi'an region, and the employees and the researchers of the XITLP management committee. There are two sections, the first part is the basic information, including the contact information, the unit name, the position, the working period, the nature of the unit. The second part is the critical assessment of Infrastructure Condition, Cost, Comprehensive Service Level, and Investment Climate. In terms of important degree evaluation of the design of four factors, the 5-point Likert scale is adopted.

Table 3. The composition of the questionnaire

Survey Item	Contents
Basic Information	Contact information, Department, Working ages, Occupation
Factor Importance	Area Location, Warehousing Capacity, Transportation Condition, Loading/ Unloading Capacity, Base Cost, Operating Cost, Service Charge, Basic Service, Layout of Logistics Facilities Function, International Multimodal Transportation System, Informatization Level, Governmental Policy, Inve stment and Financing System, Cooperation Model

First of all, this study described the significance of factors regarding the data gathered from questionnaires. The analysis of the survey response data produced mean importance values for the 14 factors ranging from 4.30 to 3.40. As shown in Table 4, all the means are above 3.00, it means that the 14 factors are considered important whether public or private sector. From the overall point of view, there are two factors, whose mean are above 4.00. Among which the factor with the highest mean, which is 4.30, refers to Governmental Policy; however, the lowest mean, which is 3.40, belongs to Service Charge. Respondents were divided into two groups: public and private sector. And according to the total ranking arrangement for each group of the mean, on some levels, there is not a big difference regarding the mean and ranking between these two groups, such as Governmental Policy，Cooperation Model，Transportation Condition and Area Location. However, a huge gap exists in the following parts, such as International Multimodal Transportation System，Base Cost，Informatization Level and Layout of Logistics Facilities Function. In order to verify the existence of differences in the perspective of statistics, in the next section, T – test is applied with SPSS data to verify each hypothesis proposed before.

Table 4. The relative importance of Factors in PPP projects

Variable	Public Sector		Private Sector		Total		Cronbach's alpha
	Mean	Rank	Mean	Rank	Mean	Rank	
Governmental Policy	4.38	1	4.22	1	4.30	1	.870
Cooperation Model	4.26	3	4.00	3	4.13	2	
International Multimodal Transportation System	4.38	2	3.44	10	3.90	3	
Transportation Condition	3.94	6	3.75	6	3.84	4	
Loading/Unloading Capacity	3.68	11	3.94	4	3.81	5	
Base Cost	3.32	13	4.14	2	3.74	6	
Operating Cost	3.59	12	3.86	5	3.73	7	
Area Location	3.85	7	3.58	7	3.71	8	
Warehousing Capacity	3.76	9	3.56	8	3.66	9	
Informatization Level	4.09	5	3.25	13	3.66	10	
Layout of Logistics Facilities Function	4.12	4	3.17	14	3.63	11	
Basic Service	3.79	8	3.44	11	3.61	12	
Investment and Financing System	3.74	10	3.36	12	3.54	13	
Service Charge	3.29	14	3.50	9	3.40	14	

In addition, this study conducted a reliability analysis of the data after the screening (Chronbach's alpha) in order to confirm that the research question was in the same field. As shown in the Table 4, Chronbach's alpha coefficient is 0.870, which is a fairly high degree of credibility, which indicates that all the problems in this study have high content consistency; meanwhile it proves that there are high reliabilities existing in all the questions and results.

As mentioned above, the aim of the study is to find whether there is a difference in the importance of different sector factors in terms of a statistics aspect. We divided the transponders into public sector and private sector by factor analysis in order to determine the difference in the importance of different factors.

A correlation matrix of 14 community variables from the research survey data was calculated. The value of the test statistic for sphericity was large (Bartlett test of sphericity 325.499) and the associated significance level was small (p=0.000), suggesting that the population correlation matrix is not an identity matrix. All the variables show a significant correlation at the 5% level, suggesting that there is no need to eliminate any of the variables for the principal component analysis. The value of the KMO statistic is 0.706,

which according to Kaiser (Norusis, 1992) is satisfactory for factor analysis.

Table 5. Total rotated factor variance

Component	Initial Eigenvalues			Rotation Sums of Squared Loadings		
	Total	% of Variance	Cumulative %	Total	% of Variance	Cumulative %
1	5.417	38.691	38.691	2.715	19.395	19.395
2	1.898	13.560	52.251	2.629	18.776	38.171
3	1.325	9.463	61.714	2.288	16.340	54.511
4	1.123	8.024	69.738	2.132	15.227	69.738
5	.839	5.996	75.734			
6	.657	4.691	80.425			
7	.571	4.079	84.504			
8	.456	3.255	87.759			
9	.402	2.871	90.630			
10	.361	2.579	93.208			
11	.301	2.147	95.355			
12	.280	1.999	97.354			
13	.217	1.549	98.903			
14	.154	1.097	100.000			

Principal component analysis produced a four-factor solution with eigenvalues greater than 1.000, explaining 69.73% of the variance, as shown in Table 6. The remaining factors together accounted for 30.27% of the variance. The factor grouping based on varimax rotation is shown in Table 7. Each variable belongs to only one of the factors, with the loading on each factor exceeding 0.50.

According to the result the 14 factors can be grouped into four principal factors and be interpreted as follows:

a. Factor grouping 1 represents Infrastructure Condition.

b. Factor grouping 2 represents Cost

c. Factor grouping 3 represents Comprehensive Service Level

d. Factor grouping 4 represents Investment Climate

Table 6. Rotated factor matrix (loading)

Survey Item	Component			
	1	2	3	4
Area Location	.597			
Warehousing Capacity	.802			

Transportation Condition	.745			
Loading/Unloading Capacity	.804			
Base Cost		.653		
Operating Cost		.784		
Service Charge		.679		
Basic Service			.787	
Layout of Logistics Facilities Function			.643	
International Multimodal Transportation System			.744	
Informatization Level			.517	
Governmental Policy				.702
Investment and Financing System				.879
Cooperation Model				.690

Table 7. Summary of comparative analysis results

Grouping	Variable	Sector	Mean	Std. Deviation	t-value	p
Infrastructure Condition	Area Location	Public	3.85	1.048	1.046	.299
		Private	3.58	1.105		
	Warehousing Capacity	Public	3.76	1.103	.833	.408
		Private	3.56	.998		
	Transportation Condition	Public	3.94	1.071	.808	.422
		Private	3.75	.906		
	Loading/Unloading Capacity	Public	3.68	1.065	1.110	.271
		Private	3.94	.955		
Cost	Base Cost	Public	3.32	1.007	3.367	.001
		Private	4.14	1.018		
	Operating Cost	Public	3.59	1.104	1.036	.304
		Private	3.86	1.099		
	Service Charge	Public	3.29	1.142	.804	.424
		Private	3.50	1.000		
Comprehensive Service Level	Basic Service	Public	3.79	1.038	1.397	.167
		Private	3.44	1.054		
	Layout of Logistics Facilities Function	Public	4.12	.769	4.286	.000
		Private	3.17	1.056		
	International Multimodal Transportation System	Public	4.38	.954	3.469	.001
		Private	3.44	1.275		
	Informatization	Public	4.09	.965	3.242	.002

	Level	Private	3.25	1.180		
Investment Climate	Governmental Policy	Public	4.38	.888	.723	.472
		Private	4.22	.959		
	Investment and Financing System	Public	3.74	1.053	1.417	.161
		Private	3.36	1.150		
	Cooperation Model	Public	4.26	.864	1.213	.229
		Private	4.00	.956		

The results of descriptive analysis and reliability analysis reveal that the most important factor is governmental policy for both of two sectors. According to the factor analysis, the 14 variables are divided into 4 groupings: Infrastructure Condition, Cost, Comprehensive Service Level and Investment Climate. In order to study the cognitive differences between the private sector and the public sector on the importance of each factor, 15 hypotheses are set and verified by T-test. The results show as follows; most of hypotheses are not rejected; it means that there were no significant differences between the public and private sector, especially in terms of infrastructure condition and investment Climate. However, there are four hypotheses, which are rejected including H5, H9, H10 and H11. As same as the result of statistical analysis, in terms of cost, private sector pays more attention than the public sector. The public sector, however, shows more attention in the aspect of "Layout of Logistics Facilities Function", "International Multimodal Transportation System" and "Informatization Level".

Conclusions and Further Research

Under the national policies of the Chinese government, such as "Go West", "One belt and one road", the development of the dry ports is increasingly valued by government. As one of the core cities along the One Belt and One Road, Xi'an shoulders the important responsibility of boosting the regional economy and strengthening the cooperation in trade between inland and oversea countries. In this regard, XITLP becomes the priority of priorities. The landlord model is adopted in the XITLP; it mainly depends on the PPP project to attract the private investments. Comparison of factor importance degrees between public and private sectors on PPP project is proposed in this research.

Based on the results, we conclude that those two sectors has cognitive differences on some factors. The private sector care more about costs, especially PPP project which requires much capital investment in initial stage. A large number of funds invested in the short term and cannot be reflowed, it imposes great pressures on private sector. In contrast, the public sector pays more attention to the comprehensive construction of XITLP and the impact on the regional economy, responding the country's various policies, which forced them eagerly to hope that corporations/settled enterprises can pay more attention

to the development of the park, influencing regional economy.

The respondents in private sector of the research are from logistics companies in Xi'an, and are mainly engaged in the domestic market, which seemed to affect the results of international market matters. First, because if they face the international market, they must reform their operational system and transport system. They need to introduce specialized talents and need to find new customers, the most important and hardest thing is the need for more government "Guanxi" in this area which greatly increased the costs of private owners. Second, facing with an unknown international market, there will be a lot of unknown risks from the domestic and international markets. Such risks make their situation even more difficult in the absence of professional guidance. However, hiring more experts will increase costs, and they are not sure whether these experts are able to deliver proposals that can be effectively implemented, if implemented blindly, the risk is unaffordable.

For the above reasons, in order to improve such a situation, the following options are proposed.

1. In addition to loans, land and other resources on the support, the public sector should strengthen private enterprises' understanding of the internationalized port construction and carry out theoretical guidance. The public sector can regularly organize the logistics seminars and conferences, invite experts from all countries to give lectures on internationalization and informatization and explain the importance and prospects with the success cases in other countries and region.

2. Introduce an incentive system. For companies which are willing to continuously optimize their operation system, the government should introduce a more favorable bonus mode, which would decrease the cost as well as risk while they seeking for optimization of their operation system. It can be tax incentives or prior opportunities when cooperating with government on public projects.

3. Private sector should take the initiative to respond to government policies, and should realize the significance of transformation and adaptability fundamentally. Also, importing special talents and paying attention to the combination of self-development and zone development can be very important.

4. Working with governmental and academic organizations more frequently, strengthening the connection between government, companies and academies shares vital significance as well. With the assistance of the government, companies can seek for new areas and bear more risks. The specialization and reformation of its own policies, such as combing of organizational structure, training of professionals, introduction of talents, researching and developing of science and technology, specialization of financial system , market operation mode and resource integration.

The limitations of the research object are as follows. First, this research mainly focused on the XITLP. Although XITLP is a very typical dry port, it also has a very important strategic position in China. However, the result of this research does not necessarily apply

to dry ports in other regions or types despites the overall research framework and methodology can be applied to other dry ports. Second, limitations exist in the questionnaire contents. In particular, most of private sector are logistics companies in Xi'an, and are mainly engaged in the domestic market. If the scope is expanded, the results may be different form this research, especially in terms of the result of International Multimodal Transportation System.

In addition to expanding the research object, many other research directions can be suggested. For example, comparing with the dry ports of other countries by using this research framework. There are differences in the social systems and policies in each country, so the factors that public and private attach importance to may also differ.

References

Beresford et al. 2012. "A study of dry port development in China", *Maritime Economics & Logistics*, no.14: 73–98.

Bian, K. A. 2011. "Application of Fuzzy AHP and ELECTRE to China Dry Port Location Selection", *The Asian Journal of Shipping and Logistics*, no. 2: 331-354.

Bichiou, K. and Gray, R. 2005. "A critical review of conventional terminology for classifying seaports" *Transportation Research Part A*, no.39: 75-92

Choi, S. H. 2008. "Empirical Analysis of the Determinants for Shippers' Selection of Gwangyang Port" *Journal of Korea Port Economic Association*, vol.24, no.4: 199-217.

Li, Bing et al. 2005. "Critical success factors for PPP/PFI projects in the UK construction industry" *Construction Management and Economics*, no. 23: 459-471.

Liu, Wei. 2015. "Theoretical Explanation of PPP Mode and Its Practical Examples," *Reform*, no.1: 78-89

Norusis, M.J. 1992. *SPSS for Windows, Professional Statistics, Release 5*, SPSS Inc., Chicago.

Roso, V. et al. 2009. "The Dry Port Concept – Connecting Container Seaports with the Hinterland," *Journal of Transport Geography*, no. 17: 338-345

Roso, V. and Lumsden, K. 2010. "A review of dry ports", *Maritime Economics and Logistics*, no.12: 196–213.

Wei, Xiaoxue. 2016. *Evaluation and Countermeasure Research on the Development Level of Xi'an International Inland Port*, Maters' Thesis.

Wu, Shu. 2015. "Study on Investment and Operation Modes of Dry Ports in China" *Research and Discussion,* 1005-152X, 06-0013-03.

Xu, Han. 2012. *Research on Investment Construction and Operation Management of Multimodal Transport Port*, Maters' Thesis.

Ye, Xiao-su and Xu, Chun-mei. 2013. "Review and Research on PPP Pattern in China," *Chinese Soft Science*, no.6: 6-9.

Yoo, H. J. 2015. *A Comparative Study on Working Environments in the Logistics Industry by Employment Types - Focused on Road Freight Transportation and Warehousing Industries*, Ph.D. Dissertation.

Zhou, Zheng-Xiang et al. 2015. "The Existing Problems in the Application of PPP Mode under the New Economic Normality and Their Solution" *Chinese Soft Science*, no.9: 82-95

Study on the residual ultimate strength of stiffened plates with central dent

Lei AO and Deyu WANG
Department of Naval Architecture And Ocean Engineering
Shanghai Jiao Tong University
Address, Shanghai, 200240, China
E-mail dywang@sjtu.edu.cn

Abstract: The residual ultimate strength of stiffened plates with dent damage under compression was investigated by using the commercial software ABAQUS. The influences of some important factors such as the dent depth, dent size and dent angle, in association with the stiffened panel's ultimate limit state, were discussed in detail. By assuming that the stiffener is always perpendicular to the involved plate elements in the dent-producing process, a simple formula was proposed to represent the lateral deflection of the stiffeners and the dent. Based on the numerical results, the reduction factors of the ultimate strength of the compressive stiffened plates are established as functions of the relative dent depth and dent length. In addition, the relationship between the residual ultimate strength of the stiffened plates and the dent inclination was also presented by a series of trigonometric functions.

Keywords: stiffened plate; dent damage; ultimate strength; uniaxial compression

Introduction

The plate and stiffened plate elements serve as the basic units of hull structure. The local plate structures first have local buckling failure under the action of external loads next to the collapse failure of hull girders. When the ship hull is subjected to vertical bending moment, the deck and bottom plate structures are subjected to tensile and compressive loads. The deck or bottom plate structures primarily exhibit buckling or yielding behaviors. Thus, it is of important significance to analyze the ultimate bearing capacity of stiffened plate structure under compressive load for the safe design of ship structures.

The general service life of the ships after their construction averages more than 20 years. During the operation process, ships may experience adverse sea conditions. Some accidental events may occur in the actual operational cases (such as grounding, collision and cargo falling) that will cause large plastic deflection of ship local plate elements. In contrast to the cracking damage, the produced dents do not destroy the component continuity of the hull structures. Compared to ship corrosion, the dents also have no significant reduction effects on the plate thickness of the local damaged region of hull structures. However, the amplitude of plastic deformation related to local dents can be several times larger than that of the structural initial deflection caused by the welding fabrication.

When a stiffened plate is subjected to a compressive load, the influence of the stiffeners may lead to different buckling failure modes of the plate structures. The local plate deformation in the dent area, however, will completely change the collapse failure mode of the stiffened plate elements and sharply reduce the compressive ultimate

strength of the stiffened structures without breaking the integrality of hull structure. Moreover, large deformation is not only introduced to the plate element during the dent-producing process but also to the corresponding stiffener elements because of the deflection of local plate. Thus, it is necessary to analyze the influence of the dents on the buckling behavior of compressive stiffened plates and evaluate the ultimate strength of damaged structure considering the lateral deformation of local stiffeners. As a result, this paper considers the influence of the main dent parameters including the dent depth Dd, dent size (transverse width DW and longitudinal length DL), and dent angle θ on the ultimate strength of stiffened plates under uniaxial compression load. The lateral deflection of the stiffener webs caused by the local dent has been considered to analyze the post buckling behavior of the compressive stiffened panel. Based on the calculated numerical data, simple equations are given to assess the residual ultimate strength of the plate structures as functions of the dent depth and dent size.

Finite element model of stiffened plate

The stiffened plate considered in this paper is obtained from the central part of the deck structures of one ordinary vessel, and the models of 1/2+1+1/2 bays in the longitudinal direction are adopted in the FE analyses. As shown in Figure 1, the dotted lines represent the position of transverse beams. To simplify the calculation, the transverse members are substituted by the corresponding boundary conditions, and the dent is initially assumed to be located in the central region of the stiffened model, wherein DW is the dent transverse width, DL is the dent longitudinal length, and s1 and s2 are the distance from the dent to the corresponding stiffened plate boundary. The geometry dimensions applied in the stiffened plate model are as follows:

Table 1 Geometry of stiffened plates

Geometry character	Value(mm)
Longitudinal span,	a = 3000
Stiffener spacing,	b = 500
Plate thickness,	t = 10, 14, 18, 22
Tee stiffener 1 (T1)	hw×tw+hf×tf = 150×10+50×15
Tee stiffener 2 (T2)	hw×tw+hf×tf = 198.6×10+61.2×21.7
Tee stiffener 3 (T3)	hw×tw+hf×tf = 250×10+80×25

The main geometrical dimensions of plate panels are a (longitudinal span), b (stiffener spacing) and t (plate thickness). To vary the column slenderness ratio, three different stiffener sizes are considered. As shown in Table 1, hw and tw are the web height and thickness for Tee stiffeners. hf and tf are the flange width and thickness. The material is assumed to behave in an elastic-perfectly plastic manner with a certain yield stress by many authors in the FEM analysis that has been proven reasonable. Thus, no material hardening effect is considered in this paper. The high tensile strength steel has been widely applied in the ship construction process especially in warship structures. Thus, the materials of the plates and stiffeners are taken as the same with yield stress of σy=590MPa. The Young's modulus is taken as E=206000 N/mm2, and Poisson's ratio is taken as λ=0.3.

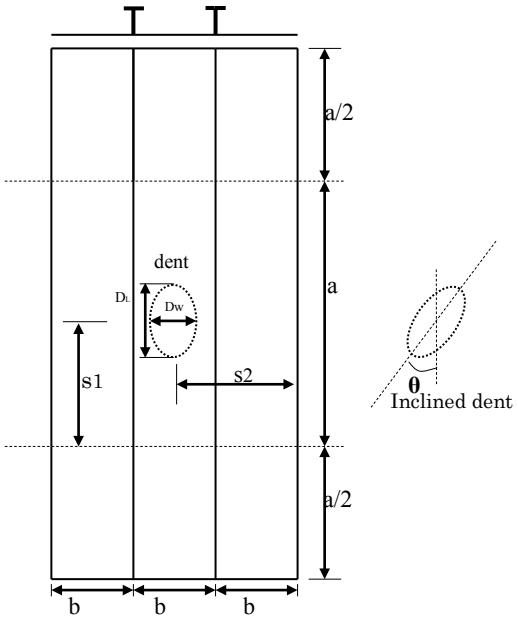

Figure 1. The geometrical schematic diagram of the stiffened plate

The initial deflection of stiffened plates will be introduced by the fillet welding in the real ship structures. This imperfection has significant influence on the ultimate strength behavior of stiffened panels including the ultimate strength values. Other initial imperfection such as the welding residual stress may also have some effects on the collapse behavior of plate structures, however, it is not considered in present study. The shape of initial deflections are considered corresponding to the buckling modes of stiffened plates including the plate initial deflection, column-type initial distortions of stiffeners with attached plating and sideways initial distortions of independent stiffeners as following:

The plate initial deflection, w_{op}

$$w_{op} = \delta_o \sin(\frac{m\pi z}{a})\sin(\frac{\pi x}{b}) \tag{1}$$

m is the buckling half-wave number in the longitudinal direction which is taken as a minimum integer corresponding to a/b, which must satisfy the following equation for plates under only longitudinal thrust :

$$a / b \le \sqrt{m(m+1)} \tag{2}$$

Column-type initial deflection of stiffeners, w_{os}

$$w_{os} = 0.0015a \sin(\frac{\pi z}{a})\sin(\frac{\pi x}{B}) \tag{3}$$

where B is the transverse span between longitudinal girders, it was taken as B=7500mm in this paper.

Sideways initial deflection of independent stiffeners, v_{os}

$$v_{os} = \frac{0.0015a}{h_w} y \sin(\frac{\pi z}{a}) \tag{4}$$

where hw is the stiffener's web height.

The maximum amplitude of local plate deflection δo is taken as a function of the slenderness ratio β in an average level[25]:

$$\delta_o = 0.1\beta_o^2 t \tag{5}$$

β is the plate slenderness ratio, expressed as follows:

$$\beta = \frac{b}{t_p}\sqrt{\frac{\sigma_y}{E}} \tag{6}$$

The nonlinear finite element analysis is conducted by employing the commercial software ABAQUS 6.13 and the nonlinear shell finite element S4R is used for modeling thin plates as a general four nodes shell element including both reduced integral method and hourglass control mode which is suitable for large deformation analysis. The Newton-Raphson algorithm is applied as a method of incremental solution to trace the proper collapse and post-buckling process in structural nonlinear analysis. The finite element model is shown in Figure 2. With respect to the boundary conditions of stiffened plate under compression in the ISSC report(2012) [26], this paper adopts the boundary conditions presented in Table 2:

Table 2. The boundary conditions for the 1/2+1+1/2 span model

Boundary	Constraint
A-B, A1-B1	URx=URy=0, Uz=uniform
A-A1, B-B1	Simple supported
C-D, C1-D1	Uy=0

The element size of 15, 30, 50mm was selected as comparison to determine the avaliable mesh size to provide accurate results. The difference ratio of ultimate stress is within 1% for these three sizes (364.2MPa for 15mm, 365.4MPa for 30mm, 368.0MPa for 50mm). As a result, 17 mesh elements between stiffeners and 108 elements between transverse members was taken for the plate, 7 mesh elements for the stiffener webs and 6 elements for the stiffener flanges in the cross section. Thus, the general fine grid size was adopted as 28 mm for providing valid numerical results. The ultimate strength of intact stiffened plate obtained by the FE method was compared with that by the

empirical methods [27-28] as shown in Table 3. The stiffener type, T2, was applied. It can be seen that most of the error rates are within 5%. As a result, the value of the ultimate strength obtained by the FE approach in this paper is valid.

Table 3 Comparison between the FEM results and empirical results for intact stiffened plates

Plate thickness	FEM	Zhang's method[27]	Ao's Method[28]	Error rate	
				Zhang's	Ao's
t=10mm	391.11MPa	400.72 MPa	408.92 MPa	2.44%	4.54%
t=14mm	419.80 MPa	430.61 MPa	443.03 MPa	2.51%	5.46%
t=18mm	461.14 MPa	450.81 MPa	466.10 MPa	2.29%	1.02%
t=22mm	478.04 MPa	464.83 MPa	481.69 MPa	2.73%	0.79%

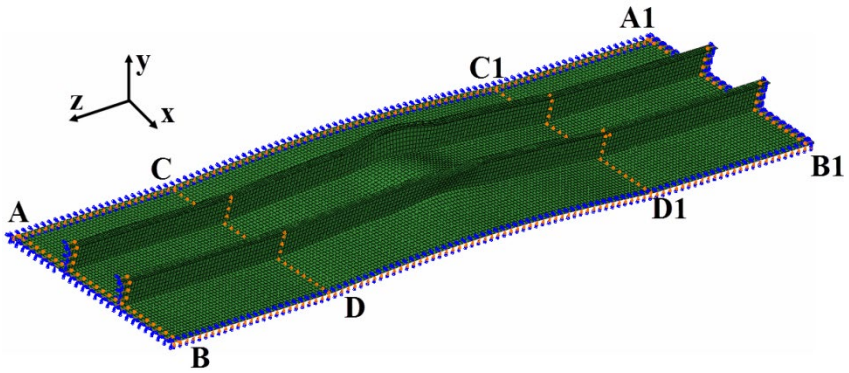

Figure 2. Finite element model for the stiffened plate

Dent shape

In numerical analysis, the dent damage can be introduced to the intact plates in two forms. Most of the previous research investigated the influence of a dent by changing the positions of the element nodes with simple equations of dent shape. Alternatively, the dent was simulated by the indenter crushing through the quasi-static method.

According to the previous summary of the dent shape (Paik et al. [5-6], Prabu et al. [7], Raviprakash et al. [29]), this paper considers three types of dent shapes for comparison, as the conical dent, the exponential dent and the sine dent. The cross sections of these three types of dent shapes are shown in Figure 3. It can be seen from Figure 3 that when the dent depth D_d, longitudinal length D_L and transverse width D_W are the same, the conical dent and sine dent have the same sectional area; in contrast, the section area of the exponential dent is relatively smaller.

Conical dent:

$$w = D_d\left(1-\frac{|z|}{D_L}\right)\left(1-\frac{|x|}{D_W}\right), \begin{cases} -0.5D_W \le x \le 0.5D_W \\ -0.5D_L \le z \le 0.5D_L \end{cases} \tag{7}$$

Exponential dent:

$$w = D_d e^{-(\frac{3z}{D_L})^2} e^{-(\frac{3x}{D_W})^2}, \begin{cases} -0.5D_W \le x \le 0.5D_W \\ -0.5D_L \le z \le 0.5D_L \end{cases} \tag{8}$$

Sine dent:

$$w = D_d \sin^2\left(\frac{\pi z}{D_L}\right)\sin^2\left(\frac{\pi x}{D_W}\right), \begin{cases} -0.5D_W \le x \le 0.5D_W \\ -0.5D_L \le z \le 0.5D_L \end{cases} \tag{9}$$

In the above equations, D_d is the dent depth, D_L is the longitudinal length and D_W is the transverse width of dent.

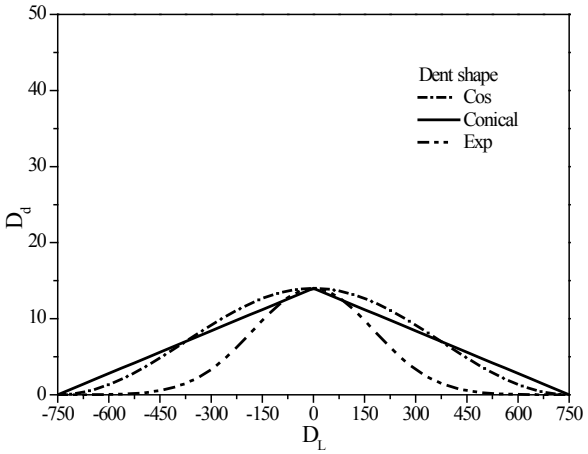

Figure 3. The geometrical schematic diagram of the dents

Figure 4 shows the comparison of the influence of different dents on the ultimate strength of the stiffened plate with respect to different dent depths. The obtained results indicate that the sine dent has the most significant reduction on the ultimate strength of stiffened plate. This observation is reasonable because the deflection volume of the exponential dent is smaller than that of the other two types of dents with the same shape parameters. As a result, we adopted the sine dent for the subsequent dent parameter studies with conservative evaluation of the ultimate strength.

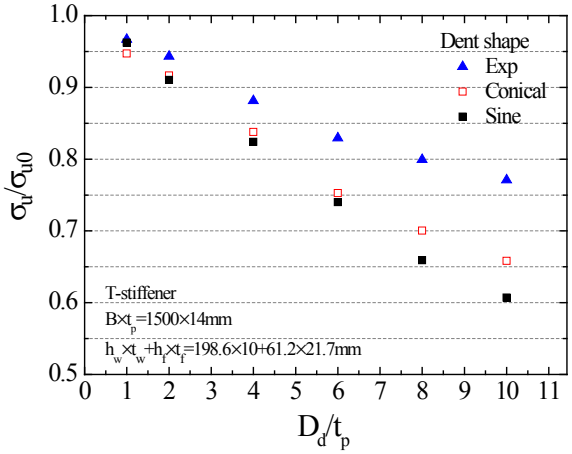

Figure 4. The influence of different dent shapes on the ultimate strength of the stiffened

plate

Xu and Guedes Soares [15] suggested that the residual plastic deformation of the plates may be separated in two parts, namely, local dent deflection and global dent deflection, expressed by a Fourier series function. In this paper, we followed their studies and assumed the amplitude of the global deflection of the dent was equal to that of the local deflection. In this case, the form of the dent can be expressed as follows:

The local dent deflection :

$$w_{dl} = \frac{D_d}{2}\sin^2(\frac{\pi x}{D_W})\sin^2(\frac{\pi z}{D_L}), \begin{cases} -0.5D_W \le x \le 0.5D_W \\ -0.5D_L \le z \le 0.5D_L \end{cases} \quad (10)$$

The global dent deflection:

$$w_{dg} = \frac{D_d}{2}\sin(\frac{\pi z}{a})\sin(\frac{\pi x}{B_0}) \quad (11)$$

The whole dent is obtained by:

$$w_d = w_{dl} + w_{dg} \quad (12)$$

Figure 5 shows the von Mises stress distribution of the compressive stiffened plate at the ultimate state. It is observed that the stress distribution pattern of compressed stiffened plate with dent damage is quite different from that of the stiffened plate without the dent. Because of the presence of the dent, the collapse failure zone of stiffened plate in the ultimate state is concentrated at the dent position instead of being distributed over the whole panel. In the buckling process of the compressive stiffened plate, the maximum stress of the plate structures first appears at the joint of the dent and the stiffened web and then expands to the local panel connected with the dent as the external load gradually grows.

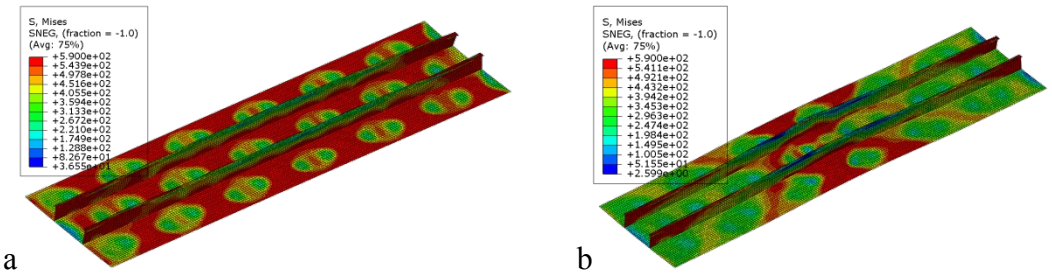

a b

Figure 5. von Mises stress distribution of the stiffened plate under compression in the ultimate state: a. without dent, b. with dent damage

Results of the finite element analysis

In contrast to cracking, the area of the net section of stiffened plate was not changed due to dent damage in case that the ship plate was not ruptured. Thus, the residual ultimate strength of damaged stiffened plate cannot be easily obtained by using the net section theory. Moreover, the presence of the dent will not cause the reduction of the

plate thickness in the locally damaged region compared to the corrosion effect. In fact, the production process of the dent is not only coupled with large deformation of local structures but also has residual stress existing in the striking area. Xu and Guedes Soares [16] employed the quasi-static method to simulate the indenter punching process and found that the introduced residual stress caused by dents has little influence on the ultimate strength of stiffened plate, with mean error of approximately 2%. Furthermore, the residual stress caused by dents may be both the tensile stress as well as compressive stress. In case of the former, the bearing capacity of the stiffened plate to resist the compressive load is increased. Otherwise, the compressive strength of the stiffened panel is decreased. Therefore, this paper does not consider the influence of residual stress in the producing process of the dents. The dents were created by changing the coordinate value of the corresponding nodes using different forms of dent shape function.

The dominant parameters of dent damage include the vertical projection size of the dent and the dent depth. Cho and Lee [2] analyzed the damage extent of a stiffened plate by using the lateral impact experimental method. Their test results found that for the stiffened plate, the maximum amplitude of the local plastic deformation caused by collision can be up to 22.77 times the plate thickness t_p. To facilitate the analysis, firstly, the longitudinal length D_L and transverse width D_W of the dent are assumed to be the same, taken as $D_L = D_W =$ 500, 1000 and 1500 mm. The dent depth D_d is taken as $D_d =$ 28, 56, 84, 112, 140. When different plate thicknesses are applied, the failure modes of the stiffened panel under compressive load will change. The thickness of the stiffened plate is chosen in the range of $t_p =$ 10, 14, 18 and 22 mm. Three stiffener sizes are considered, namely as T1, T2, T3 in Table 1. The lateral plastic deformation of the local stiffeners was considered and the amplitude of the lateral deformation was determined by $w_s / h_s = h_w / D_p$.

Figure 10 - Figure 12 shows the influence of dent size and depth on the residual ultimate strength of stiffened plate with respect to different plate thicknesses. It is observed from the results that both the dent size and dent depth have great influences on the ultimate strength of the stiffened plate. With the increase in dent length and depth, the residual ultimate strength of the stiffened plate is significantly reduced to 63.0% of the ultimate strength of the intact plates. The dent size and the dent depth should be considered together for the assessment of the ultimate strength of dented stiffened structures. If either of the factors is too small, the influence of the dent on the ultimate strength of the stiffened plate can be ignored. In this section, both local and global deflection of the dents expressed in Eq. (10)-(12) are considered.Thus, the size of the local dent deflection have less effect than the dent depth on the residual ultimate strength of the stiffened plate.

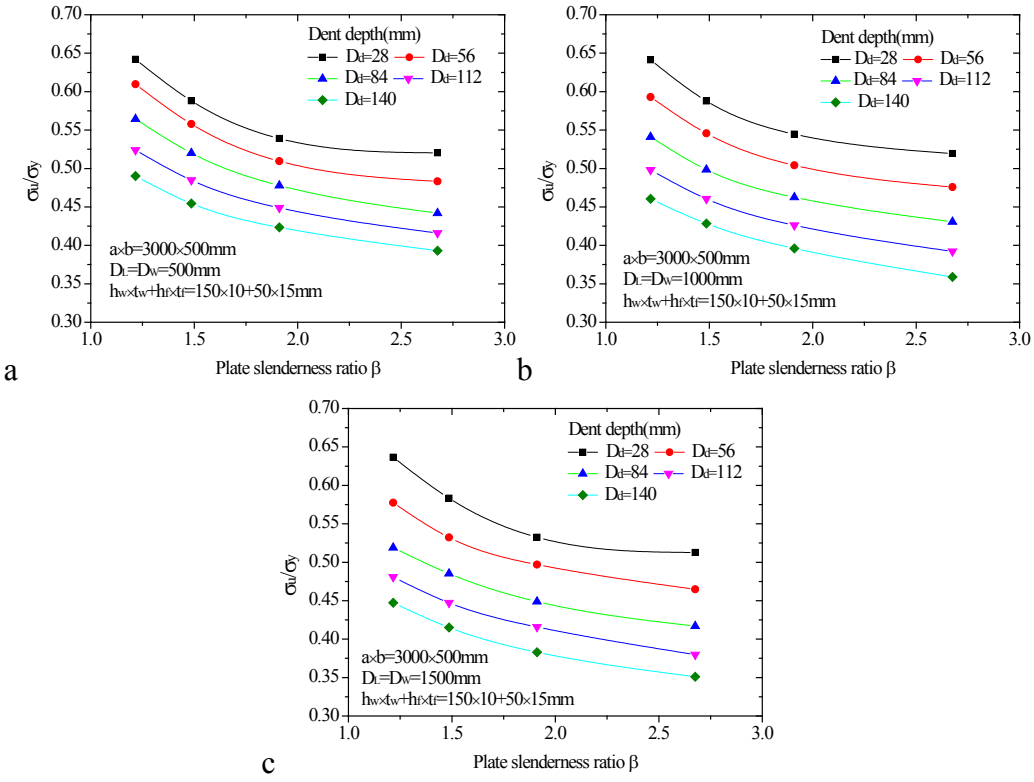

Figure 6. The influence of dent size and depth on the ultimate strength for T1 the stiffened plate: a. $D_L = D_W = 500mm$, b. $D_L = D_W = 1000mm$, c. $D_L = D_W = 1500mm$.

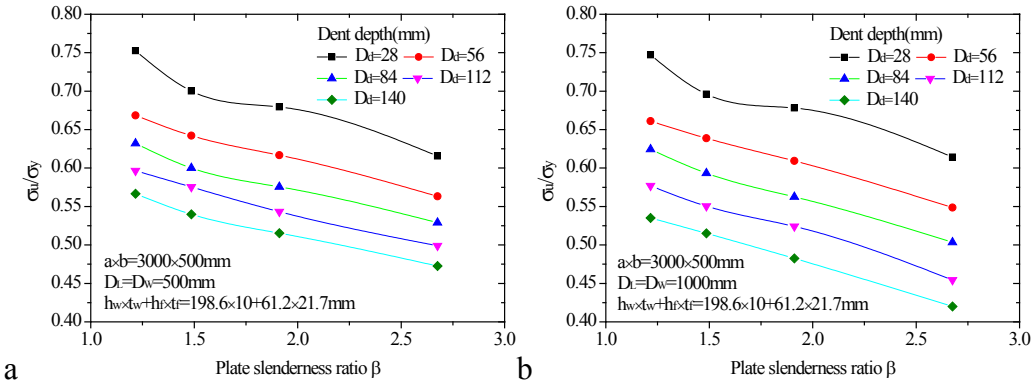

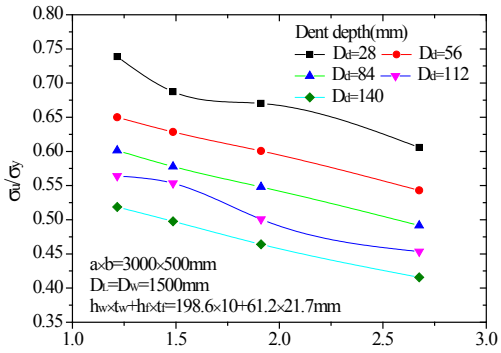

c

Figure 7 The influence of dent size and depth on the ultimate strength for T2 the stiffened plate: a. $D_L = D_W = 500mm$, b. $D_L = D_W = 1000mm$, c. $D_L = D_W = 1500mm$.

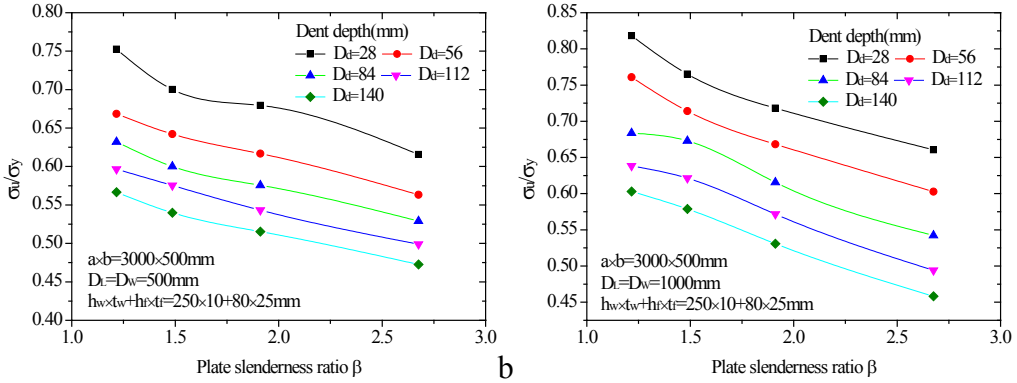

a b

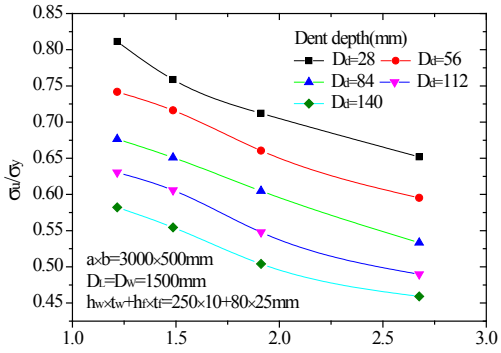

c

Figure 8 The influence of dent size and depth on the ultimate strength for T3 the stiffened plate: a. $D_L = D_W = 500mm$, b. $D_L = D_W = 1000mm$, c. $D_L = D_W = 1500mm$.

It can be observed that the dent effects on stiffened plate is not directly related to the plate thickness but decided by the relative depth Dd/tp. Therefore, the paper proposed a reduction factor to evaluate the residual ultimate strength for stiffened plates as a function of relative depth:

$$\frac{\sigma_u}{\sigma_y} = a \cdot e^{(-b \cdot D_d / t_p)} \tag{13}$$

$$a = 0.065 \cdot \beta^2 - 0.34 \cdot \beta + c \tag{14}$$

$$c = -0.593 \cdot (\frac{I_s}{A_s})^2 + 2.005 \cdot (\frac{I_s}{A_s}) - 0.4969 \tag{15}$$

$$b = 0.006697 \cdot \beta^2 - 0.02361 \cdot \beta + 0.0586 \tag{16}$$

where σu is the ultimate strength of the stiffened plate with dent damage, I_s and A_s are the geometrical moment of inertia and sectional area of one stiffener.

Compared to the FE results shown in Figure 11, the proposed formula is verified to be valid with most of the error band in 5%. The residual ultimate strength of dented stiffened plate can be calculated by using Eq. (15). It should be noticed that both the local-globle dent deflection and lateral deformation of the stiffeners corresponding to the dents need to be counted when the predicted formula is applied.

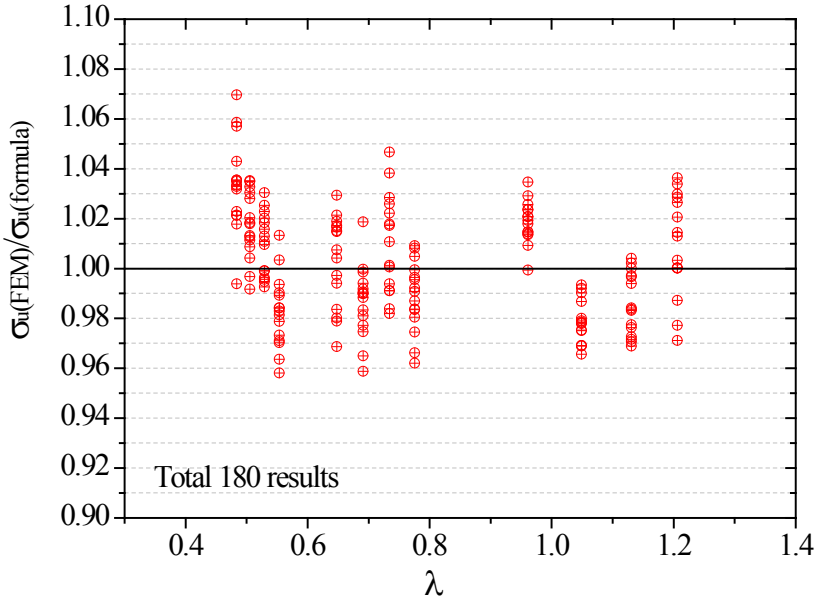

Figure 9. Comparison of the results between the predicted formula and the finite element analysis.

Conclusion

Casual accidents, such as grounding, collision, and object falling, that occur during the ship operation period would introduce dent damage to the local plate elements of the hull structures. Compared to the welding-induced deflection during the ship construction process, the amplitude of the dent plastic deflection will be significantly much larger. This paper employed the nonlinear finite element method to analyze the influence of dent damage on the ultimate strength of a stiffened plate. The dominating dent parameters considered include dent depth, dent size, dent angle, and plate thickness.

Considering that the plate large deformation induced by dents is always coupled with lateral deflection of related stiffeners, this paper proposed a simple equation to simulate the local damage of stiffeners caused by dents and analyzed the influence of lateral deflection of the stiffeners on residual ultimate strength of stiffened plate. Based on the finite element results, the following conclusions can be drawn:

(1) The comparative analysis regarding the dent shape of exponential, conical and sine shape illustrated that the influence of dent shape on the ultimate strength of a stiffened plate is determined mainly by the volume of dent plastic deformation. With larger deformation volume, the dent will have more significant reducing effect on the ultimate strength of stiffened plates.

(2) Assuming that the stiffener is still vertical to the local plate in the process of large plastic deformation, this paper proposed a simple formula to represent the local lateral deflection of stiffeners as well as the dent. The residual ultimate strength of stiffened plate was found to have the largest reduction of 18.5% via the influence of the lateral deflection of the stiffener with respect to various plate thicknesses.

(3) The dent depth and dent size are two main parameters that have crucial influences on the ultimate strength of stiffened plates. If either of the two considered factors is too small, then the dent damage will have little effect on the residual ultimate strength of the stiffened plate. This paper proposed the reduction factor of the ultimate strength for stiffened plates with dent damage as functions of the relative dent depth Dd/tp. Both the local-globle dent deflection and lateral deformation of the stiffeners corresponding to the dents have been counted in.The comparison of the proposed reduction factor with the finite element results revealed an error band of less than 5%.

Acknowledgements: The present work is co-supported by the Chinese Government Key Research Project KSHIP-II Project (Knowledge-based Ship Design Hyper-Integrated Platform No 201335) and High-tech Ship Research Projects Sponsored by MIIT(No. [2016]25). The authors would like to acknowledge the Project support.

References

1. Paik, J.K.; Seo, J.K. A method for progressive structural crashworthiness analysis under collisions and grounding[J]. Thin-Walled Structures, 2007; 45(1):15-23.
2. Cho, S.R.; Lee, H.S. Experimental and analytical investigations on the response of stiffened plates subjected to lateral collisions[J]. Marine Structures, 2009; 22(1):84-95.
3. Harding, J.E.; Onoufriou, A. Behaviour of ring-stiffened cylindrical members damaged by local denting[J]. Journal of Constructional Steel Research, 1995; 33(3):237-257.
4. Paik, J.K.; Lee, J.M.; Lee, D.H. Ultimate strength of dented steel plates under axial compressive loads. Int J Mech Sci 2003; 45: 433-448.
5. Paik, J.K. Ultimate strength of dented steel plates under edge shear loads[J]. Thin-Walled Structures, 2005; 43(9):1475-1492.
6. Prabu, B.; Bujjibabu, N.; Saravanan, S.; et al. Effect of a Dent of Different Sizes and Angles of Inclination on Buckling Strength of a Short Stainless Steel Cylindrical Shell Subjected to Uniform Axial Compression[J]. Advances in Structural Engineering, 2007; 10(5):581-591.
7. Luís, R.M.; Guedes Soares, C.; Nikolov, P.I. Collapse strength of longitudinal plate assemblies with dimple imperfections. Ships Offshore Struct 2008; 3:359-370.
8. Witkowska, M.; Guedes Soares, C. Ultimate strength of locally damaged panels. Thin Walled Struct, 2015; 97:225-240.

9. Raviprakash, A.V.; Prabu, B.; Alagumurthi, N. Ultimate strength of a square plate with a longitudinal/transverse dent under axial compression[J]. Journal of Mechanical Science & Technology, 2011; 25(9):2377-2384.
10. Raviprakash, A.V.; Prabu, B.; Alagumurthi, N. Effect of size and orientation of a centrally located dent on the ultimate strength of a thin square steel plate under axial compression[J]. International Journal of Steel Structures, 2012; 12(1):47-58.
11. Lang, N.C.; Kwon, Y.W. Investigation of the Effect of Metallic Fuselage Dents on Compressive Failure Loads[J]. Journal of Aircraft, 2012; 44(6):2026-2033.
12. Xu, M.C.; Guedes Soares, C. Assessment of residual ultimate strength for wide dented stiffened panels subjected to compressive loads[J]. Engineering Structures, 2013; 49(2):316-328.
13. Xu, M.C.; Guedes Soares, C. Effect of a central dent on the ultimate strength of narrow stiffened panels under axial compression[J]. International Journal of Mechanical Sciences, 2015; 100:68-79.
14. Ghazijahani, T.G.; Jiao, H.; Holloway, D. Experiments on dented cylindrical shells under peripheral pressure[J]. Thin-Walled Structures, 2014; 84:50-58.
15. Saad-Eldeen, S.; Garbatov, Y.; Guedes Soares, C. Strength assessment of steel plates subjected to compressive load and dent deformation[J]. Structure & Infrastructure Engineering, 2016; 12(8):995-1011.
16. Peroumal, D.; Sidhuvilaji, E.; Prabu, B.; et al. Numerical Study about Combined Effect of Distributed Initial Imperfections and Dent on Ultimate Strength of Square Plates under Uni-Axial Compression[J]. Applied Mechanics & Materials, 2015; 813-814(1):1037-1041.
17. Li, Z.; Zhang, D.; Peng, C.; et al. The effect of local dents on the residual ultimate strength of 2024-T3 aluminum alloy plate used in aircraft under axial tension tests[J]. Engineering Failure Analysis, 2015; 48:21-29.
18. Cerik, B.C. Ultimate strength of locally damaged steel stiffened cylinders under axial compression[J]. Thin-Walled Structures, 2015; 95:138-151.
19. Saad-Eldeen, S.; Garbatov, Y.; Guedes Soares, C. Ultimate strength analysis of highly damaged plates[J]. Marine Structures, 2016; 45:63-85.
20. ISSC. Ultimate Strength (Committee III.1)[C]. In: Proceedings of the 18th International Ship and Offshore Structures Congress, Rostock, Germany. 9-13 September, 2012.
21. Zhang SM (2016). "A review and study on ultimate strength of steel plates and stiffened panels in axial compression," Ships Offshore Struc, 11(1), 81-91.
22. Ao L, Wu JM, Wang DY. A modified formula for predicting the ultimate strength of stiffened panels under longitudinal compression [J]. International Journal of Offshore & Polar Engineering, 2018 (accept).
23. Raviprakash, A.V.; Prabu, B.; Alagumurthi, N. Residual ultimate compressive strength of dented square plates[J]. Thin-Walled Structures, 2012; 58(3):32-39.
24. Liu, K.; Wang, Z.; Tang, W.; et al. Experimental and numerical analysis of laterally impacted stiffened plates considering the effect of strain rate[J]. Ocean Engineering, 2015; 99:44-54.
25. Liu, B.; Villavicencio, R.; Guedes Soares, C. Simplified method for quasi-static collision assessment of a damaged tanker side panel[J]. Marine Structures, 2015; 40:267-288.
26. Witkowska, M.; Guedes Soares, C. Ultimate strength of stiffened plates with local damage on the stiffener[M]// Analysis and Design of Marine Structures. 2009;145-154.

STUDIES ON IMPROVING BEYPORE PORT,INDIA

R. Sundaravadivelu 1 S.Sakthivel 2, P.K.Suresh 3 Nikhil Kumar Singh, 4
1,2,4 Dept of Ocean Engineering, IIT Madras, India-600036
3 Meenakshi Sundararajan Engineering college, Kodambakkam, Chennai, India-600024
E Mail : rsun@iitm.ac.in,sureshpk2000@gmail.com

Abstract: The coast of India is bordered on the east by bay of Bengal and along the west by Arabian sea. Beypore ($11^0$9'48.96"N and $75^0$48'27.74" E) in Kerala state is one such river side port located along the west coast of India facing Arabian Sea. Beypore port is one of the oldest ports in Kerala sine first century with historical values and is located along estuary. It consists of a pair of breakwater and berths. The existing berth which is directly exposed to waves travelling in between breakwaters in monsoon has been observed to be severely affected due to direct wave attack. Now it is proposed to build another berth and increased the depth. The coast is more influenced by South West monsoon during June to September. Mike 21 software was utilized for wave propagation studies. The studies indicate that the wave disturbance within the harbour has decreased with the introduction of proposed berth and percentage of operability has increased. The details of field data, numerical studies in arriving an optimum layout of the new berth are discussed in the paper.

Keywords: port,wave,wharf,breakwater

Introduction

Beypore port is a small port in Kerala state along the south west coast of Indian peninsula. It is an estuarine port, where Beypore (11.1736° N, 75.8040° E) river discharges into the Arabian Sea.. Beypore port is the second biggest port in Kerala and currently handles about 100,000T of cargo and 7500 passengers per annum (Fig 1). Now the port has a depth of about 5 meters alongside wharf and approach channel and it is proposed to be developed in stages. It has a depth of (-)7m adjacent to wharves and (-)4m along approach channel. Now it is proposed to expand the port to accommodate bigger vessels up to 12000 DWT. The berth which is directly facing thewaves in south west monsson has been observed to be severely affected due to direct wave attack. Hence, Beypore port authority proposes to construct a new berth which can also act as a protective structure to improve the tranquility condition at old berth (Fig 2).

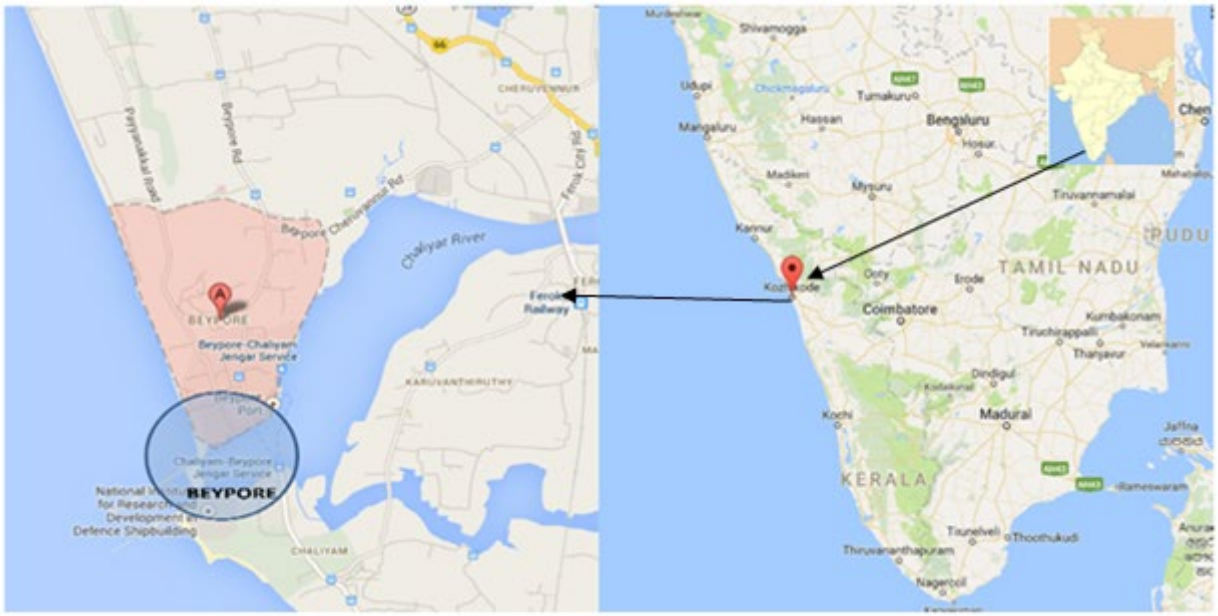

Fig1 Index map

Proposals for improvement

- Study of existing tranquility
- Based on study optimize layout of a new berth
- By dredging approach channel and turning circle up to (-) 10.20m so that 12000DWT vessels can approach.
- Apart from this some infrastructural facilities were also planned.

Fig2 Proposal formulated

Bathymetry

The study area considered here is 4.4 km along shoreline and 5.0 km normal to the

shoreline. The creation of suitable bathymetry is essential for obtaining reliable results from the model. Setting up the bathymetry requires more than just specifying an array of accurate water depths covering the area of interest. It also includes the appropriate selection of the area to be modelled and the grid spacing.

The hydrographical survey was carried out using Global Positioning System to fix the horizontal coordinates and a sounding rope to measure the water depth. Soundings were noted at intervals of 20 X 20 m. The appropriate tidal correction was incorporated to the water depth, which were obtained from the tidal values. Bathymetry chart obtained from the hydro graphic study is as depicted in Fig 3.The bathymetry covers up to the water depth of 5.5 m from shore line. The bathymetry is specified as a dfs2 file when running a normal simulation, or a dfs1 file when only running a profile simulation.

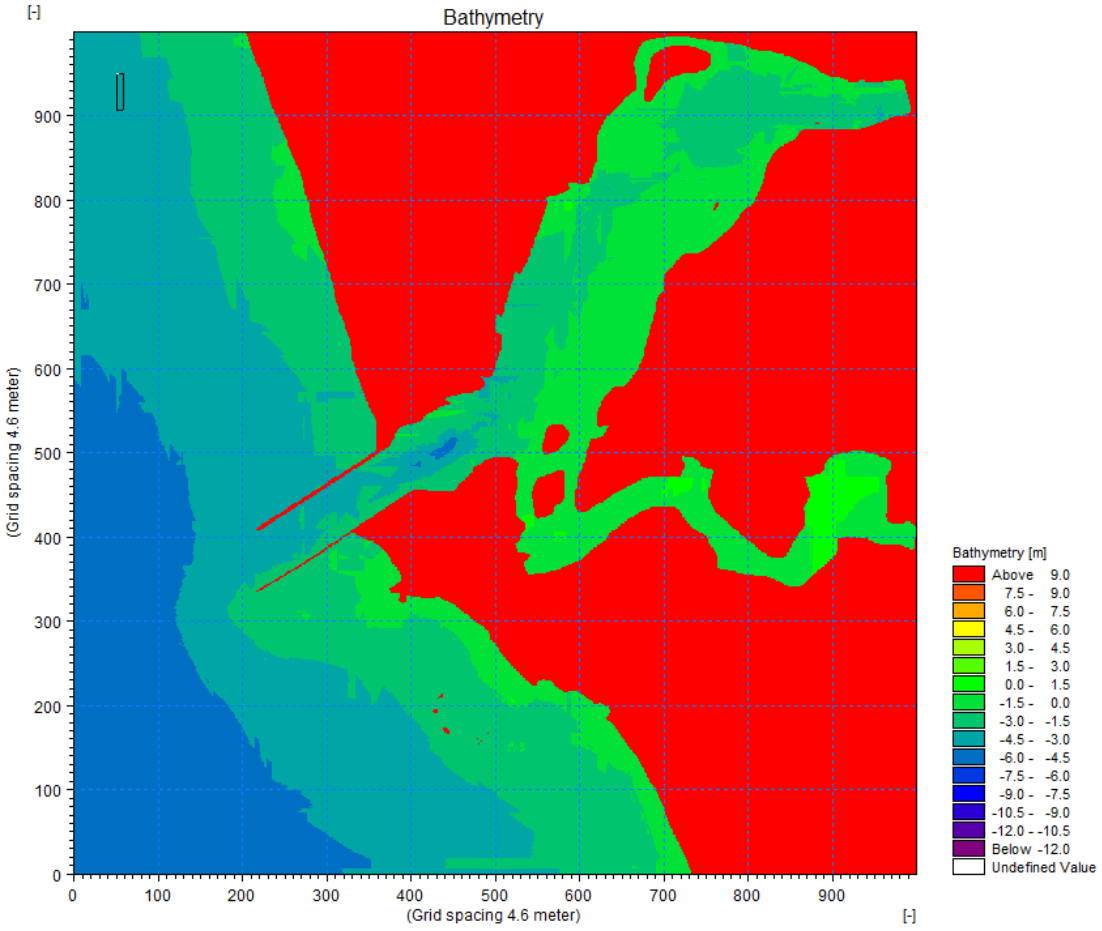

Fig3 Bathymetric details

Wave climate

The wave climate pertaining to the coast was adopted from the wave atlas (1990) and furnished vide Table 1.

Table1 Wave climate

Month	Wave direction w r t North	Wave height (m)	Wave period (sec), T
January	330	1.0	6.5
February	330	1.0	6.5
March	330	1.0	6.5
April	315	1.0	6.5
May	275	1.0	7.5
June	260	1.0	7.5
July	270	1.0	7.5
August	270	1.0	7.5
September	290	1.0	6.5
October	285	1.0	6.5
November	350	1.0	6.5
December	350	1.0	6.5

Tidal data

The tidal range is in order of 1.35 m. The various tide levels with respect to chart datum are as under:

Lower Low Water springs - + 0.18 m
Mean Low Water - + 0.37 m
Mean Higher Low Water - + 0.77 m
Mean Sea Level (MSL) - + 0.88 m
Mean Lower high Water - + 1.11 m
Mean Higher High Water - + 1.31 m
Higher high water spring - + 1.51 m

MODEL SETUP

The present numerical model was developed based on the mild slope equation derived by Berkhoff (1972.

- $\nabla^2(CCg\phi)+\omega(Cg/C)\phi=0$ Where
- ∇-Operator
- C-Phase speed
- Cg-Group velocity

$\phi(x,y)$-Mean free surface velocity potentia

For the conduct of the numerical study four cases were considered suitably varying the alignment of the structure and bathymetry to get results for various conditions .The following four conditions are adopted. The model run was performed with wave conditions furnished vide Table 1.

t.

The conditions for model trial are

1. **Case 1** – As per the existing site condition
2. **Case 2** - With the proposed berth on the original bathymetry.
3. **Case 3** - With the proposed berth and dredging for all the berths with dredge level of – 10m
4. **Case 4** - With the proposed berth and dredging in turning circle and front of the proposed berth up to -10 m and in front of the existing berth up to(–) 5 m.

The wave height at the following locations are selected for analyzing the wave penetrations and tranquility conditions (Fig 4)

1. **Point 1 and 2** – At two points along the existing berth.
2. **Point 3** - At the Proposed Berth.
3. **Point 4 and 5 –** In front of the proposed Diaphragm wall

Fig 4 Locations of wave data analysed

The basic output data from the model are integral wave parameters such as root mean square wave height, the peak wave period and the mean wave direction. The analyses of wave climate indicate that dominating directions are from 270^0 N and the required tranquility is not obtained without the new berth. Based on the analyses the operations

of the port are worked out based on the tranquility criteria and shown vide Table 2

Typical results for wave height of 1m with period of 7s from 270^0 is shown vide fig 5

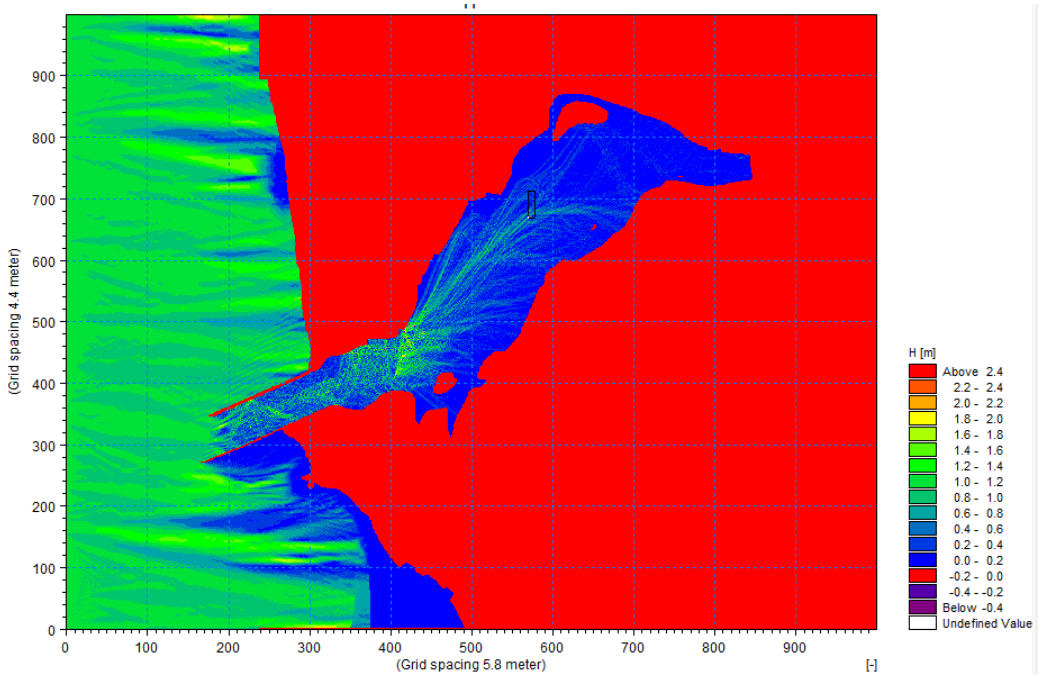

Fig 5 Typical results for waves from 270^0N

The criteria for tranquility are based on very little movement of boats to reduce the likelihood of the damage due to collisions of the boats moored close to another. For the fishing harbours the maximum significant wave height is recommended to be less than 0.3 m. Based on this criteria the Mike21 PMS module was run and results at five points are extracted With the construction of new berth with a protective arm on the west of the old wharf, the operability of existing wharf can be improved to 100%.Typical results of the study are furnished vide Table 2 to 6

Table 2 Operation conditions of the port (Point1)

Month	Case I	Case II	Case III	Case IV
January	77.60	77.62	41.49	82.67
February	65.51	65.51	41.49	82.67
March	72.74	79.51	27.59	94.21
April	56.55	86.55	75.00	74.87
May	83.58	77.58	96.30	87.63

June	43.34	93.34	83.33	91.67
July	28.80	68.80	71.20	74.32
August	100	100	82.89	100
September	100	100	94.07	98.65
October	60.89	80.89	75.93	100
November	42.51	77.51	40.00	82.57
December	35.70	65.70	33.81	71.54

Table 3 Operation conditions of the port (Point2)

Month	**Case I**	**Case II**	**Case III**	**Case IV**
January	59	61	37	87
February	59	61	37	87
March	34	54	40	95
April	46.07	66.07	85.00	89.61
May	81.85	91.31	56.69	100
June	36.71	96.59	51.34	58.96
July	51.97	78.21	93.60	55.74
August	68.75	88.65	81.08	67.97
September	71.52	91.52	100	100
October	100	80.79	100	87.65
November	100	100	40.00	94.67
December	55.74	100	33.81	89.54

Table 4 Operation conditions of the port (Point3)

Month	**Case II**	**Case III**	**Case IV**
January	42.51	47.63	49.36
February	42.51	47.63	53.51
March	54.37	51.72	61.58
April	32.57	49.56	47.51
May	66.82	63.78	51.96

June	79.62	71.62	82.97
July	51.79	45.65	54.61
August	62.31	41.27	49.82
September	88.46	91.65	100
October	76.71	97.48	91.63
November	48.75	29.68	41.78
December	62.57	26.67	31.63

Table 5 Operation conditions of the port (Point4)

Month	Case II	Case III	Case IV
January	56.53	31.63	42.58
February	56.53	31.63	42.58
March	65.51	54.97	67.45
April	91.61	78.47	81.79
May	71.65	69.58	82.57
June	45.57	35.97	63.37
July	95.78	52.73	75.86
August	100	61.59	82.51
September	86.79	91.96	100
October	100	100	95.56
November	22.87	34.48	41.75
December	31.79	39.63	47.63

Table 6 Operation conditions of the port (Point5)

Month	Case II	Case III	Case IV
January	41.57	47.63	51.91
February	41.57	47.63	51.91
March	33.78	51.72	57.76
April	26.81	49.56	65.31
May	63.57	63.78	73.36

June	71.46	51.62	69.67
July	53.67	45.65	72.45
August	57.51	41.27	79.56
September	87.89	91.65	89.54
October	92.63	97.48	81.76
November	22.91	29.68	41.67
December	23.59	26.67	37.37

Result and Discussions

The model was initially run with existing conditions of the port and also with the new berth and increased dredge level. It was observed that tranquility of the berth is severely affected when the mean wave direction is 270^0degrees. The acceptable limit of wave disturbance is 30 cm based on the laid down limits of harbor tranquility for medium sized vessels. The number of operable days for point 1 in the existing berth increases from 233 days to 295 days with the introduction of proposed berth. The number of operable days for point 2 in the existing berth increases from 232 days to 294 days with the introduction of proposed berth. The existing berth location will have protection by the construction of protective jetty on its west.

Conclusions

The results revealed that the harbor layout was not adequate (Case 1) especially for the calmness criteria defined for the monsoon wave conditions for medium draught vessels. The wave disturbance within the harbour has decreased with the introduction of proposed berth (Case 2) with the alignment parallel to the eastern arm of the existing wharf. The percentage operability of the harbor at the selected points is found to have increased resulting in the increase in the number of operable days for ships in the harbour. In particular, during June to October, the operability of existing wharf location will improve from an average of 20% -25% to nearly 100% operational.

The dredge level for the navigation channel also plays an important role in influencing the harbour tranquility within the harbour. It has been found that the wave disturbance in the harbour increases with the increase in the dredge level of the entire navigational channel and the berths (Case 3). The dredging in the turning circle and the new berth (Case 4) is found to provide necessary tranquility. Hence, a compromise is to be made between the dredge level and harbour tranquility while carrying out the new

development.

References

(1972)"Computation of combined refraction diffraction",Proceedings of 13th international conference of coastal engineering,Canada,p471-490 Berkhoff,J,C.W

(1990) Wave atlas for Indian coast 1990 , National Institute of Oceanography,India

(2004). MIKE 21 Wave Dynamics PMS Module Release 2.4, User Guide and Reference Manual Danish Hydraulic Institute, Denmark

Probabilistic Analysis of Ship-Bank Collision under Environmental Loads in Yangshan Port

Han Liu[1,2,3], Ning Ma[2,3], Xiechong Gu[2,3]
1 School of Naval Architecture, Ocean & Civil Engineering, Shanghai Jiao Tong University
2 State Key Laboratory of Ocean Engineering, Shanghai Jiao Tong University
3 Collaborative Innovation Center for Advanced Ship and Deep-Sea Exploration, Shanghai Jiao Tong University
Shanghai, 200240, China
ningma@sjtu.edu.cn

Abstract: Probability of ship-bank collision and consequent hull breach is a crucial part of estimating the potential risk of ship damage and oil spill in the operation of a port. This study presents a performance-based approach to evaluate the probability of ship-bank collision and consequent hull damage for a container ship passing a channel. The impact scenarios are screened from a data base of substantial course keeping failure candidates that are obtained by Monte Carlo simulation approach. The wind loads and bank effect generated according to the probability distribution of wind condition and ship-bank distance are introduced into the simulations of ship manoeuvring for entering the channel of Yangshan Port. The proposed approach is demonstrated through the probabilistic analysis for a 10000TEU container ship at different ship speeds and container layout schemes. The minimum ship speed and related container layout strategies in critical meteorological conditions are proposed to avoid the potential collisions.

Keywords: Ship-bank collision; probabilistic analysis; Yangshan port; performance-based approach; environmental loads

Introduction

The Shanghai International Shipping Center Yangshan deepwater port, as the world's largest port to handle container throughput, will reach the throughput of 40 million TEUs per year (People's Daily, July 26th, 2017). The heavy traffic in the port will also see a growing risk of ship collisions and much more, particularly since more and more in-and-out port container ships are holding over 10000 TEUs. The consequent accidents (like ship damage, explosion and oil spill) will bring economic loss and casualties, and meanwhile, pose a great threat to the marine environment and ecosystem of the port area. Such environmental concern looms large in Yangshan port, since it is close to the Zhoushan fishery that is the largest fishery of China. More attention to the risk probability of ship arriving and departing the port need to be paid.

Prolific research works have provided the theoretical basis and analysis procedures in predicting the probability of ship accidents such as collision and grounding. Pedersen (2010) gave a comprehensive summary of related studies and concluded that the performance-based analytical procedures is a first step to reduce the risk of accidents.

Sharing the same idea, van Dorp & Merrick (2011) incorporated the probabilistic risk model with accident scenario detection based on time domain simulation of vessel traffic in certain water areas. The attributes of vessels and route conditions are obtained from the data of Automatic Identification System (AIS). The probabilistic evaluation are performed using methods like Monte Carlo simulation (MCS) (Brown & Chen, 2002, Goerlandt & Kujala, 2011) and expert judgement (Ulusçu et al., 2009). Soon the research has been extended to the prediction of the collision risk by calculating the consequences of ship encounters based on evasive manoeuvring and deformation energy (Ståhlberg et al., 2013). But the studies above focus on the holistic navigational risks in a water area, while the risk probability of individual ship is not studied. Balmat et al. (2009) developed a fuzzy logic based system to define the risk factor and quantify the degree of risk for individual ship navigation. A highlight in this work is that the meteorological conditions are included in the risk factor. Similarly, Zhang et al. (2013) used Bayesian network to establish the navigational risk model of the Yangtze River, considering meteorological causation factors like wind and visibility.

Figure 1 shows the electronic nautical chart of the Yangshan deepwater port. The narrowest section of the entrance to the berths (marked as A) is merely 1.05km wide, and the approach channel is close to the dock with the width of no more than 650m. The channel's depth varies from 80m to 16m. Such conditions make a restricted water area for the ships passing through the channel. The ships will suffer from a suction force towards the bank and a bow-out or bow-in moment, which is called the ship-bank interaction or the bank effect. Moreover, wind load on the container ship superstructure is also significant to affect the course keeping performance. Ship-bank distance and wind condition are important factors to cause manoeuvring problem in the channel, therefore, the statistics of the port area such as frequency distribution of wind condition and ship route is helpful to conduct the probabilistic analysis of ship-bank collision.

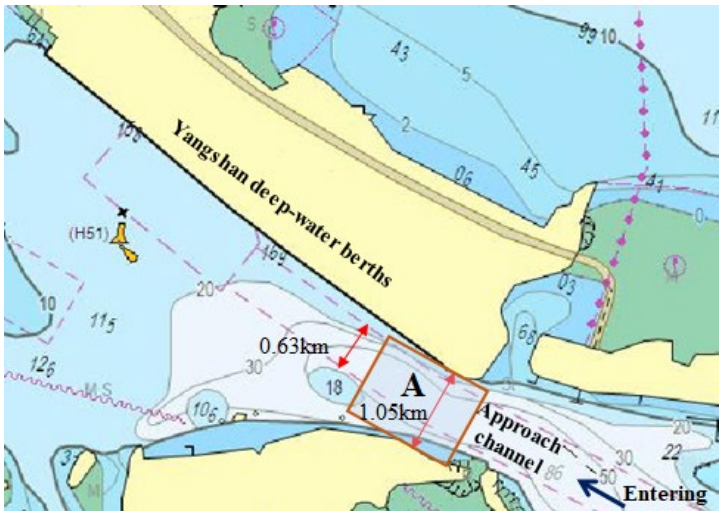

Figure 1. Electronic nautical chart of the Yangshan deepwater port

The objective of this article is to present a performance-based approach to assess the probability of container ship ship-bank collision and collision with banks, while at the same time obtaining detailed results that can be used in the consequence modeling, bridging the separation between unwanted collision and hull damage. Some researchers have revealed the impact of the angle of collision, the vessel speeds, ships' dimensions and loading conditions on the collision energy (Zhang 1999), the resulting probability of hull rupture (Ehlers et al. 2008) and the oil outflow (Montewka et al. 2010).

In this paper, a 10000TEU container ship entering the narrowest part of the channel is taken as an example to present the application of the proposed approach. First, the architecture of probability analysis based on the distribution of wind conditions and ship routes through the MCS is proposed. Then the manoeuvring equations as well as the resulting state-space framework to identify the events of course keeping failure are described, and the methodology for case study of the probabilistic damage is expressed in terms of probability of hull breach. Finally, probabilistic assessment of ship-bank collision and hull rupture together with discussion on reducing the probability are given for various ship speeds and container layout schemes.

Architecture of Probability Analysis

The overall process to predict the probability of ship-bank collision is outlined in Figure 2. The core methodology is to identify the ship-bank impact scenarios through the MCS. A large numbers of navigation conditions are generated according to a set of probability density functions (PDFs) and the attributes of the ship (main dimensions, speed and load condition). From the replicated simulations of manoeuvring, the impact scenarios are identified and stored. The criterion for the assessment of ship-bank collision is regarded as: whenever the ship-bank distance is less than 0.02 L_{PP} (which is assumed to touch the bank), the ship-bank collision occurs. Then, the available deformation energy in the ship-bank collision is calculated for each selected scenario by applying the method that Zhang proposed (Zhang 1999). The hull breach criteria is based on the formula that is derived from the results of finite element modeling by Ståhlberg et al. (2013), and the criteria refers to the required deformation energy for inner hull rapture. When the available deformation energy E_{ξ} is no less than the critical hull capacity for inner hull breach, the hull breach happens. Finally, the program returns the storage of parameters of ship-bank collision and hull breach for the risk probability analysis.

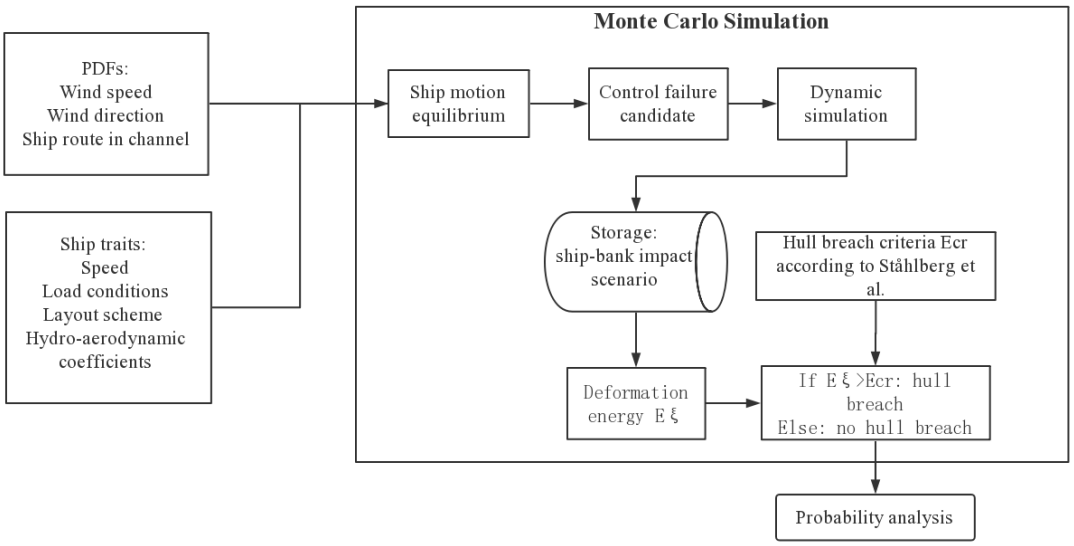

Figure 2. Schematic of probability prediction for ship-bank collision.

To increase the efficiency of computing the course keeping failure candidates across the large numbers of MCS runs, a preliminary screening is performed based on the equations of the ship's equilibrium condition. The cases whose solutions meet the criterion for control failure are collected in the control failure candidate group and further used for time-domain simulation. This method will be detailed in section 3.1 and 3.2.

Distributions of wind speed, wind direction and ship-bank distance are investigated prior to the MCS. For the frequency distribution of wind in the area of Yangshan port, the daily wind data recorded by the Shengsi National Level Surface Observational Station from 2012 to 2016 were recounted in terms of speed and direction. These historic files are shared online by China Meteorological Data Service Center (2017). Figure 3 shows the distribution of the probability of maximum wind speed P_{WS} and the distribution of wind direction at maximum speed.

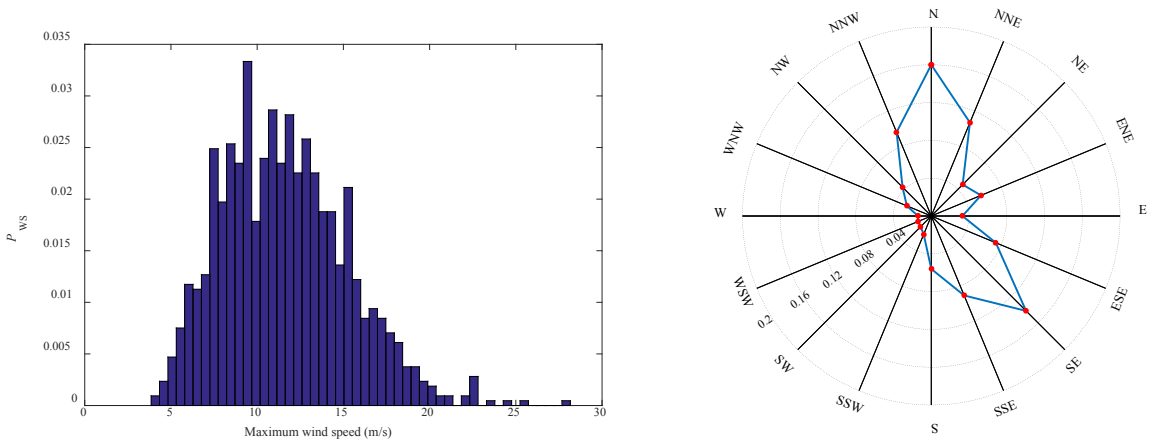

Figure 3. Distribution of P_{WS} and distribution of wind direction at maximum speed at Yangshan port.

The direction of the approach channel is almost the same to the wind direction ESE (for entering ships) or WNW (for leaving ships). The ship is assumed to follow the route parallel to the channel, and the ship's lateral position in the channel follows a normal distribution. The ship-bank distance is determined by knowing the lateral position in the channel. The mean of the normal distribution with respect to the centreline of waterway can be seen in Figure 4. According to Inoue (1977), if no centreline light buoy is installed in the channel, the distance between the mean of the normal distribution and the centreline of waterway D can be estimated by

$$D = 0.1W \tag{1}$$

where W is the width of waterway and W=630m, and the variance of the normal distribution is

$$\sigma = -7.170 + 0.105W + 2.168Q \tag{2}$$

where σ is the variance and Q is the traffic volume per hour.

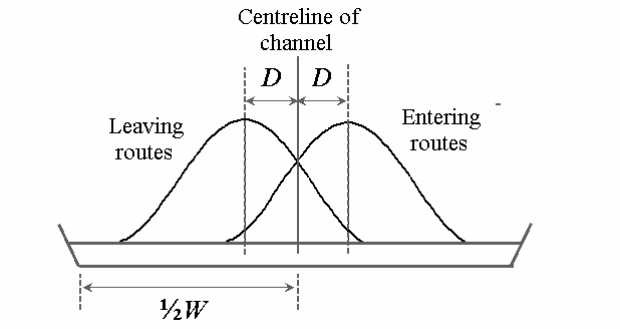

Figure 4. Location of the mean of ship route distributions with respect to the centreline of approach channel (Inoue, 1977).

Performance-Based Identification of Impact Scenario

Figure 5 shows the coordinate systems as well as the variables used in the equations of ship motion. The earth-fixed coordinate system O_0-$\xi\eta\zeta$ and ship fixed coordinate system O-xyz are right-handed coordinate systems. The ship initially moves in the direction of the ξ axis with speed, U. U_w and θ_w denote the absolute value of the wind speed and wind direction. Affected by the environmental forces, the ship's velocities are generated as the vector [u, v, r], and the heading angle ψ as well as the drift angle β appears. A rudder deflection δ is required to maintain the ship's direction. y_{bank} is the distance between the ship and the bank.

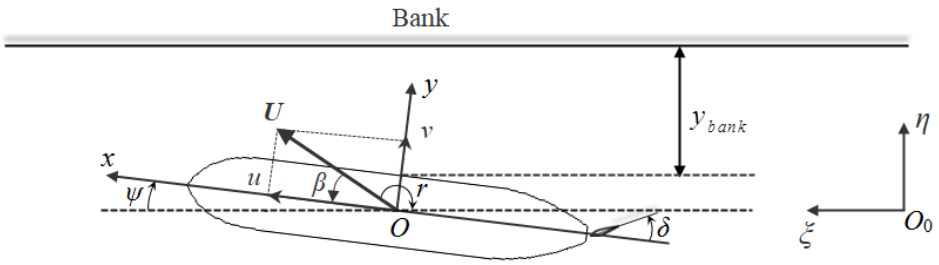

Figure 5. Coordinate systems.

To simplify the manoeuvring problem, the ship's engine power adjusts with the wind loads to keep the speed U constant, and small deviation in sway and yaw motion is caused by the rudder deflection and wind/bank forces. Therefore, the equation of surge motion is neglected and the non-dimensional equations of ship motion are given as

$$m'\left(\dot{v}' + u'r' + x'_G\dot{r}'\right) = Y'_H + Y'_A \tag{3}$$

$$I'_z\dot{r}' + m'x'_G\left(\dot{v}' + u'r'\right) = N'_H + N'_A \tag{4}$$

where m is the ship mass, I_z is the moment of inertia about the z axis. Y_H and N_H are the hydrodynamic force and moment acting on the ship, and Y_A and N_A are the aerodynamic force and moment due to wind. The non-dimensional treatment are performed based on water density ρ, ship length between perpendiculars L_{PP} and speed U. Some examples are given as follows and readers can get the idea of non-dimensionalization of other variables, too.

$$\begin{aligned} &\dot{v}' = \frac{\dot{v}L_{PP}}{U^2}, \quad \dot{r}' = \frac{\dot{r}L_{PP}^2}{U^2}, \quad u' = \frac{u}{U}, \quad r = \frac{rL_{PP}}{U} \\ &Y'_H = \frac{Y_H}{0.5\rho L_{PP}^2U^2}, \quad N'_H = \frac{N_H}{0.5\rho L_{PP}^3U^2} \end{aligned} \tag{5}$$

The hydrodynamic lateral force and yaw moment acting on the ship are expressed by the following polynomial equations

$$Y'_H = Y'_0 + Y'_{\dot{v}}\dot{v}' + Y'_{\dot{r}}\dot{r}' + Y'_v v' + Y'_r r' + Y'_\eta\eta' + Y'_\delta\delta \tag{6}$$

$$N'_H = N'_0 + N'_{\dot{r}}\dot{r}' + N'_{\dot{v}}\dot{v}' + N'_v v' + N'_r r' + N'_\eta\eta' + N'_\delta\delta \tag{7}$$

The constant terms Y'_0 and N'_0 represent the steady force and moment due to the asymmetric hydrodynamics of propeller rotations. According to the study of Liu et al. (2016), the ship-bank interaction forces are measurable if $y_{bank} \le 0.7L_{PP}$. The forces vary

with the change of ship-bank distance. To mathematically model this feature, the initial lateral position of the ship is set as η=0, and the variation of the forces when η changes is written as $Y'_\eta\eta'$ and $N'_\eta\eta'$. The coefficients Y'_η and N'_η are called asymmetric derivatives.

The aerodynamic lateral force and yaw moment are based on Isherwood (1972)

$$Y'_A = (\rho_A/\rho)V'^2_A C_{YA}(\theta_A) \tag{8}$$

$$N'_A = (\rho_A/\rho)V'^2_A C_{NA}(\theta_A) \tag{9}$$

where $V'^2_A = u'^2_A + v'^2_A$, $u'_A = u' + U'_W\cos(\theta_W - \psi)$, $v'_A = v' + U'_W\sin(\theta_W - \psi)$, and $\theta_A = \tan^{-1}(v'_A/u'_A)$.Herein ρ_A is air density, A_Y is the lateral projected area above the waterline, and the wind force coefficients C_{YA}, C_{NA} are wind force coefficients corresponding to each relative wind direction angle θ_A.

Yasukawa et al. (2013) considered that when the sway and yaw motion is assumed small, the magnitude of v, ψ and β can be taken as the order $O(\varepsilon)$. Then, Eqs. (8) and(9) can be rewritten as

$$Y'_A = Y'_{A0} + Y'_{A\beta}\beta + Y'_{A\psi}\psi + O(\varepsilon^2) \tag{10}$$

$$N'_A = N'_{A0} + N'_{A\beta}\beta + N'_{A\psi}\psi + O(\varepsilon^2) \tag{11}$$

Readers can refer to (Yasukawa et al., 2012) for the expressions of Y'_{A0}, $Y'_{A\beta}$, $Y'_{A\psi}$, N'_{A0}, $N'_{A\beta}$ and $N'_{A\psi}$. When the ship reaches the motion equilibrium, the acceleration terms in Eqs. (3) and (4) are eliminated. By taking Eqs. (6)- (11) into Eqs. (3) and (4). the following equations for the equilibrium condition is obtained

$$0 = Y'_0 + Y'_{A0} + (Y'_v + Y'_{A\beta} + Y'_{A\psi})\psi_0 + Y'_\eta\eta'_0 + Y'_\delta\delta_0 \tag{12}$$

$$0 = N'_0 + N'_{A0} + (N'_v + N'_{A\beta} + N'_{A\psi})\psi_0 + N'_\eta\eta'_0 + N'_\delta\delta_0 \tag{13}$$

By substituting the wind condition and ship's lateral position into Eqs. (12) and (13), the rudder angle δ_0 and heading angle ψ_0 can be solved. Once δ_0 is larger than the maximum steering angle, that is, 35°, the criterion for control failure is satisfied. The corresponding wind condition and ship lateral position are treated as the input to the dynamic simulation module.

When the control failure scenario is confirmed, the ship performs crash stopping to avoid probable collisions. The stopping time is evaluated based on the regression formula by Nippon Kaiji Kyokai (1979)

$$TIME = 7.17\left(mUC_b/(HP)^{1/2}\right)^{1/2} \tag{14}$$

where C_b is the block coefficient and HP is the horsepower at U. The dynamic manoeuvring simulation is carried out in this time period to check whether the collision occurs. Eqs. (3) and (4) are rearranged by the state vectors $[v\ r]^{\mathrm{T}}$ to yield the state-space equation as follows

$$\mathbf{M}\begin{bmatrix}\dot{v}'\\ \dot{r}'\end{bmatrix}+\mathbf{N}\begin{bmatrix}v'\\ r'\end{bmatrix}-\mathbf{L}[\eta']=\mathbf{F}_R[\delta]+\mathbf{F}_A \tag{15}$$

where

$$\mathbf{M}=\begin{bmatrix}-Y'_{\dot{v}}+m' & -Y'_{\dot{r}}+m'x'_G\\ -N'_{\dot{v}}+m'x'_G & -N'_{\dot{r}}+I'_z\end{bmatrix} \tag{16}$$

$$\mathbf{N}=\begin{bmatrix}-Y'_v & -Y'_r+m'\\ -N'_v & -N_r+m'x'_G\end{bmatrix} \tag{17}$$

$$\mathbf{L}=\begin{bmatrix}Y'_\eta\\ N'_\eta\end{bmatrix}\quad \mathbf{F}_R=\begin{bmatrix}Y'_\delta\\ N'_\delta\end{bmatrix}\quad \mathbf{F}_A=\begin{bmatrix}Y'_A\\ N'_A\end{bmatrix} \tag{18}$$

Moreover, ψ and r satisfies the relationship of . By adding it to the equation above, the final state-space equation expands as

$$\begin{bmatrix}\dot{v}'\\ \dot{r}'\\ \dot{\psi}'\\ \dot{\eta}'\end{bmatrix}=\begin{bmatrix}-\mathbf{M}^{-1}\mathbf{N} & \begin{matrix}0\\0\end{matrix} & \mathbf{M}^{-1}\mathbf{L}\\ \begin{matrix}0 & 1\\1 & 0\end{matrix} & \begin{matrix}0 & 0\\1 & 0\end{matrix}\end{bmatrix}\begin{bmatrix}v'\\ r'\\ \psi\\ \eta'\end{bmatrix}+\left[\mathbf{M}^{-1}\mathbf{F}_R\right][\delta]+\left[\mathbf{M}^{-1}\mathbf{F}_A\right] \tag{19}$$

Since Eq. (19) is actually a linear time invariant system as $\dot{\mathbf{x}}=\mathbf{A}\mathbf{x}+\mathbf{B}\mathbf{u}$, the rudder angle as the state-feedback $\mathbf{u}$ is adjusted by a Linear Quadratic Regulator (LQR).

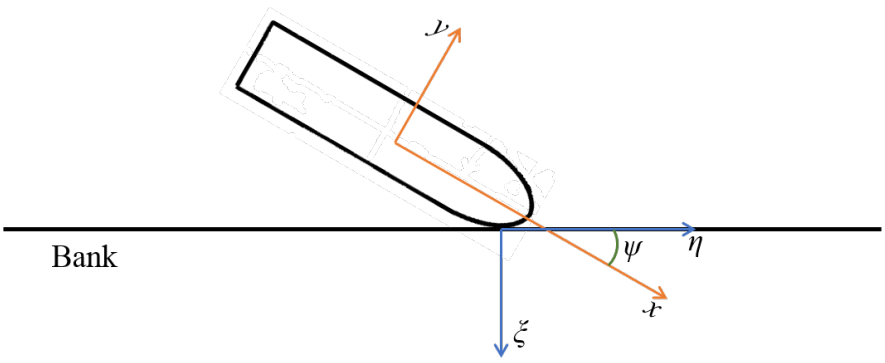

Figure 6. Definition of axis and angles for ship-bank collision.

The available deformation energy, resulting from the impact of the ship and the bank, is determined based on the model proposed by Zhang (1999). It is based on rigid body mechanics considering three degrees of freedom. Relevant axes and notations are defined in Figure 6. The deformation energy calculation method presented by Zhang will not be reproduced here in full, but it is noted that the formulation by Zhang allows calculation of deformation energy in longitudinal and perpendicular directions, respectively denoted and E_η and E_ξ. In this work, only E_ξ is applied.

The vessel specific hull rupture criteria are determined according to the vessel particulars that is interpolated in scalable rupture criteria obtained from a series of FEM damage model calculations (Ståhlberg et al., 2013). The required energy for rupture of inner skin is approximated as follows:

$$E_{\mathrm{cr,in}} = L_{ref}\left(100\frac{L_b}{L_{ref}}\right)^{2.87} \tag{20}$$

with $E_{\mathrm{cr,out}}$ in Joules, L_{ref} 188.3 m and L_b the length of the striking ship.

Probabilistic Assessment of 10000TEU Container Ship Collision

A 10000TEU container ship, which normally has a large wind pressure area, is studied in this case study. According to the official file of 10000TEU Container Ship Vessel Trim and Stability Booklet, the paper chose a typical non-full loaded condition marked *10T/TEU DEP. AT DESIGN DRAFT* with 7453 containers overall and each of those containers weights 10t. Principle dimensions of the ship and shipping information for the loaded condition are listed in Table 1. Five layout schemes with the same container number are selected to investigate the effect of layout scheme on the probability of ship-bank collision. Diagrams and numbering regulation for the five chosen layout schemes are presented in Figure 7.

Table 1. Principle dimensions of 10000TEU and shipping information of loaded condition *10T/TEU DEP. AT DESIGN DRAFT*

Length btw. perpendiculars L_{PP}	320.0m
Breadth B	48.2m
Mean draft T	12.94m
Displacement Δ	124337t
Block coefficient	0.602
Long. position of LCB x_G	4.33m
Container number - in hold	4578TEU
Container number - on hatch cover and deck	2875TEU
Rudder area A_R	72.0m^2

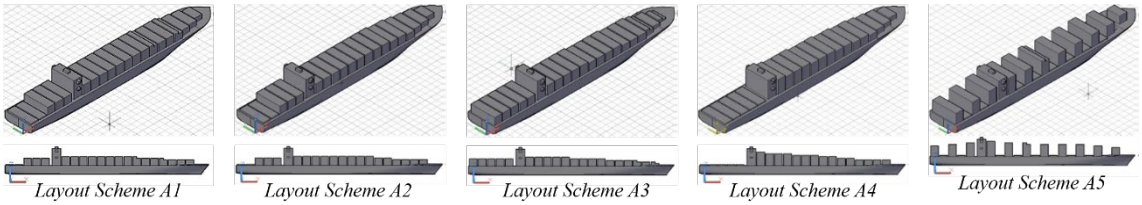

Figure 7. Diagrams and numbering regulation for chosen layout schemes.

Qiao et al. (2017) measured the wind force coefficients, C_{YA} and C_{NA}, through systematic wind tunnel tests in the Wind Tunnel and Circulating Water Channel (CWC) of Shanghai Jiao Tong University. Figure 8 shows the wind load coefficients C_{YA} and C_{NA} for the 5 chosen layout schemes. The asymmetric derivatives, Y'_η and N'_η, are analysed from the ship-bank interaction forces measurement. In this experiment, the ship was placed laterally off the centerline of the CWC with different displacements (Liu et al. 2017), and water flowed past the ship at speed U. Apart from the asymmetric derivatives, the added mass, and other hydrodynamic derivatives are measured through a series of PMM test in the CWC. Table 2 shows all the hydrodynamic derivatives.

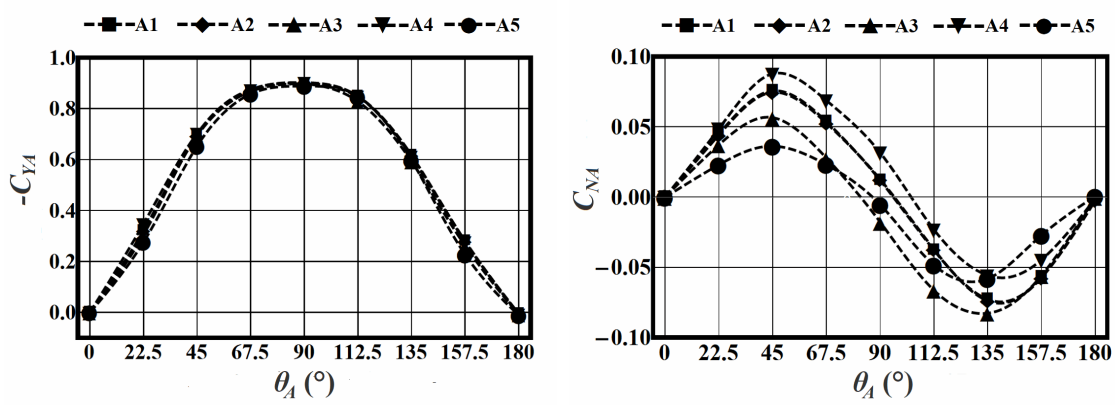

Figure 8. Wind force coefficients for the 10000TEU for five layout schemes.

Table 2. Hydrodynamic derivatives during 10000TEU manoeuvring

Y'_η	1.6E-5	N'_η	-7.7E-6	$Y'_{\dot{v}}$	-0.0521	$N'_{\dot{v}}$	-0.0001
$Y'_{\dot{r}}$	-0.0004	$N'_{\dot{r}}$	-0.0002	Y'_v	-0.0066	N'_v	-0.0038
Y'_r	0.0015	N'_r	-0.0015	Y'_δ	-0.0016	N'_δ	0.0007

In this paper, investigation is made on the probability of collision and consequence in the process of passing through the narrowest part of the channel (the rectangle section marked with A in Figure 1). The MCS is individually conducted for the five layout schemes and three ship speeds, which are 14.25kn, 9.5kn and 7.13kn corresponding to 60% V_S, 40% V_S and 30% V_S (V_S refers to the service speed of the ship), respectively.

Each MCS calls the PDFs of environmental factors, including wind condition and ship routes, to generate 1000000 cases to become the input arrays.

The probability of ship-bank collision for given layout schemes and speeds are listed in Table 3. No failure is detected for all layout schemes at 60% V_S. The maximum probability appearing at 40% V_S is 0.17‰ and the value increases to 2.5‰ when ship speed drops to 30% V_S. The ship with layout scheme A5 faces more impact scenarios than that with the other 4 layout schemes. The lowest probability remains scheme A4 at 40% *Vs* and scheme A1 at 30% *Vs* respectively.

The probability of inner hull breach is defined as the ratio between the number of inner hull breach and the number of collision occurrence. Considering no collision occurs for all layout schemes at 60% V_S, Table 4 presents the probabilities of inner hull breach at 40% V_S and 30% V_S. The ship with layout scheme A5 is expected to have the highest possibility of hull breach, and the scheme A3 and A4 seem to be good for avoiding hull rapture. The results can function as indicative value of potential occurrence of oil spill and further used in estimating the risk of ship-bank collision.

Table 3. Probability of ship-bank collision for 10000TEU passing through section A.

Layout scheme	60% V_S	40% V_S	30% V_S
A1	0	2.6E-6	6.4E-4
A2	0	4.1E-6	7.8E-4
A3	0	6.5E-6	1.0E-3
A4	0	1.7E-6	6.7E-4
A5	0	1.7E-4	2.5E-3

Table 4. Probability of inner hull breach for different layout schemes and speeds.

	40%V_S	30%V_S
A1	0.0000	0.0589
A2	0.0204	0.0381
A3	0.0000	0.0000
A4	0.0000	0.0000
A5	0.0096	0.0943

Statistics of Impact Scenarios and Discussions

A crucial characteristic of the presented simulation model is the ability to provide the detailed information about some of the conditions in which the collision occurs. The statistics of wind speed and direction, and the initial lateral position of the ship can be

studied in terms of ship speed and layout scheme. Figure 9 and Figure 10 illustrate the probability of course keeping failure by these factors at 30% V_S as an example.

Probability of ship-bank collision by wind speed and wind direction is plotted in Figure 9. In subplot a, the probability of collision occurrences is mainly in the range of 17.5m/s-21.5m/s. In subplot b, the probable wind direction is mainly in the range of 60°-120°, and a slight likelihood of failure shows between -120° and -80°, both representing a beam wind to the ship. The highest summit in each figure appears in the PDFs of scheme A5, and the width of risky speed and direction distribution to cause collision is broader than that in the other schemes. Therefore, A5 is quite an adverse layout scheme for the ship passing the area.

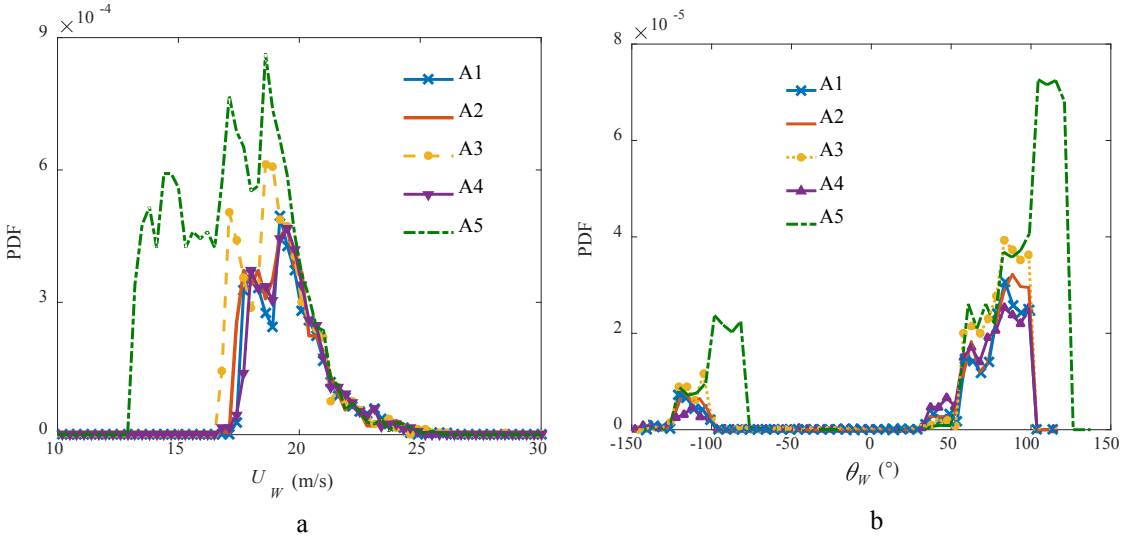

Figure 9. Probability of ship-bank collision by wind speed and wind direction for passing through section A at 30% V_S.

In Figure 10, the zero point of the abscissa is the centreline of the channel, and the mean of the PDF for ship entering routes (shown in Figure 4) is shown with a dash line. When the ship follows a route on the right-hind side of the line, the bank effect need to be considered in the hydrodynamic forces. It can be found that the majority of ship-bank collisions occurring in A1-A4 do not stem from the bank effect. As to A5, the bank effect show a positive correlation with the increase of ship-bank collision. This is because the aerodynamic yaw moment counteracts the bank induced yaw moment. As shown in Figure 7, the magnitude of aerodynamic yaw moment for layout A5 shows a sharp decrease and the moment becomes too weak to cancel out the bank induced yaw moment.

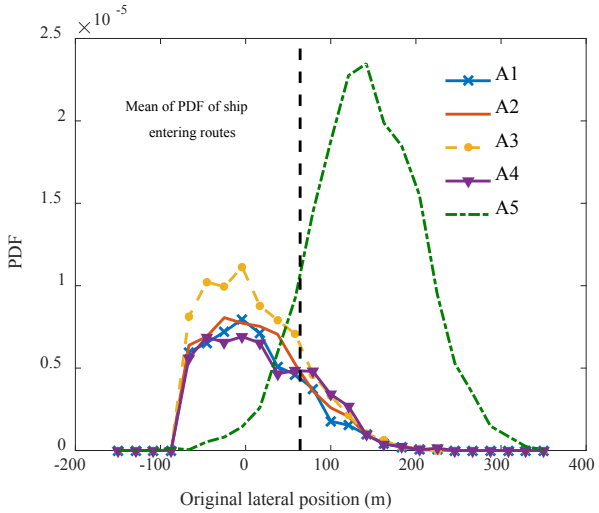

Figure 10. Probability of ship-bank collision by initial lateral position at 30% V_S.

From the results in Table 3, it is evident that the speed of 60% V_S is capable to avoid ship-bank collision during passing section A. The speed of 30% V_S leads to a fairly high risk level that is over 1‰. If the probability of ship-bank collision is required to be in the order of 10^{-6}, ship speed needs to be higher than 40% V_S. According to the study by Briggs et al. (2009), the maximum ship speed in a given channel is about 80 percent of a parameter called the Schijf limiting speed. For the 10000TEU ship, the maximum speed to pass section A is 18.6kn, which is approximately 80% V_S. So keeping a speed of ≥ 40% V_S is a feasible strategy for the 10000TEU container ship to reduce manoeuvring risks during passing the channel.

The results also indicate that the design of layout scheme significantly affects the course keeping performance of the container ship. The distributions in Figure 9 and Figure 10 show that A5 is a relatively hazardous layout scheme in terms of the meteorological condition and the waterway width in Yangshan port. As shown in Figure 6, layout scheme A5 is provided with the highest permeability, which means the gaps between containers on the hatch cover and deck, causing the yaw moment coefficient C_{NA} smaller than the other layouts. This is a main factor to deteriorate the ship's course keeping ability in the circumstance of bank effect. The layout scheme with a lower permeability, e.g. A4, will be a good choice in confronting high wind speed condition.

The critical meteorological condition to confront in the entering port process is the beam wind with a speed higher than 17.5m/s. When the container ship confronts such scenario, ship crews are suggested to turn the ship to the weather-vane direction, and meanwhile, perform crash stop.

Conclusions

This paper presents a manoeuvring performance based approach for the modelling of probability of ship course keeping failure and ship-bank impact and the application to the scenario a 10000TEU container ship entering Yangshan port is demonstrated. The two major stochastic external factors in causing the risk, wind load and bank effect, are modelled by PDFs, and the probabilistic trait of them in the failure event are predicted using the MCS technique.

The simulations are conducted to investigate the influence of ship speed and container layout scheme on the probability of collision and consequence. Layout schemes with higher permeability and speeds lower than 40% service speed face higher risk of collision and hull rupture. The minimum ship speed to avoid course keeping are proposed higher than 40% V_S. The lower lateral projected area is required in designing the container layout.

The approach is capable of providing detailed information about the circumstances in which the container ship lose course keeping control and collide the bank. If combined with the method to evaluate ship damage extent in a collision, as presented by Brown & Chen (2002), the proposed model can be used to predict the risk level of ship-bank or ship-ship collision in ports.

Acknowledments

This study is supported by the National Key Basic Research Program of China: No. 2014CB046804, and the China Ministry of Education Key Research Project "KSHIP-II Project": No. GKZY010004. Sincere thanks are expressed to Mr Yi Dai, Dr Fei Wang, Mr Dan Qiao and Mr Qiang Chen for their help in the model tests.

References

Balmat, J. F., Lafont, F., Maifret, R., and Pessel, N.. 2009. "Maritime risk assessment (marisa), a fuzzy approach to define an individual ship risk factor", *Ocean Engineering*, Vol. 36: 1278-1286.

Briggs, M. J., Vantorre, M., Uliczka, K., and Debaillon, P.. 2008, "Prediction of squat for underkeel clearance", *Handbook of Coastal and Ocean Engineering*, 723-774.

Brown, A., and Chen, D.. 2002. "Probabilistic method for predicting ship collision damage", *Ocean Engineering International Journal*, Vol. 6: 54-65.

China Meteorological Data Service Center, 2017, Dataset of daily surface observation values in individual years in China, http://data.cma.cn/en/?r=data/detail&dataCode=A.0029.0001.

Ehlers S, Broekhuijsen J, Alsos HS, Biehl F, Tabri K. 2008. "Simulating the collision response of ship side structures: a failure criteria benchmark study", *International Shipbuilding Progress*, 55(1–2):127–44.

Goerlandt, F., and Kujala, P.. 2011. "Traffic simulation based ship collision probability modelling", *Reliability Engineering and System Safety*, Vol. 96: 91-107.

Inoue, K.. 1977. "On the separation of traffic at straight waterway by distribution model of ship's paths", *The Journal of Japan Institute of Navigation*, Vol. 58: 103-115.

Isherwood, R. M.. 1972. "Wind Resistance of Merchant Ships", *Transaction of the Royal Institution of Naval Architects*, Vol. 115: 327-338.

Nippon Kaiji Kyokai. 1979. “About ship stopping performance (General Technology)” *Transactions of Nippon Kaiji Kyokai*, Vol. 166: 1-6.

Liu, H., Bao, Y. X., Yuan, C. S., and Xie, X. J.. 2014. “Study on spatiotemporal distribution characteristic of strong breeze and strong crosswind in Jiangsu section of the Yangtze River waterway”, *Journal of Natural Disasters*, Vol. 23: 155-169, in Chinese.

Liu, H., Ma, N., Shao, C., and Gu, X. C.. 2016. “Numerical Simulation of Planar Motion Mechanism Test and Hydrodynamic Derivatives of a Ship in Laterally Restricted Water”, *Journal of Shanghai Jiaotong University*, Vol. 50: 115-122, in Chinese.

Montewka J, Ståhlberg, K, Seppala T, Kujala P. 2010. “Elements of risk analysis for collision of oil tankers”, *Proceedings of the ESREL conference*, 1005-1013.

Pedersen, P. T.. 2010. “Review and application of ship collision and grounding analysis procedures”, *Marine Structures*, Vol. 23: 241-262.

People’s Daily. July 26th of 2017. http://en.people.cn/n3/2017/0726/c90783-9246682-2.html.

Qiao, D., Ma, N., Gu, X. C., Wang, G. C., and Chen, Q.. 2017. “Study on energy efficiency design for large container ship with the consideration for the influence of wind load”, *Proc. 11th International Conference of Port-city Universities League*: 96-116.

Ståhlberg, K., Goerlandt, F., Ehlers, S., and Kujala, P.. 2013. “Impact scenario models for probabilistic risk-based design for ship–ship collision”, *Marine Structures*, Vol. 33: 238-264.

Ulusçu, Ö. S., Özbaş, B., Altıok, T., and İlhan, Or. 2009. “Risk analysis of the vessel traffic in the strait of Istanbul”, *Risk Analysis*, Vol. 29: 1454–1472.

van Dorp, J. R., and Merrick, J. R. W.. 2011. “On a risk management analysis of oil spill risk using maritime transportation system simulation”, *Annals of Operations Research*, Vol. 187: 249-277.

Yasukawa, H., Hirono, T., Nakayama, Y., & Koh, K. K.. 2012. “Course stability and yaw motion of a ship in steady wind”, *Journal of Marine Science & Technology*, Vol .17: 291-304.

Yasukawa, H., Sano, M., and Amii, H. 2013. “Wind effect on directional stability of a ship moving in a channel”, *Journal of the Japan Society of Naval Architects and Ocean Engineers*, Vol. 18: 45-53, in Japanese.

Zhang, D., Yan, X. P., Yang, Z. L., Wall, A., and Wang, J. 2013. “Incorporation of formal safety assessment and bayesian network in navigational risk estimation of the Yangtze river”, *Reliability Engineering & System Safety*, Vol. 118: 93-105.

Zhang S. 1999. “The mechanics of ship collision”, Ph.D. thesis, Technical University of Denmark.

A Classification System For Port Cities To Improve Understanding Of Port-City Maritime Pollution

Toby Roberts[1], Prof George Attard[1,2], Dr Mario Brito[1,2], Florentin Bulot[1], Natasha Easton[1], Dr Simon Gerrard[2], Gareth Giles[1,3], Prof Jang Kim[4], Dr Robert Mayon[1,2], Tafta Nugraha[1], Dr Peter Shaw[1,2], Prof Damon Teagle[1,2], Andrew Wright[5], Dr Sevil Deniz Yakan[6], Prof Ian Williams[1,2], Dr Matthew Loxham[1,2],

[1]The University of Southampton, [2]Southampton Marine and Maritime Institute, [3]Public Policy Southampton, [4]Incheon National University, [5]Lloyd's Register, [6]Istanbul Technical University,
Email for correspondence: Dr Matt Loxham (m.loxham@soton.ac.uk), Prof Ian Williams (i.d.williams@soton.ac.uk)

Abstract: Ports are vital to the global economy, providing a range of local, regional, national, and international benefits. However they also give rise to negative impacts, which are often concentrated within the local area. Amongst these, maritime pollution of the air and water may have considerable consequences for the environment, as well as human health and well-being. In order to improve understanding of how maritime pollution varies between cities, a classification system was developed based on a range of variables. These variables include passenger numbers, annual throughput (TEU), World Bank Port Infrastructure Quality indices, urban area characteristics, human development index, adherence to environmental conventions, port structure, local climate zone, and local infrastructure. Information on these variables was collected for 200 large port cities selected from Lloyd's list top 100 container ports, AAPA world port rankings, regional lists of large ports and members of Port-City Universities League. Cruise passenger numbers and cargo tonnage appear to be a useful way of grouping ports. A provisional system using these variables was created which offers an improved system for grouping ports by size and function.

Keywords: Port-City, Classification system, Pollution,

Introduction

Ports play a crucial role in driving international trade and provide vital services to the local, regional and national economy. In order for future ports to be developed in a more sustainable way, it is important to be able to categorise ports effectively. An improved understanding of the different types of ports, and how they may be defined by groupings of their individual characteristics, can enable improved understanding of the different ways varying types of ports interact with their environment, such as pollution emissions. At present the understanding of the negative impacts of ports such as pollution is limited due to a lack of understanding regarding which characteristics of ports are key drivers of pollution.

Ports produce a range of positive and negative impacts on the cities they serve, with the

negative impacts being largely concentrated relatively close to the port and the positive impacts being spread further afield, across the city, region and country. This has led to increasing tensions between ports and cities. If future port development is to be sustainable, it must more effectively balance social, environmental and economic considerations.

Ports produce a range of environmental impacts such as air pollution, water pollution, soil pollution, waste, noise, light and biological pollution. The impacts created by ports have a range of social consequences such as negative impacts on human health and wellbeing. In addition to this, pollution from ports has been shown to produce large economic costs for the cities they impact (Castells Sanabra et al. 2013). It is therefore of great importance that ports reduce pollution if sustainable development in ports is to be achieved.

Pollution is a considerable negative impact of ports which can be created by shipping within the port, the use of port land and the impact of transport to and from ports (Miola et al 2009). Within a port city, the emissions created by the port can form a large percentage of total city emissions. A good example of this is Hong Kong, where port activities were estimated to contribute 54% of SO_2 and 33% of NO_x within the city (OECD 2013).

Potential options for mitigation of maritime pollution may also vary between different types of ports. For example, a vessel speed reduction zone (also known as slow steaming) has been shown by Lindstad et al (2011) to be more effective at reducing pollution from container ships than from passenger ferries. The economic value added by the port also varies depending on the function, with OECD (2013) showing the economic value added by cruise ports to be small when compared to the value added by cargo and industrial facilities. The varying economic benefits of ports may influence decision making when methods to reduce pollution are proposed. Therefore it is important to have an improved system for grouping ports in order to further investigate what influences pollution levels, as well as to improve understanding of which pollution reduction methods may be best suited to certain types of ports.

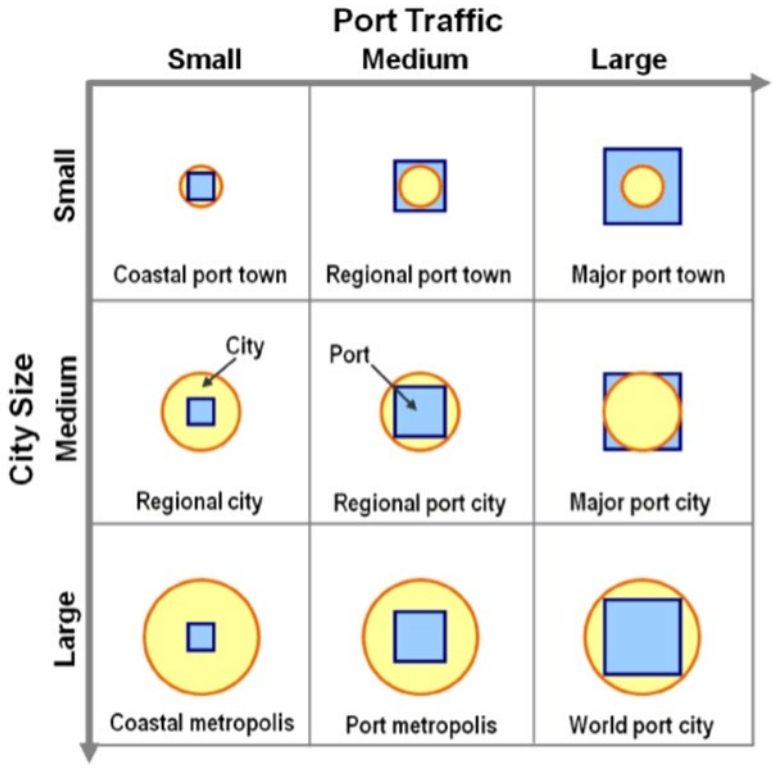

Figure 1: Existing typology of Port Cities (OECD 2013). This demonstrates the potential outcomes of combinations of different sized cities (yellow circle) hosting ports of different sizes (blue square).

Figure 1 is an example of an existing classification system used by the OECD for port cities, which groups port cities by city size and port traffic volume. Whilst this system has its uses, it is unable to differentiate between different types of ports such as passenger ports or cargo ports, which may create different levels of pollution. This system may also place ports which are very different in terms of function together. There is also a lack of information in regard to how small, medium and large for each group are measured, without which the definitions are somewhat arbitrary. An improved classification system with clearly defined groupings may offer a greater insight into how ports vary and how these differences influence levels of pollution.

The purpose of this research is to investigate the following aim:

1. What are the common groupings of ports?

Which is intended to lead on to further work addressing the subsequent aims:

2. Which port characteristics influence levels of maritime pollution?
3. Are port cities associated with elevated levels of pollution?

Methods

In order to better understand the key drivers of pollution in port cities, a classification

system was developed using publically available data. The following variables were collected:

- Cargo Tonnage and annual throughput (TEU)
- Passenger numbers (Cruise and ferry separately)
- Urban area size, population and population density
- Developmental indices
- World Bank quality of port infrastructure index
- Inner and outer urban area urbanization
- Distance to other ports
- Adherence to emissions restrictions (MARPOL I-VI, Ballast water and anti-fouling conventions)
- Maximum vessel size
- Shelter afforded
- Port type (Coastal, River etc.)
- Climate zone (Koppen-Gieger classification)
- Facilities present (Airport, railway, bunkering etc)
- Types of vessels handled (Container, ro/ro, dry bulk, cruise etc)

Information on these variables was collected for 200 large port cities selected from Lloyd's list top 100 container ports, AAPA world port rankings, regional lists of large ports and members of Port-City Universities League.

When necessary TEU was converted into cargo tonnage using a value for the maximum potential weight per TEU. This value is 21,600 per TEU (Emase 2018). This will not be as accurate as having recorded cargo tonnage values, however it should allow a sufficient understanding of the freight volume. Cruise passenger numbers were also estimated when necessary from recorded cruise ship calls in port, using an average number of passengers per vessel of 3000 (Cruisemapper 2018). This was required for many of the ports in Asia.

Cluster analysis was then used to create groupings of common characteristics using all or different selections of the collected data. In addition to this, Microsoft Excel was also used to sort data by selected variables and then subjective judgements made in regard to suitable groupings based on the range of values include in each data set.

Provisional Results

Initial cluster analysis of the data revealed that grouping ports based on all of the variables collected does not produce any meaningful classification system. Using only a small number of variables has so far produced more meaningful outcomes.

Cruise passenger numbers and cargo tonnage were chosen as potential variables to use to group the data, due to the fact cruise ships and container ships have both been highlighted as providing a large percentage of emissions within ports. The OECD (2013) stated that in a port with container ships making 26% of total port calls, container ships were responsible for 33.6% of NO_x emissions. In addition to this if cruise ships constituted 14% of total port calls they contributed 32.5% of CO_2 emissions within the port area. This suggests that cruise ships and container ships create large environmental impacts in port areas. Cargo tonnage was chosen due to greater data availability, with TEU being converted into cargo tonnage were possible.

Table 1: Range of passenger number and cargo tonnage values used for each group. This shows how ports are assigned to each group.

Passenger group	Range of values (Cruise passenger numbers)	Freight Group	Range of values (Kilotons of cargo tonnage)
A	1 million +	5	300,000 +
B	500,000 – 999,999	4	200,000 – 299,999
C	200,000 – 499,999	3	100,000-199,999
D	100,000-199,999	2	50,000-99,999
E	0-99,999	1	0-49,999

A potential system based on groupings of passenger numbers and groupings of cargo tonnage appears to offer a greater level of differentiation between port types than the system illustrated in figure 1. This separates ports not only by their size, but also by the function they provide. The proposed ranges of values for each group are shown in table 1. These values were decided upon after subjectively assessing the range of possible values found in the data set. This system uses 5 groupings for passenger numbers and 5 groupings for freight volume, producing 25 combination groups. For this system, whichever is largest between TEU converted into cargo tonnage and recorded cargo tonnage was used.

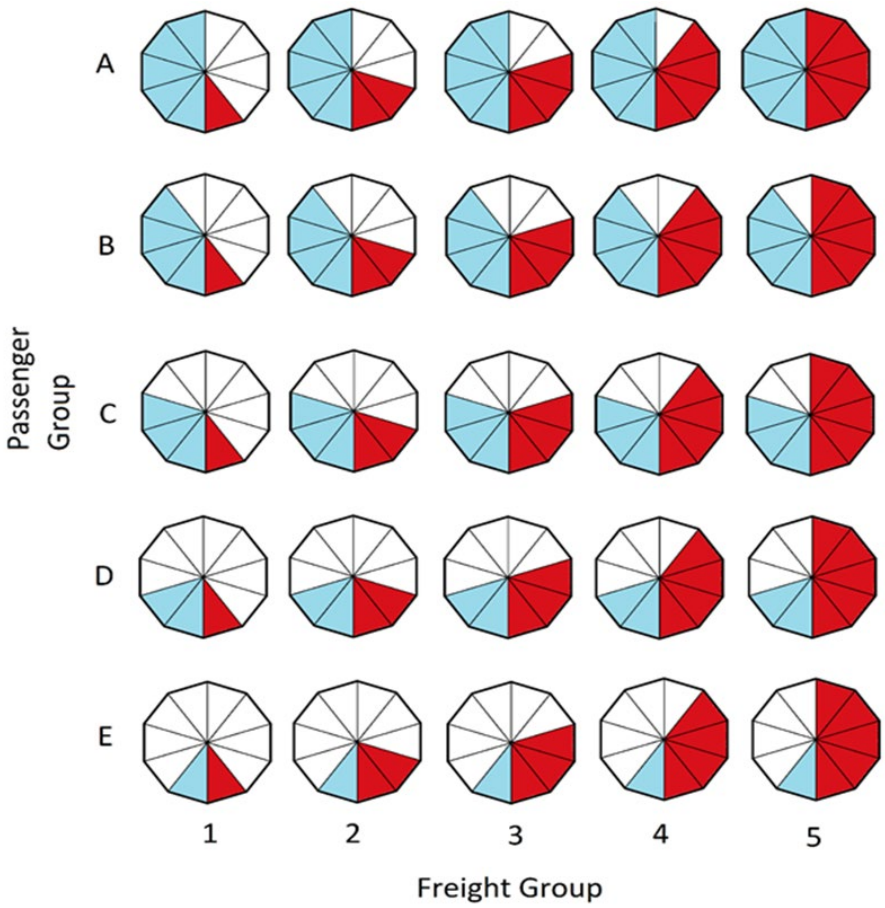

Figure 2: A potential system for port classification. Blue illustrates passenger number grouping (A to E) and red illustrates freight grouping (1 to 5).

Figure 2 illustrates visually how each group differs in terms of passenger numbers and cargo tonnage.

Table 2: Selected examples of ports located within each group

	Freight group 1	**Freight group 2**	**Freight group 3**	**Freight group 4**	**Freight group 5**
Cruise passenger group A	Miami Nassau	Southampton Marseille	New York/ New Jersey	None in port set	Shanghai Singapore
Cruise passenger group B	Lisbon Copenhagen	Amsterdam St Petersburg	Vancouver Hamburg	None in port set	Busan Hong Kong
Cruise	Da Nang	Valencia	Yokohama	Port Klang	Tianjin

passenger group C	Nagasaki	Abu Dhabi	Incheon Ho Chi Minh city		
Cruise passenger group D	Sanya Kagoshima	Kobe	None in port set	Xiamen Antwerp	Guangzhou
Cruise Passenger group E	Alexandria Valparaiso	Chennai Felixstowe	Nagoya Ulsan	Yeosu-Gwangyang Kaohsiung	Ningbo-Zhoushan Dalian

This system successfully separates large ports of varying function from each other, however its uses are limited in regard to smaller ports, which may all fall into the same grouping (i.e. Freight Group 1, Passenger Group E). An additional complimentary system could also be developed for small ports if this system is developed further. This would expand the usage of this system which is at present only useful for large ports.

Some of the groups in this system contain few or no ports, however this may just be a reflection of the fact these particular combinations of passenger numbers and cargo tonnage are unusual. Using fewer groups could be considered, however this produces less separation and leads to groupings of ports with vastly different passenger and freight numbers. This is due to the fact there are a small number of ports with values far greater than the majority of other ports used in this system. The groups which have no ports within them may not be useful at present, however if the system is to remain useful it should be able to continue to categorise ports in the future. It is possible these groups will contain ports in the future. A further possible method for grouping ports could be by grouping them in terms of the position in the data set, such as pentiles.

This system is also limited by data availability, with not all of the data being available for all of the 200 ports. Further data collection will take place to make the dataset as complete as possible

Next Steps

The cruise/cargo classification system proposed in figure 2 will be improved by an iterative method using different numbers of clusters and different ranges of values until a useful system is achieved. Ferry passenger numbers could also be added if it is possible to find a method to directly compare ferry and cruise passenger numbers. In addition to

this, cluster analysis of the data will continue and further systems considered, until a final system for clustering ports has been chosen.

The final system will be presented to a range of experts in port-related industries as part of a workshop in Southampton. In addition to this, it will also be presented to the Ports and Maritime group of a leading engineering consultancy at a workshop in Copenhagen. The final system will be decided once it can be approved by industry experts attending these workshops.

After this, groups will be investigated in more detail considering the other variables presented in the methods, with ports chosen from each group being investigated in more detail. This will provide an insight into the common characteristics of each group. This will then enable further work investigating how these characteristics influence maritime pollution levels within and between groups.

Conclusions

Initial results suggest a suitable way to categorise large ports may be to use passenger numbers and cargo tonnage. This method produces groupings which separate ports by size and function more effectively than existing widely used systems. Future work will focus on the refinement of these categories, the introduction of study of further categories, and research into understanding characteristic differences between ports within the same clusters and different clusters.

References

Castells Sanabra M., Usabiaga Santamaría J. J., Martínez De Osés F. X. (2013), "Manoeuvering and hotelling external costs: enough for alternative energy sources?" Maritime Policy and Management. The flagship journal of international shipping and port research, pp. 1-19

Cruisemapper, 2018, Cruise ship passenger capacity, available at http://www.cruisemapper.com/wiki/761-cruise-ship-passenger-capacity-ratings, accessed, 1/09/2018

Emase, 2018, Shipping containers, available at https://web.archive.org/web/20090420143514/http://emase.co.uk/data/cont.html, accessed 1/09/2018

Lindstad, H, Asbjornslett, B, E, Stromman, A, H, 2011, Reductions in greenhouse gas emissions and cost by shipping at lower speeds, Energy Policy, Vol 39, issue 6, pp 3456-3464

Miola A., Paccagnan V., Mannino I., Massarutto A. Perujo A., Turvani M. (2009), External Costs of Transportation. Case Study: Maritime Transport. European Commission, Joint Research Centre, Institute for Environment and Sustainability, pp. 1-109

OECD, 2013, The competitiveness of global port cities: synthesis report, available at http://www.oecd.org/cfe/regional-policy/Competitiveness-of-Global-Port-Cities-Synthesis-Report.pdf accessed 1/09/2018

Numerical Prediction of the Oil Spill Triggered from Tsunami at the Japan Costal Area with Chemical Complex

Youhei Takagi[1]
1 Department of System Design for Ocean-Space, Graduate School of Engineering
Yokohama National University
79-5 Tokiwadai, Hodogaya-ku, Yokohama, Kanagawa 240-8501, Japan
takagi-yohei-hn@ynu.ac.jp

Abstract: The large earthquake due to the Nankai-trough assumes to occur at Japan in near future. Tsunami caused by such a large earthquake gives large damage to the costal area in Japan. Ocean countries with large chemical complex at costal area have the risk of oil spill triggered from tsunami, and we have to estimate the damage from possible large earthquake and tsunami and develop an innovative technology for reducing the disaster damage. In the present study, we have developed the simulation model to numerically predict the oil spill behavior at the Japan costal area. By using the developed tsunami and oil-spill simulator, we investigated the risk of oil spill in the Osaka Bay area. The Osaka Bay has many small oil tanks and some large ones. From our numerical simulation under the scenario of the Nankai-Trough earthquake, it was found that wide city and business towns will be suffered from the oil spill. To reduce the damage from the oil spill, new resilient technologies are now supposed and developed.

Keywords: Tsunami, Oil Spill, Numerical Simulation

Introduction

Oil spill from tanker, oil/gas platform, and chemical complex is a very serious problem that affects environment and economy at marine and coastal area. At 2011, a huge earthquake occurred at Japan east area and a large tsunami arrived at the Tohoku coastal area. The tsunami washed away many buildings and structures, and many peoples were missed. At the Kesen-numa Bay area, 22 oil storage tanks were broken and collapsed and the oil of 11,700 kL was spilled[1]. The spilled oil was burned on the sea surface and the tsunami-triggered fire disaster was observed for the first time at Japan. In the future, the large earthquake due to the Nankai-trough assumes to occur at the Pacific Ocean near Japan, and we have to reduce the risk of oil spill and fire disaster by tsunami when such a large earthquake will happen. The Osaka Bay is one of the large ports with chemical complexes and many disaster risks are estimated by some researchers in recent years. However, the risk of oil spill is hardly discussed. In the present study, we have developed the hybrid numerical model combining oil parcel tracing with tsunami wave simulator in a wide area and estimated the damage due to oil spill in the Osaka Bay area.

Numerical model

Tsunami firstly occurs offshore and gradually approach coast, and finally break over land. Therefore, the phenomena in tsunami are multi-scale and muli-physics. Our numerical model consists of two calculations, that is, the two-dimensional tsunami simulator and the oil tracking from the broken storage tanks.

The tsunami simulator was originally developed by Prof. Tomita and co-researchers in the Port and Airport Research Institute and the simulation code is named as the Storm Surge and Tsunami Simulator in Oceans and Costal area (STOC)[2]. The governing equations for solving tsunami motion are the continuity and Navier-Stokes equations. The order of the Navier-Stokes equation is reduced to two-dimension, and the approximated equation with the static pressure assumption is actually calculated in the simulator. These governing equations are discretized with the finite difference scheme. The output data from the simulator are velocity, pressure, and surface height at each grid. Because the tsunami calculation is generally conducted in a wide area, the computational grid was a hierarchal multi-grid system and the minimum grid spacing in the nested grid is 50 m. The initial condition of tsunami along the Nankai-trough was given by the fault model proposed from the cabinet office of Japan[3].

After conducting the tsunami simulator, the motion of oil parcel from broken storage tanks is calculated with the velocity data from the STOC. As the dispersed oil droplets are very small compared with the scale of tsunami wave, we treat the cluster of oil droplets as “parcel” and the modeled oil parcel is tracked with the Lagragian method. In this calculation, the convective motion due to tsunami flow and the diffusive effect in the oil parcel are considered. At the initial stage of released oil parcel, the diffusion rate of oil is large since the concentration of oil in a single parcel is high. On the other hand, at the final stage of spilled oil motion, oil is fully dispersed and the diffusion effect becomes very weak.

As shown in Figure 1, the Osaka port has large two industrial parks: North port and Sakai-Senboku areas. The North port area has small oil tanks, on the other hand, the Sakai-Senboku area has large tanks. The maximum amount of spilled oil from the storage tanks in each area under the worst scenario of the Nankai-trough earthquake was estimated by the Osaka prefecture, and we used the published data as the initial conditions of our simulation. By using the aerial photographic map shown in Figure 2, the location of storage tanks was manually checked, and we determined that the release points of oil parcel in our calculation were 8 points at the North port area and 4 points at the Sakai-Senboku area. The total amount of spilled oil in the Osaka port was 32,000 kL and the number of oil parcels used in the present simulation was 5000.

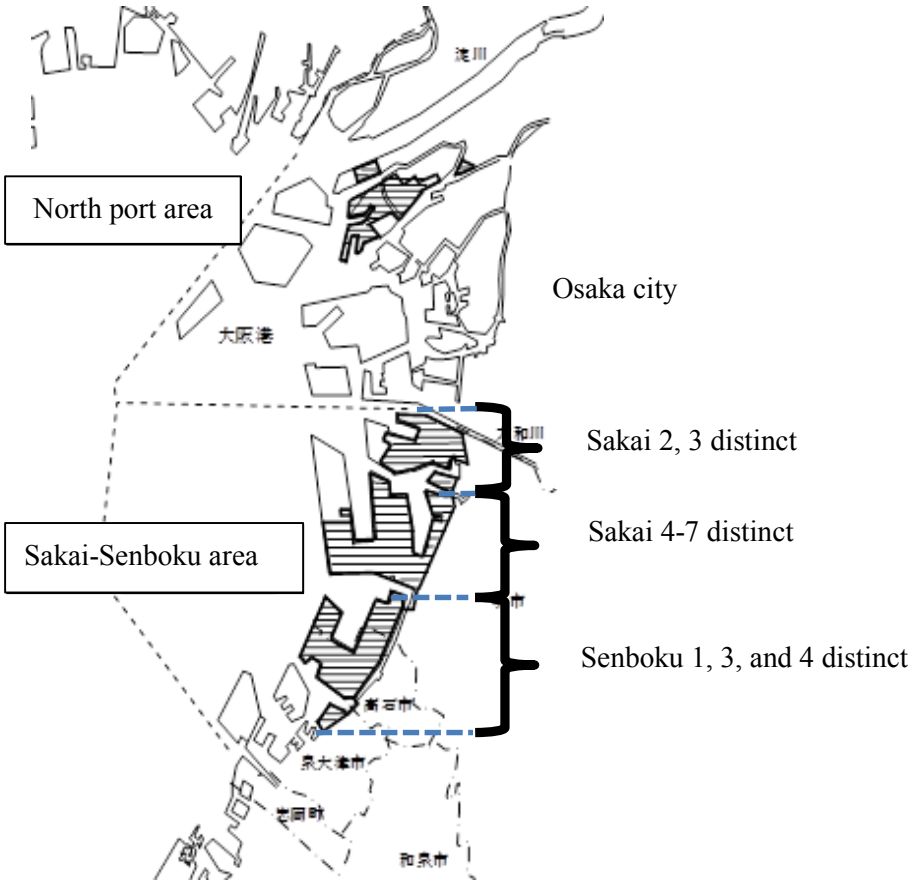

Figure 1. The industrial parks in the Osaka Bay area. The hatched areas are the tank-clustered regions.

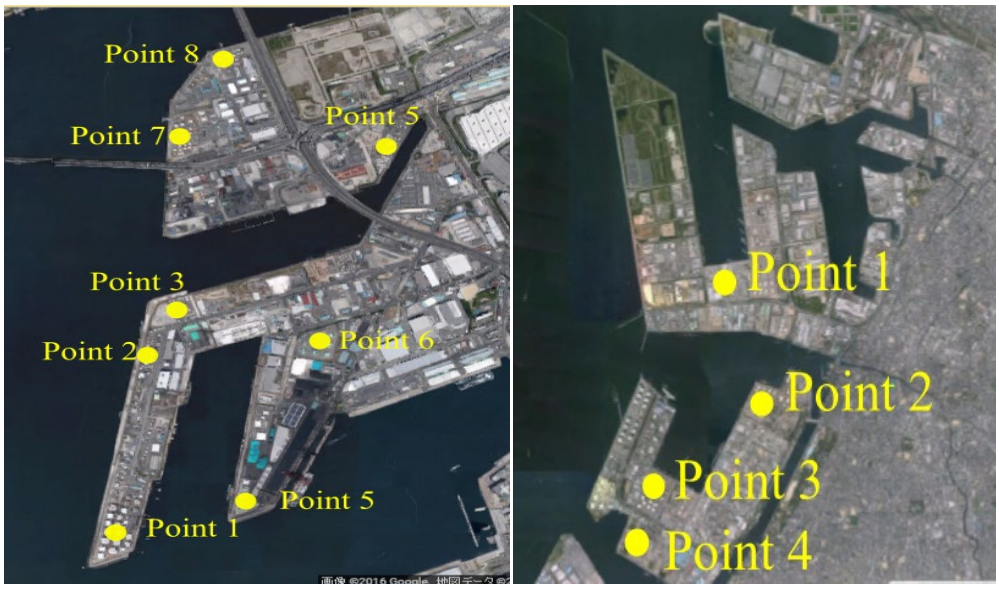

Figure 2. The released points of oil parcels in the calculation: (left) North port, (right) Sakai- Senboku.

Results and discussion

Firstly we carried out the tsunami simulation assuming the Nankai-trough earthquake. A tsunami wave arrived at the Osaka bay area after about 2 hours of the earthquake oscillation and the averaged wave height at the industrial parks shown in Figure 2 was about 2.4 meters. These estimations of tsunami motion were well agreed with other numerical predictions by researchers and local governments.

By using the generated tsunami data, the spilled oil motion from the clustered storage tanks was calculated after the tsunami arrival. When the present fault model for the Nankai-trough was used, the two peaks of tunami wave height were observed and the oil parcel tracking was continued until 90 minutes after the first wave arrival. Figures 3 and 4 are the calculated oil parcel positions after 70 minutes after the first wave arrival in the North port and Sakai-Senboku areas, respectively. At the North port area shown in Figure 3, many oil parcels arrived inside the costal area, it was found that the business city such as Namba was polluted and had the risk of fire disaster as same as the 2011 great Japan earthquake. In addition, the half of spilled oil were flowed out into the sea and might give the risks to tankers and container ships staying in the evacuation area of Osaka bay. On the other hand, at the Sakai-Senboku area shown in Figure 4, the oil parcels were not widely diffused on the land because this region has the Uemachi fault in the north-south direction. However, the risk of fire disaster was very large at the oil-accumulated points. As same as Figure 3, many oil parcels were flowed on the sea surface, the oil-polluted regions in the sea might be expanded if the sea current was rapidly changed.

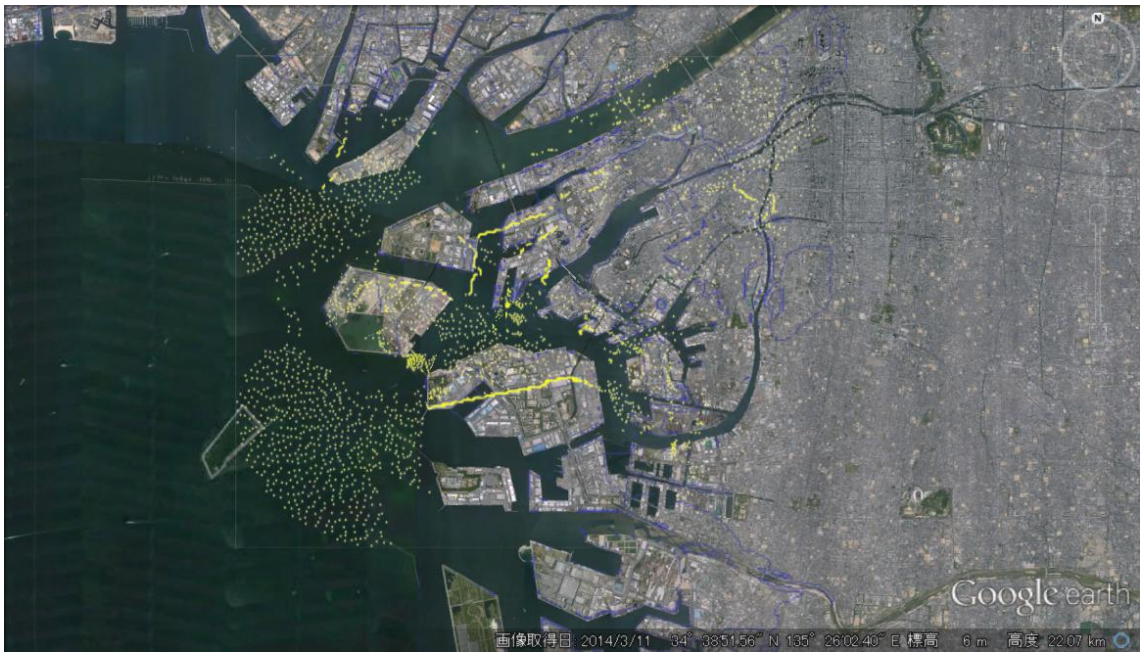

Figure 3. The distribution of oil parcels after 70 minutes after the first wave arrival in the North port area. The oil parcels colored in yellow are plotted on the aerial map.

Figure 4. The distribution oil of parcels after 70 minutes after the first wave arrival in the Sakai-Senboku area. The oil parcels colored in yellow are plotted on the aerial map.

Conclusions

We successfully developed the hybrid simulation model for predicting the oil spill triggered from tsunami. In the present study, we used the worst scenario of the Nankai-trough earthquake and the total amount of spilled oil from the broken storage tanks was maximum value. The present simulator is useful for estimating the risk of oil spill and related fire disaster at the coastal area, and we can investigate the risk for other ports and bay areas at Japan. In order to improve the numerical accuracy of the prediction, we are developing a new model for capturing the three-dimensional fluid physics around the storage tanks with the advanced numerical schemes and the high-performance computer resources.

References

[1] S. Zama, H. Nishi, K. Hayatama, M. Yamada, H. Yoshihara, and Y. Ogawa (2012) “On Damage of Oil Storage Tanks due to the 2011 off the Pacific Coast of Tohoku Earthquake (Mw9.0) Japan”, WCEE2012.

[2] T. Tomita, K. Honda, T. Kakinuma (2007) “Application of Three-dimensional Tsunami Simulator to Estimation of Tsunami Behavior around Structures”, Proc. 30th Int. Conf. Coastal Eng.: 1677-1688.

[3] The disaster prevention countermeasure for the Nankai-trough earthquake, The Cabinet Office, the Government of Japan (in Japanese), http://www.bousai.go.jp/jishin/nankai/index.html

Microscale toxicity testing with the marine macroalga *Ulva pertusa*

Jihae Park[1], Murray T. Brown[2], Stephen Depuydt[1], Hojun Lee[3], Soyeon Choi[3], Geonhee Kim[3], Jonghwa Shin[4], Taejun Han[1,3*]

[1]Ghent University Global Campus, Songdomunhwaro 119, Incheon 21985, South Korea, [2]School of Biological and Marine Sciences, University of Plymouth, Plymouth PL4 8AA, United Kingdom, [3]Department of Marine Science, Incheon National University, Academyro119, Incheon 22012, South Korea, [4]Department of Urban Policy and Administration, Incheon National University, Academyro 119, Incheon 22012, South Korea

Abstract: The global significance of detecting toxicants in the environment and assessing their impacts on biota has resulted in the development and adoption of a range of methodologies. A toxicity test based on the inhibition of reproduction in a green seaweed, *Ulva pertusa*, provides many practical advantages over other currently employed techniques including no specialist expertise required, cost- and time effectiveness, and the high sensitivity. Since reproduction is the means by which population recruitment is facilitated, the measured endpoint is also ecologically significant. The *Ulva* reproduction bioassay would be a valuable addition to the existing suite of tests routinely used to monitor coastal and estuarine ecosystems.

Keywords: Bioassay; reproduction; *Ulva pertusa*

Introduction

It was once thought that the solution to pollution was dilution and that marine environments, provided convenient, effective and resilient locations for disposal of anthropogenic-derived wastes. However, this was not the case with coastal waters constantly under threat from the thousands of chemicals derived annually from industrial and municipal sources. To formulate effective protective legislation for marine habitats the ecological risks posed by toxicants need to be evaluated by assessing the biological responses of the biota [1, 2].

The global awareness of the necessity of detecting toxicants in the environment and assessing their impacts on biota has resulted in the development and adoption of a range of methodologies.

Conventional chemical analysis has several drawbacks including the complexity of the procedures for preparing samples, the need for expensive analytical equipment and interference from secondary pollutants during analysis. In addition, this approach fails to account for temporal changes in exposure or the interactive effects of pollutants, nor does it provide ecologically significant information [3].

To compensate for these limitations, various biological assays have been developed to provide information on pollutant-induced toxic effects that can be used to assess environmental risks [4]. As early as 1960's fish was the first organism adopted as a test organism for bioassays, but, from the 1980's onwards, a large number of bioassays

using microorganisms, invertebrates, fish and algae are increasingly being used in toxicity testing [5, 6].

Seaweeds play an important role in marine ecosystems as primary producers, providers of habitat and nursery grounds for fish and invertebrates. Some ecotoxicity testing methods were developed with seaweed including reproduction tests with the red seaweed, Ceramiun strictum, Champia parvula and the brown seaweed, *Fucus spiralis*, *Hormisira bankii*, *Saccharina latissima* (formerly *Laminaria saccharina*) and *Macrocystis pyrifera* and growth tests with the red seaweed *Gracilaria tenuistipitata* and *Ceramium* spp. [7-12]. As for the green seaweed, fewer test methods have been developed, while it is notable that the number of seaweed species used for toxicity testing was 65 of which only 11 species are green seaweeds [11].

Ulva spp. are important representatives of seaweed communities in coastal waters that are under threat from the frequent inundations of toxic waste derived from industrial and municipal sources. These seaweeds are primary producers constituting the basis of costal ecosystem and, moreover, provide shelter and habitats for other marine organisms; they are also important natural sources of food and pharmaceutical products.

In the life cycle of *Ulva*, reproduction is a critical process by which populations perpetuate, and disturbance of this process can cause failure in recruitment, leading to the disappearance of the population and ultimately to modifications in a whole community structure and dynamics in an ecosystem where *Ulva* belongs to.

The *Ulva* toxicity test to be introduced in the present study provides many practical advantages over other currently employed techniques. No specialist expertise is required. The test is cost- and time effective, since it only requires a cell plate, a small volume of water and takes a total of approximately 3 h to conduct around a 96 h incubation period. The sensitivity of the *Ulva* method is similar to, and in many cases better than, commonly available or well established bioassay methods, and since reproduction is the means by which population recruitment is facilitated, the measured endpoint being ecologically significant cannot be disputed. In addition, field-collected samples of unialgal *Ulva* plants can easily be held and acclimated in a holding tank for 1 to 2 month(s), and artificial induction of reproduction in a laboratory is easily achieved using vegetative thalli, allowing all year round testing to be performed. The *Ulva* reproduction bioassay would be a valuable addition to the existing suite of tests routinely used to monitor coastal and estuarine ecosystems.

Principle of the *Ulva pertusa* reproduction bioassay

Ulva spp. have an interesting reproductive pattern involving direct transformation of vegetative cells into reproductive cells via generative divisions. One of the most striking features during progression of reproduction in *Ulva* is a visible change in color of the thallus from yellow-green when in a vegetative state to dark olive when reproductive, to white after release of reproductive cells (Fig. 1). Thallus disks of *U. pertusa* are allowed

to grow as unialgal and static cultures in different concentrations of the test sample for 96 h, and the extent of reproduction is determined by image analysis measurements, and/or visual inspection of the proportion of the reproductive area out of the total area.

Summary of test methods

The protocol for the methods using the reproduction inhibition of *U. pertusa* is summarized in Table 1.

First, the optimal environmental conditions for undertaking the test are 60-200 μmol photons m^{-2} s^{-1}, 25-35 psu and 15-20^{o}C for photon irradiance, salinity and temperature, respectively. Then, to test the protocol, disks of *U. pertusa* are exposed to toxicants concerned. From the test results EC_{50} values of the individual toxicants are derived.

Percent reproduction is assessed from the proportion of the disk area with a color change out of the total thallus disk area. Visual evaluation of reproduction can be rated on the scale: 0 % denoted vegetative state (yellow-green color), 25 %, 50 %, 75 %, and 100 % denoted reproductive state (dark olive and white color) in less than one quarter, a quarter to a half, a half to three quarters, and more than three quarters of the total thallus disk area (see Fig. 2). However, this can be done more objectively using a 16 grid measurement template. At the end of the 96 h exposure period, determine the color change of each of the 16 grid areas of each microplate used. A definitive rating is to be determined of each grid area based on the greatest color response within each area. The scale outlined in Figures 3-5 can be used to quantify the percentage of color change.

A novel method using the green macroalga *U. pertusa* can be used for the toxicity test on more than 75 different environmental samples of contaminants, including metals, volatile organic compounds, herbicides, oils, dispersants, slag-waste, etc. [13-17].

Tables and Figures

Table 1. Summary of test conditions and test acceptability criteria for marine seaweed *Ulva pertusa* reproduction inhibition toxicity tests.

Parameters	Test conditions
Test type	static, non-renewal
Endpoint	reproduction inhibition (EC_{50})
Test organism	*Ulva pertusa*
Test duration	96 h
Test temperature	15±2 °C
Test salinity	25-3 5‰ (32 ‰ recommended)
Light quality	cool white fluorescent lighting
Light intensity	80-100 µmol m^{-2} s^{-1} (approx. 5,000-6,400 lux)
Photoperiod	12:12 h L:D
Test vessel	24-well cell plate (Ø 15 mm)
Test solution volume	2.5 ml
Test specimen/well	4 disk (Ø 4 mm each) for image analysis or 1 disk (Ø 10 mm) for visible inspection
Dilution water	nutrient enriched artificial sea water
Renewal of test solution	none
Aeration	none
Culture media	nutrient enriched artificial sea water
Test concentrations	minimum 4+ control
Number of replicates per concentration	4 (depending on statistical analysis chosen)
Sample volume required	50-100 ml depending on test volume
Test acceptability criterion	> 80 % of reproduction in control

Figure 1. Indices of reproductive percentage of *Ulva* based on order classification of the proportion of reproductive area with thallus color change. It is noticeable that the color ("creamier white") of dead disks due to high toxicity compounds is different from that ("ivory white") of the thallus having discharged reproductive cells (adapted from Han et al. 2007[17]).

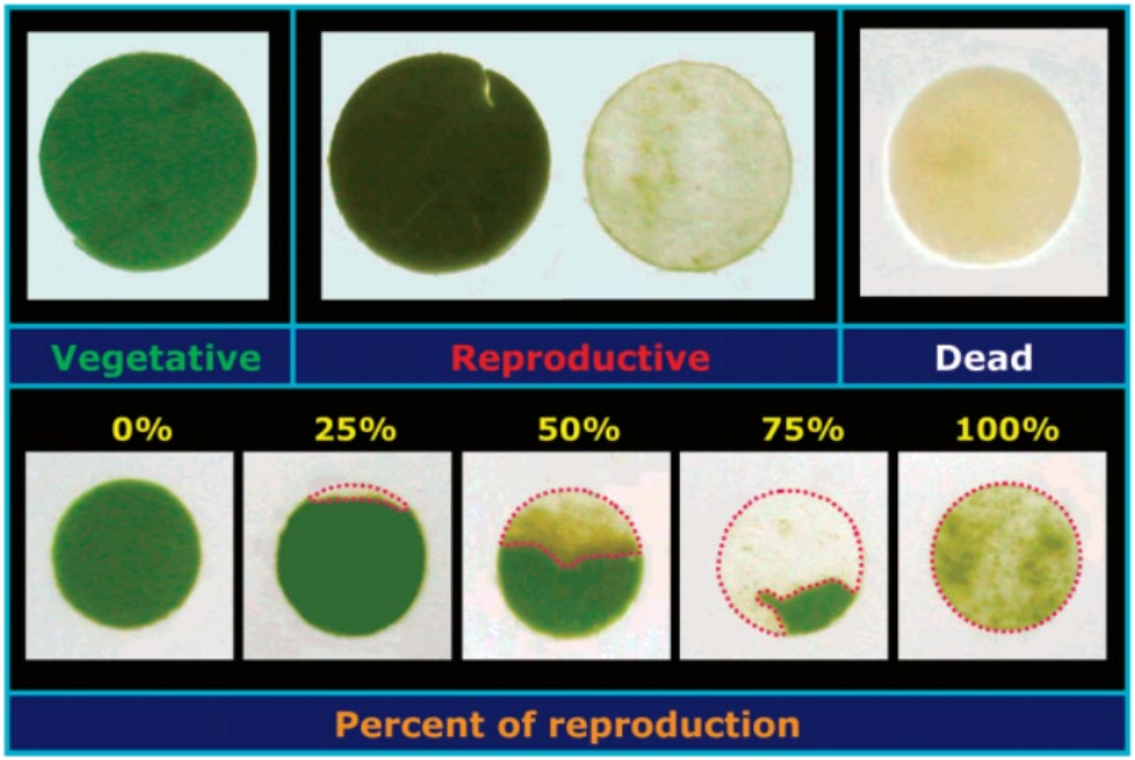

Figure 2. A photograph of 4 replicate disks (R1-4) exposed to different concentrations of toxicant (Con: control, T1-5: concentrations of toxicants from lower to higher concentrations, respectively).

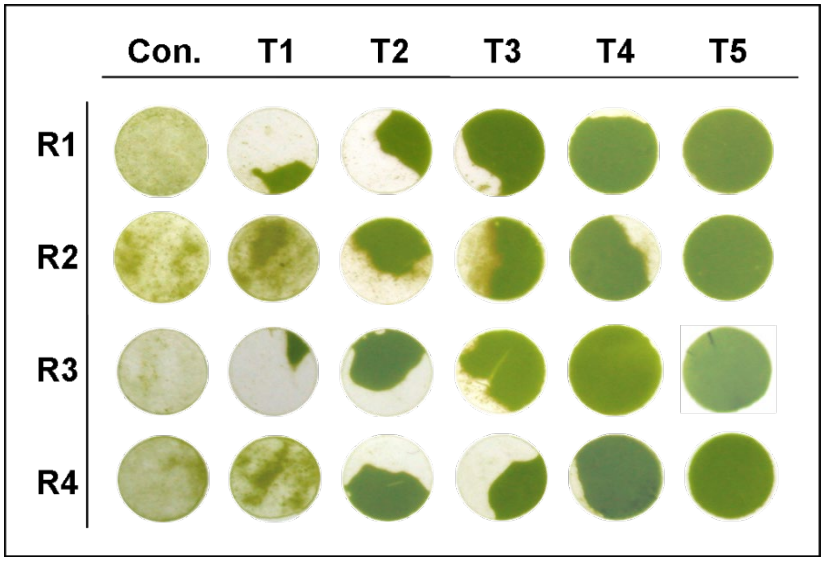

Figure 3. A photograph of a 16-grid measurement film on the surface of 4 replicate disks (R1-4) exposed to different concentrations of toxicant (Con: control, T1-5: concentrations of toxicants from lower to higher concentrations, respectively).

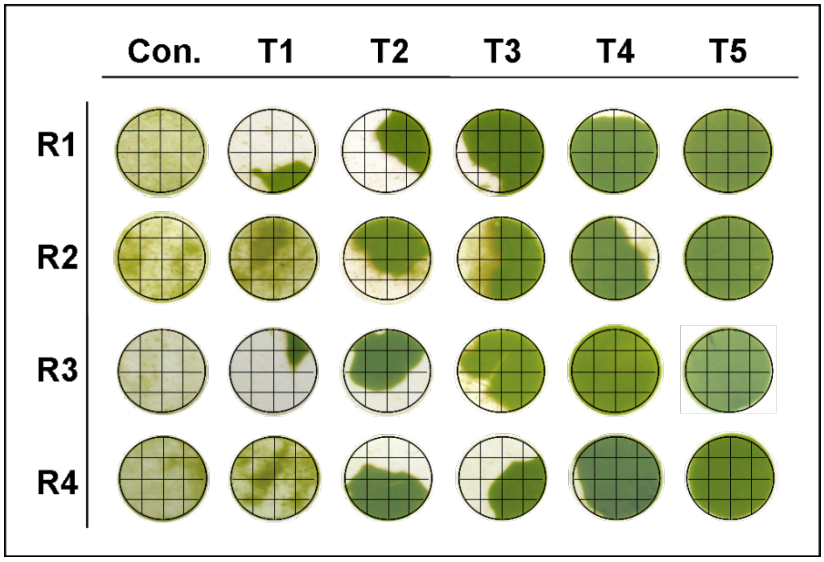

Figure 4. A schematic drawing of the number of grids with a colour change on the 4 replicate disks (R1-4) exposed to different concentrations of toxicant (Con: control, T1-5: concentrations of toxicants from lower to higher concentrations, respectively). The numbers are indicated in the circles. When counting the number of grids, a colour change over a half the grid size is considered as a full grid whereas less than a half is counted as a grid with no colour change.

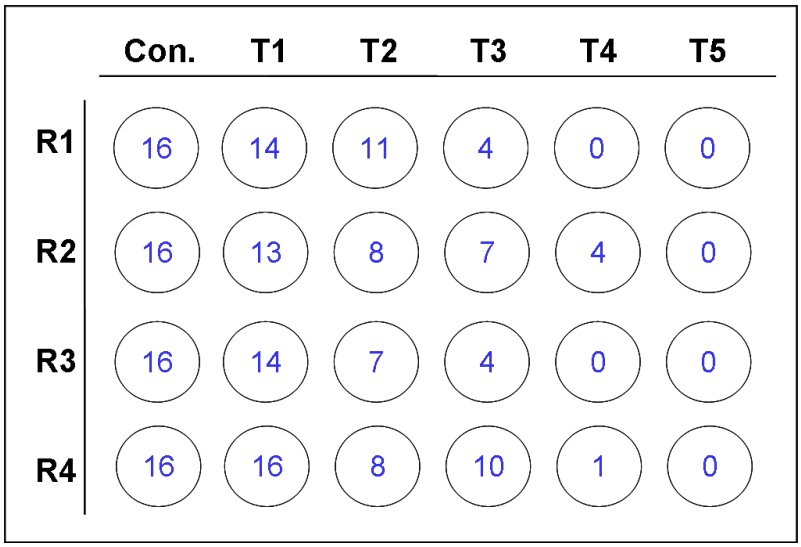

Figure 5. A schematic drawing of the percentage of disk areas with colour change on 4 replicate disks (R1-4) exposed to different concentrations of toxicant (Con: control, T1-5: concentrations of toxicants from lower to higher concentrations, respectively). The percentage is calculated based on the Table provided on the right hand side.

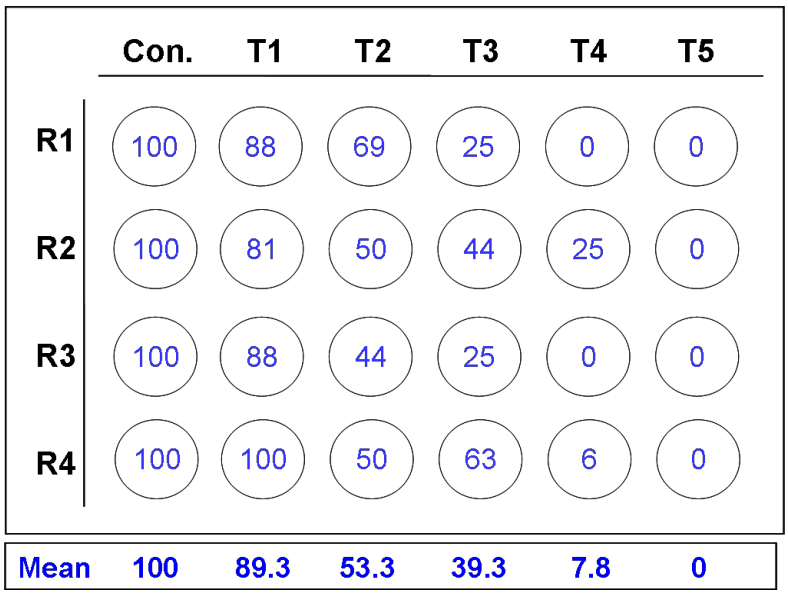

NUMBER OF OBSERVED AREAS	PERCENTAGE OF AREA WITH COLOR CHANGE(%)
0	0
1	6
2	13
3	19
4	25
5	31
6	38
7	44
8	50
9	56
10	63
11	69
12	75
13	81
14	88
15	94
16	100

Conclusions

The key to the process of creating eco-toxicological techniques is the selection of appropriate test species, which are ideal characteristics of the species, such as habitat fixation, broadness of distribution, ease of harvesting, and sensitivity of toxic reactions.
Attractive features of the *Ulva* method include simplicity of testing, miniaturization, high sensitivity and resolution power of sample-specific toxicity, cost-effectiveness and small sample volume and bench space requirements.
There are many advantages, but several pending issues therein to be solved in the future. Firstly, the *Ulva* method has not been confirmed to have applications to other *Ulva* species than *U. pertusa*. As there are taxonomic difficulties to identify *Ulva* species, it may require some experts' help to find out *U. pertusa* on the beach. Secondly, the shelf time for *Ulva* disks and thalli is not long enough, and further developments may be required for construction of a complete kit system of the *Ulva* method. Thirdly, this method employs a technique to quantify percentage reproduction by measuring the area of color change on a given area of thallus disk, which is liable to subjectivity relating to skill levels of personnel and variability of instruments etc. A more objective way of quantifying the reproductive status of the seaweed awaits being developed.
Overall, however, the *Ulva* system seems to be a good method of determining the toxicity of a variety of water samples including wastewaters.

References

1. Mallick, N., Rai, L. 2002. "Physiological responses of non-vascular plants to heavy metals." In: Prasad, M.N.V., Strzałka K. (eds), Physiology and Biochemistry of Metal Toxicity and Tolerance in Plants, Springer, Dordrecht, pp. 111-47.
2. Bidwell, J.R., Wheeler, K.W., Burridge, T.R. 1998. "Toxicant effects on the zoospore stage of the marine macroalga *Ecklonia radiata* (Phaeophyta: Laminariales)." Marine Ecology Progress Series, 163:259-65.
3. Han, Y.-S., Kumar, A.S., Han, T. 2009. "Comparison of metal toxicity bioassays based on inhibition of sporulation and spore release in *Ulva pertusa*." Toxicology and Environmental Health Sciences, 1:24-31.
4. Eullaffroy, P., Vernet, G. 2003. "The F684/F735 chlorophyll fluorescence ratio: a potential tool for rapid detection and determination of herbicide phytotoxicity in algae." Water Research, 37(9):1983-90.
5. Klaine, S.J., Lewis, M.A. 1995. "Algal and Plant Toxicity Testing." In: Hoffman, D.J., Rattner, B.A., Burton Jr., G.A., Cairns Jr., J. (eds), Handbook of Ecotoxicology, Lewis Publishers, Boca Raton, pp. 163-84.
6. Williams, T., Hutchinson, T., Roberts, G., Coleman, C. 1993. "The assessment of industrial effluent toxicity using aquatic microorganisms, invertebrates and fish." Science of the Total Environment, 134:1129-41.
7. Eklund, B.T., Kautsky, L. 2003. "Review on toxicity testing with marine macroalgae and the

need for method standardization—exemplified with copper and phenol." Marine Pollution Bulletin, 46(2):171-81.

8. USEPA. 1998. "Short-term methods for estimating the chronic toxicity of effluents and receiving waters to marine and estuarine organisms." Environmental Protection Agency of USA, Contract No.: EPA/600/491/003, Method 1009.0.

9. Haglund, K., Björklund, M., Gunnare, S., Sandberg, A., Olander, U., Pedersén, M. 1996. "New method for toxicity assessment in marine and brackish environments using the macroalga *Gracilaria tenuistipitata* (Gracilariales, Rhodophyta)." Hydrobiologia, 326:317-25.

10. Thursby, G., Steele, R. 1995. "Sexual reproduction tests with marine seaweeds (macroalgae)." In: Rand, G.M. (eds), Fundamentals of aquatic toxicology effects, environmental fate, and risk assessment, Taylor and Francis, Washington, DC, pp. 171-88.

11. Eklund, B.T. 1998. "Aquatic primary producers in toxicity testing: emphasis on the macroalga *Ceramium strictum*." Stockholm University, Stockholm.

12. Hooten, R.L., Carr, R.S. 1998. "Development and application of a marine sediment pore-water toxicity test using *Ulva fasciata* zoospores." Environmental Toxicology and Chemistry, 17(5):932-40.

13. Han, T., Kong, J.-A., Brown, M.T. 2009. "Aquatic toxicity tests of *Ulva pertusa* Kjellman (Ulvales, Chlorophyta) using spore germination and gametophyte growth." European Journal of Phycology, 44(3):357-63.

14. Yoo, J., Ahn, B., Oh, J.-J., Han, T., Kim, W.-K., Kim, S., Jung, J. 2013. "Identification of toxicity variations in a stream affected by industrial effluents using *Daphnia magna* and *Ulva pertusa*." Journal of Hazardous Materials, 260:1042-9.

15. Han, T., Han, Y.-S., Park, C.Y., Jun, Y.S., Kwon, M.J., Kang, S.-H., Brown, M.T. 2008. "Spore release by the green alga *Ulva*: A quantitative assay to evaluate aquatic toxicants." Environmental Pollution, 153(3):699-705.

16. Han, Y.-S., Kang, S.H., Han, T. 2007. "Photosynthesis and photoinhibition of two green macroalgae with contrasting habitats." Journal of Plant Biology, 50(4):410-6.

17. Han, Y.-S., Brown, M.T., Park, G.S., Han, T. 2007. "Evaluating aquatic toxicity by visual inspection of thallus color in the green macroalga *Ulva*: testing a novel bioassay." Environmental Sience and Technology, 41(10):3667-71.

COASTAL PROCESSES IN CUA DAI BEACH: FUTURE INFLUENCE OF SEA LEVEL RISE IN COASTAL AREAS

DANG HOANG ANH, NGUYEN DANH THAO
Department of Port and Coastal Engineering, Ho Chi Minh City University of Technology
268 Ly Thuong Kiet street, Ho Chi Minh City, Viet Nam
E-mail: 81300052@hcmut.edu.vn

Abstract: Vietnam's coastline stretches over 3,260 km with many small islands. Among the country's 63 provinces in which the coastal zone takes over 28 provinces located accounting for 17% of the total country's area. Its coastal area is the home to 20 million inhabitants who main income from tourist and fishing. Therefore, the Vietnam's coastal zone contribute to the national socio-economic development, but the coastline of Vietnam has been suffered severe impacts from both natural forces and human activities that makes it sensitive to erosion and sea level rise. The purpose of this paper is firstly to provide current erosion in Cua Dai Beach Hoi An. Secondly, the effects of sea level rise on coastal defenses in Cua Dai Beach will be analyzed, highlighting the future challenges facing this coastal communities.

Keywords: Cua Dai Beach, Beach Erosion, Sea Level Rise, Coastal Defenses.

1. Introduction

Severe erosion of Cua Dai Beach, with its many resorts, hotels and restaurants, has become a huge issue for Hoi An. The shoreline variation became problematic since the construction of the first buildings along the beach and currently it is costly to adapt to the retreating coastline. Satellites have recorded large changes in the coastline in the past decades, from an onshore migrating sand bank to the formation of a spit and its erosion. There are several contributors to the recent erosion. The following were excluded as significant reasons for the current erosion: changes in watershed, deforestation, land subsidence due to groundwater extraction, tectonic subsidence, changes in near shore underwater conditions and sediment blockage by hydropower dams, although the latter could be of influence in the future. A recent study claimed that Vietnam's coastal problems were triggered by rapid economic development and strong forces of human interference over the last two decades. Coastal erosion issues were closely connected with land use changes which had originally formed through the dynamic equilibrium of erosion by complex forces of sea waves and sand deposition built-up by rivers (Nguyen Danh Thao et al., 2014).

Other problem which Vietnam coastal zone was facing is sea level rise. In 2013, IPCC publish AR5 Report which base on the AR4 and they conducted more study. This research predicts global sea level keep increase in 21th century around 2,0 mm/year and main reasons are the rising temperature to the ice melting. Another reason contributes to GSLR

that we can mention like changing ice in Greenland, Human activity exploited underground water. The IPCC AR4 (IPCC,2007) projected sea levels would reach 0.18 to 0.59m above present by the end of the twenty-first century. More recently, The IPCC AR5 (IPCC, 2013) announced the projections of SLR base on two different approaches, namely Process Based Projections (PBP) and Semi Empirical Projections (SEP). Until 2015, Viet Nam have 180 weather observation station but only the places have full data over 30 years which can be used for calculating the climate change scenario. After checking and considering all the data, Viet Nam have 150 weather station enable to establish climate change in Viet Nam (Resources and Environments Ministry 2016). The result indicate East Sea tend to increase 4,05 $\pm$0.6 mm/year and some station such as Phu Quy predict rise 5.6 mm/year. In addition, Southern Viet Nam next the sea can be rise 5.6 mm/year. SLR rise is a well-known driver for coastal retreat. The SLR at Hoi An is around 6 mm/year (Ministry of Natural Resources and Environment, 2016).

The purpose of this paper is firstly to identify coastal erosion in recent years. Secondly, the effects of sea level rise on coastal defenses in Cua Dai Beach will be analyzed, highlighting the future challenges facing this coastal communities and introduction of countermeasures for coastal management.

2. Study Sites and Methods

The main methods of this study are literature review and field surveys. A wide range of previous documented studies in Vietnam's coastline and central coastal zones were examined. Accordingly, based on the preliminary studies from the historical coastline images that provided by @Google Earth, and from the field survey combine satellite photo we analyzed coastal erosion and processes, and their possible coastal hazards in the studied sites in the future under the scenario of sea level rise. The site investigations were conducted in coastal zone in Hoi An. The field surveys, in combination of meetings with local authorities, were carried out from 2nd to 5th August 2017 to examine the effectiveness of coastal defense (sea dikes, revetments, groins and tidal control works) and topography in Hoi An Beach.

3. Result and Discussions

3.1 General Coastal Erosion in Cua Dai Beach

Cua Dai Beach from North to South is divided by Thu Bon river. Shoreline changes at the North beach since 2004 are spatially recorded in Figure 2. The authors conduct a field survey of this beach during the summer season of August 2017 in order to observe current coastal erosion problems. During the survey, Palm resort (Figure 1) which seems to be one of the most vulnerable area losing land in Hoi An. As a result of this erosion, the beach has progressively moved inland. Although some of resort have tried to stop the erosion by installing a variety of improvised coastal defense measure, such as seawall and rubble mound breakwater. However, it would clearly require stronger revetments made

of rock or concrete but stronger revetments do not solve the problem of sand transport, which might finally undermine the revetments and cause them to collapse.

Figure 1 Number 1 is Cua Dai Beach in 2017 and number 2 is Cua Dai Beach in 2014 (Tanaka et al., 2017)

Severe erosion has occurred along the coastline, in particularly in Cua Dai beach which seats on estuary of Thu Bon river. Therefore, the major driving forces of coastal erosion in Hoi An coastline remain controversial and debatable. This study has investigated the changes of morphology on Cua Dai Beach. Shoreline has been retreated severely in recent years. The erosion of sandy beach is more severe in the zones which are closer to the river mouth. Coastal structures have significant influences on adjacent beaches. The wedge toe of sandy beach on the left side of river mouth propagates to the north.

A series of satellite images taken in 2004, 2011, 2012, 2014, 2015 and 2017 (Figure 2) show the historical evolution of the coastline in this area. Prior to 2004, it seems that some coastal erosion had taken place, though a small sandy beach still remained in front of hotels and along the beach. However, it seems that the situation was drastically altered after many storm approuch and lack of sand supply from river led to lose more than 60 ha in 2011. With many dams appears to have been very effective in retaining sand within its vicinity, and a wide sandy beach is losing in front of the hotel as a result. During 2012, there are accretion on the left side of river it contributed more than 5 ha and create a spit. The changes in coastline from 2014 to 2017 reveal how the jetty hindered longshore sediment transport (in the predominant south to north direction) and caused a loss of sand in front of resorts.

Erosion in Cua Dai Beach was the dominant process during this period. The total losing area was around 85 ha (Figure 2). However, accretion occurred in the right side around 10 ha, but the trend is go down. During 2014-2016, there are many storms so that the new gate is opened in the north, which is expecting to allow sediments move to the resort side and reduce erosion. As the result, the erosion trend go up faster than accretion trend that warming Cua Dai Beach need the effective measure and more sustainable.

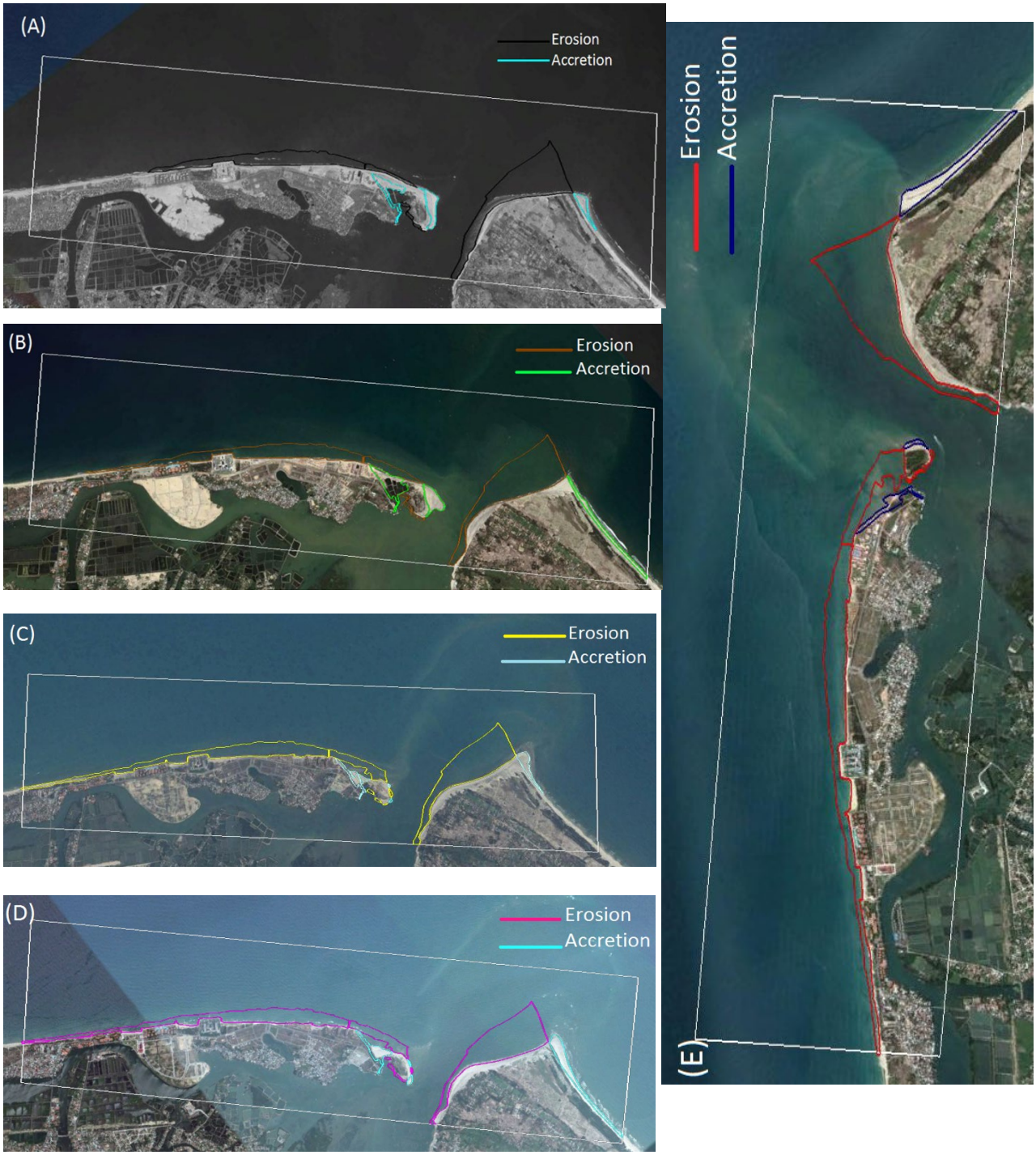

Figure 2 Change in coastline of Cua Dai Beach from 2004 to 2017: (A) coastline change from 2004 to 2011, (B) coastline change from 2004 to 2012 , (C) coastline change from 2004 to 2014, (D) coastline change from 2004 to 2015, (E) coastline change from 2004 to 2017.

3.2 Coastal Erosion Estimation

Based on measurements with Google Earth view from 2004 to 2017, the yearly erosion

is 13 meters a year for a stretch of 3.5 kilometer after which it gradually reduces. The active depth was estimate with (Hallermeier, 1981) the extrapolated yearly wave height and period date from survey (H_s = 2.33 m , T =11.64s) the closure depth is estimated to be 5.03 meters. The cross section of a given beach tends to follow a given profile relative to the sea. Bruun (1954) demonstrates calculations vary, the beach profile will respond to relative sea level. As the wave and water level conditions vary, the beach profile will respond by changing, and consequently the beach profile is always unstable. However, a useful concept called equilibrium beach profile is used to estimate the average cross section of the beach. Bruun (1954) proposed the following equation to give an equilibrium beach profile:

$$h(y) = Ay^{2/3} \tag{3.1}$$

Where h(y) is the water depth at a distance y from the shoreline and A is the profile scale parameter, which can be determined according to the diameter of beach material (Dean, 1987)

According to Dean (1987), the profile scale parameter A is set to be 0.115, assuming 0.25mm as the mean diameter of sand (Fila et at,.2016). According to this calculation, it can be erosion more than 43 m as it approaches the equilibrium beach profile and 13 m on the surface. As the collect the data by (Nguyen Ngoc The, 2017) and (Fila J., 2016), the beach face just underneath the coastal defense appears to be unstable, and hence the beach profile can easily be altered by episodes of intense or even normal waves. In Figure 3.6, the equilibrium beach profile on the coast of Cua Dai Beach, calculated by Eq. (3.2), is shown, together with the present beach profile. According to Dean (1987), the profile scale parameter A is set to be 0.115, assuming 0.25 mm as the mean diameter of sand. According to this calculation, it can be anticipated that the shoreline would retreat by more than 20 m as it gradually approaches its equilibrium beach profile. Thus, these communities can be expected to continue losing their lands and properties.

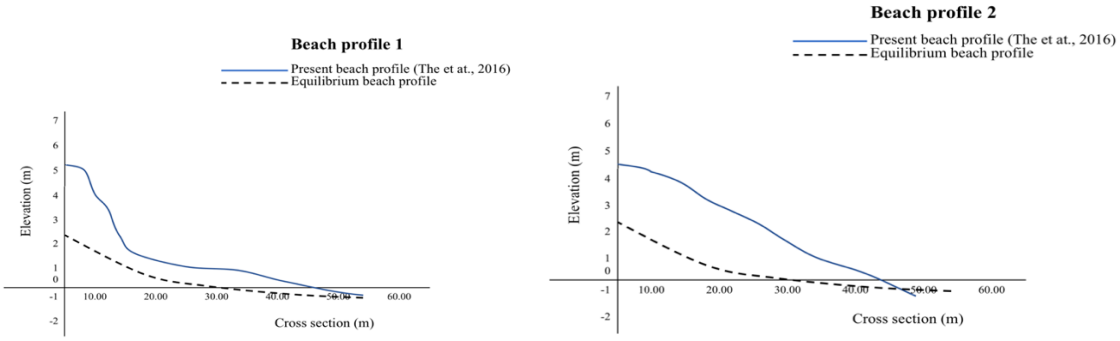

Figure 3 Present and estimated equilibrium beach profile at Cua Dai Beach

3.3 Four SLR Scenario For This Study

This study defines the scenario base on the criteria introduce by (Esteban et al., (2014)) which include IPCC scenario and available data:

Scenario 1: 0.15 m rise, which would correspond to an annual increase of 3 mm, similar to that at the end of the twentieth century;

Scenario 2: 0.44 m rise, which would be similar to the increase suggested by the worst IPCC 4AR scenario in the period between 2050 and 2100;

Scenario 3: 0.9 m rise, which would be halfway between scenarios 2 and 4;

Scenario 4: 1.3 m rise, similar to the increase suggested by (Vermeer M. R., 2009) for the period 2050 - 2100.

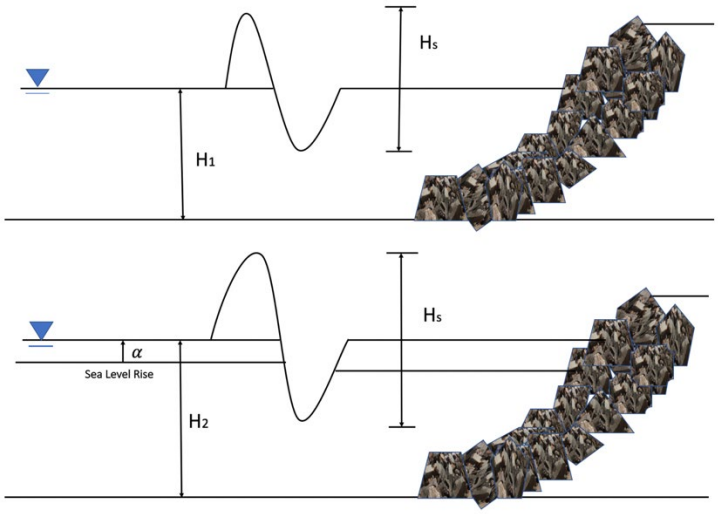

Figure 4 Problem of coastal revetments under sea level rise. Sea level rise will increase water depth in front of the structure (from H1 to H2), resulting in an increase in the significant wave height (Hs) possible in front of the structure. This can amplify the damage caused by the waves and create other problems such as overtopping

3.5 Sea Level Rise Impact On The Height Of The Structure

To understand the effects that future increases in sea level will have on the design and construction of coastal defenses around southern Vietnam, it is important to understand that the coast in this area is mention about the height of the structure. Thus, the height of the waves reaching the coastline is limited by the depth-limiting breaker height. Figure 4 shows the average increase in rubble mound breakwater cross section (including the increase in required breakwater height as a consequence of sea level rise and increased run-up, and the required increase in armor size) for the various sea level rise scenarios

calculated Future increases in sea level rise will allow higher waves to reach the coast-line and will require coastal defenses to be built to a higher standard than today.

Equation TCVN9901, Height of the structure Eq. (4.4):

$$Z_đ = Z_t + R_l + a + b \quad (3.2)$$

In which: $Z_đ$ is the height of the structure, Z_t is the height of sea level in case of tide frequency, storm surge and influence of nature, R_l is the height of Run-up, a is the increase figure for calculated-mistake and b is the increasing figure calculated for sea level rise. Figure 4.10 indicate the increasing height of coastal defense apply in Cua Dai Beach for sea level this century. Essentially what this would mean is that a breakwater built without taking into account sea level rise in the area will have to be reinforced at a later stage in its life with stronger armor, as and when it suffers damage (or if sea level rise is considered from the outset, then the initial structure will be considerably more expensive than if sea level rise is not considered).

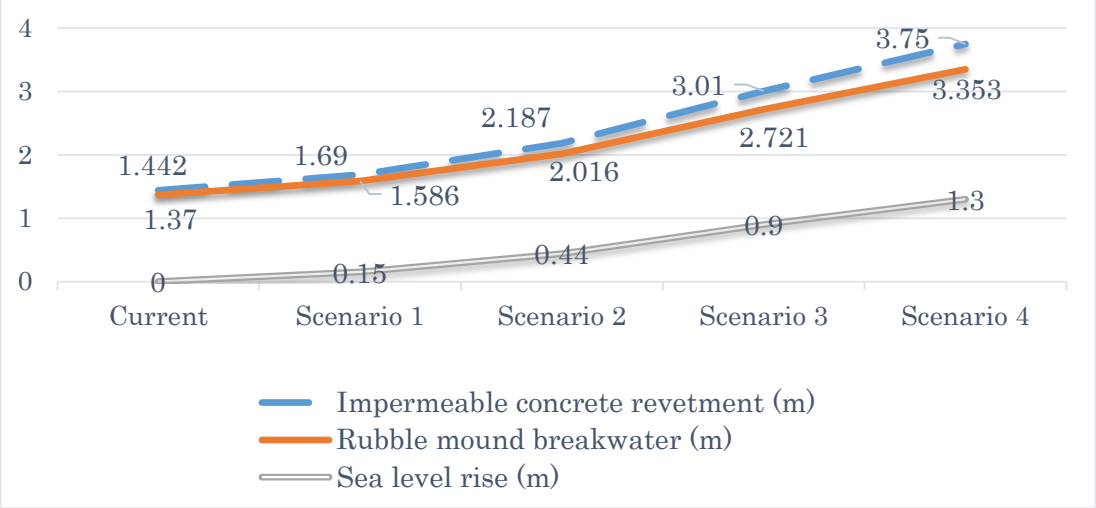

Figure 5 Increase in height of coastal defense requirements for each of the four sea level rise scenarios considered.

4. Conclusions

Hoi An Beach on the northern coastline is experiencing severe erosion due to northward longshore sediment transport and shoreline retreat. According to this calculation, it can be anticipated that the shoreline would retreat by more than 20 m as it gradually approaches its equilibrium beach profile. Thus, these communities can be expected to continue losing their lands and properties. As Cua Dai has been undergone irreversible impacts from both natural and anthropogenic forces which cause severe erosion – a negative coastal process. Stark erosion was a long due recorded in the coastlines of Hoi An city in which erosion situation is increasingly exacerbated because of man-made engineering structures. Besides, Climate change and sea level rise represent

an important challenge to the Vietnamese economy and society, especially coastal area in Cua Dai beach. A significant length of this coastline is already protected by coastal revetments and there are also a number of resorts that serve tourism. Sea level rise will require these structures to be strengthened, in Cua Dai beach are characterized by shallow bathymetries, future increases in sea levels will allow higher waves to reach the coastline

There are many elements reasons impact to coastal erosion, thus the government need to seek the full data about sediment transport, local wave and future climate change to make a fulfil picture about coastal evaluation. Furthermore, it is necessary that coastal management procedures are also improved, as at present it appears that many local erosion problems are the result of lacking integrated coastal defense in Cua Dai Beach and different engineering measures can be applied for environment friendly, but natural rules should be well understood and adequate considered and coastal processes need to be carefully examined before adopting.

References

Thao, N. D. (2014). *Coastal Disasters and Climate Change in Vietnam.* London Elsevier.

IPCC. (2007). *Climate Change (2007) The Physical Science Basis Contribution of Working Group I to the Fourth Assessment Report of the Intergovernmental Panel on Climate Change.* Cambridge University Press, Cambridge, UK.

IPCC. (2013). *Working Group I Contribution to the IPCC Fifth Assessment Report Climate Change 2013.* The Physical Science Basis, Final Draft Underlying Scientific-Technical Assessment.

Environment, M. o. (2016). *Climate change, sea level rise scenarios for Vietnam.*

Tanaka, D. &. (2017). *Evaluation of longshore sediment transport along the Cua Dai Delta coastaline*

Bruun, P. (1954). Coast erosion and the development of beach profiles. *Beach Erosion Board, Corps of Engineers, 44*, 82.

Dean, R. (1987). *Equilibrium beach profiles: U.S. Atlantic and Gulf coasts.* Department of Civil Engineering, University of Delaware. Technical Report .

Esteban, T. &. (2014). Tropical Cyclone Damage to Coastal Defenses: Future Influence of Climate Change and Sea Level Rise on Shallow Coastal Areas in Southern Vietnam . London Elsevier.

Fila J., K. M. (2016). *Coastal Erosion Hoi An.* Multidisciplinary Project Report, Delft University of Technology.

Hallermeier, R. J. (1981). *A Profile Zonation for Seasonal Sand Beaches from Wave Climate.* Coastal Engineering, Vol. 4, .

Nguyen Ngoc The, D. C. (2017). *Study on seasonal trends of evolution for Hoi An shoreline and Cua Dai beach with sbeach model* .

Vermeer, M. R. (2009). *Global sea level linked to global temperature.* PNAS. 106, .

QUANTITATIVE ANALYSIS OF THE EFFECTS OF EARTHQUAKE ACTION ON THE PORT STRUCTURES IN VIETNAM

NGUYEN KIET, NGUYEN THE DUY
Department of Port and Coastal Engineering, Ho Chi Minh City University of Technology
268 Ly Thuong Kiet street, Ho Chi Minh City, Vietnam
E-mail: kietnguyen2608@gmail.com

Abstract: In Vietnam, the load induced by earthquake had not been considered in the structure design until 2006, when the Code Design of Structures for Earthquake Resistances was first issued. However, this Code is prepared only for the building design. Hence, there still exists the quest regarding the importance of seismic load in the design of Port Structures which are often associated with high seismic risk. The aim of this study is to look into whether it is necessary to consider this type of load in the Port structure design.
Keywords: Wharf Structures, Seismic Condition, Superstructure, Earthquake

1. Introduction

Seismic design of maritime structures need to be considered due to coastal regions are often associated with high seismic risk [1]. The magnitude of earthquakes which may occur on the Vietnam territory is presented in the Map of Ground Accelerations which has a type of soil A. This will take into account the ground motion criteria such as peak ground accelerations and ground response spectra. The ground acceleration varies with the studied areas and is the dominant parameter used in the modeling of earthquake action on any type of structures.

2. Mechanism of earthquake action on structures

2.1 General case

The seismic waves which propagate to the soil strata under the structures cause the displacement and then the inertia force acting on the structures.

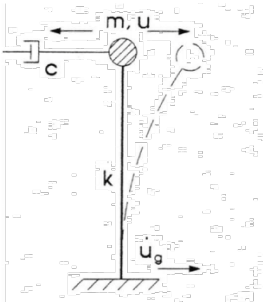

Figure 1. Definition sketch of structure displacement induced by soil exciting Earthquake

The basic differential equation for structure displacement is

$$m\ddot{u} + c\dot{u} + ku = -m\ddot{u}_g \quad (1)$$

in which

u: relative displacement of the mass m with time

$\dot{u}$: relative velocity of the mass m with time

$\ddot{u}$: relative acceleration of the mass m with time

$\ddot{u}_g$: ground acceleration with time

$m\ddot{u}_g = P_{eq}$: seismic load acting on structure

2.2 Marine structures

Under seismic load action, the marine structures displace in the water environment. Due to the resistance of water, the motion of the marine structures become "slower" than other structures, i.e. the periods of vibration of the system are greater than those in the air. The resistance in the system due to the friction between the structures and water also increase. Therefore, it is necessary to re-calculate the periods of vibration of the system.

In general, the second order differential equation for the displacement of a marine structure subjected to dynamic load is

$$[M]\{\ddot{u}\} + [C]\{\dot{u}\} + [K]\{u\} = [F] \quad (2)$$

in which

[M], [C], [K]: matrices of mass, resistance factor and stiffness system, respectively

[F]: dynamic loads acting on the system (wave force, current force, impact of vessels)

In the water, the mass of water adjacent to the structure elements moves with the elements and this affects the displacement of the entire system. The mass of the elements of the structure system which are submerged in water can be calculated as follows

$$[M] = [M_s] + [M_w] + [M_{en}] \quad (3)$$

in which

$[M_s]$: self-weight of structure material (including uplift)

$[M_w]$: mass of water contained in the structure elements

$[M_{en}]$: mass of entrained water (mass of water volume adjacent to the structures which moves with the structures)

In case of earthquake occurrence, the inertial mass, M_{eq}, which generates earthquake load is calculated as:

$$\left[M_{eq}\right] = [M_s] + [M_w] \quad (4)$$

The inertial force (earthquake load) is then equal to

$$[F] = \left[M_{eq}\right]\{\ddot{u}_g\} \quad (5)$$

in which

$\{\ddot{u}_g\}$: vector of ground acceleration

Note: there exists a number of methods for the input of ground acceleration in the structure analysis models. In the present study, the design response spectrum method has been applied.

The second order differential equation for the displacement of the marine structures subjected to earthquake load then can be rewritten as

$$[M]\{\ddot{u}\} + [C]\{\dot{u}\} + [K]\{u\} = [M_{eq}]\{\ddot{u}_g\} \quad (6)$$

The solution of Eq. (6) provides the displacements of the structure system which is subjected to earthquake load.

3. Quantitative analysis of the effects of earthquake load on wharf structures

Open-type wharves on piles are the most popular port structure in Vietnam because this type of structure is appropriate with most topographical and soil conditions in Vietnam and it is also the most economical one.

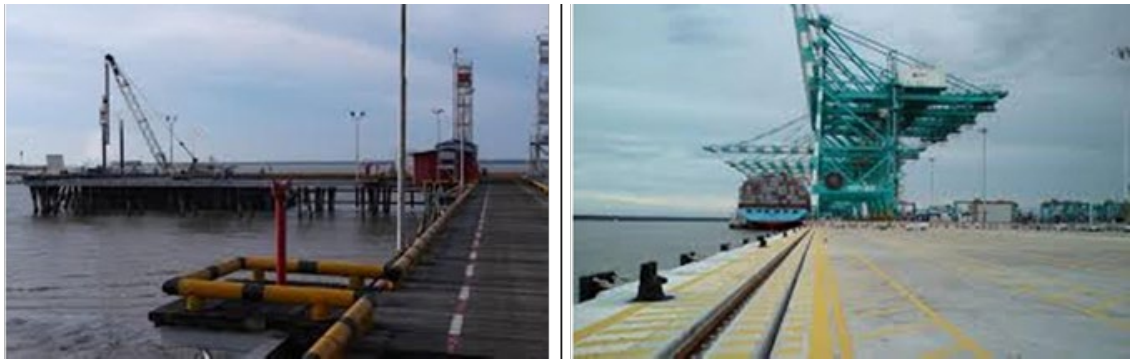

Figure 2. An open-type wharf on piles

3.1 Design external forces

The main external forces acting on the pile-supported section of an open-type wharf are listed as below with regard to the vertical forces and horizontal forces:

Vertical forces	Horizontal forces
✓ Deadweight of the superstructure ✓ Static loads Live loads Vehicle load ✓ Cargo handling equipment load ✓ Sidewalk live load Temporary live load Tractive force of vessel ✓ Uplift	✓ Wind load ✓ Reaction force of the fender Tractive force of vessel Earthquake forces which are mooring and anchoring forces

3.2 Structure analysis model

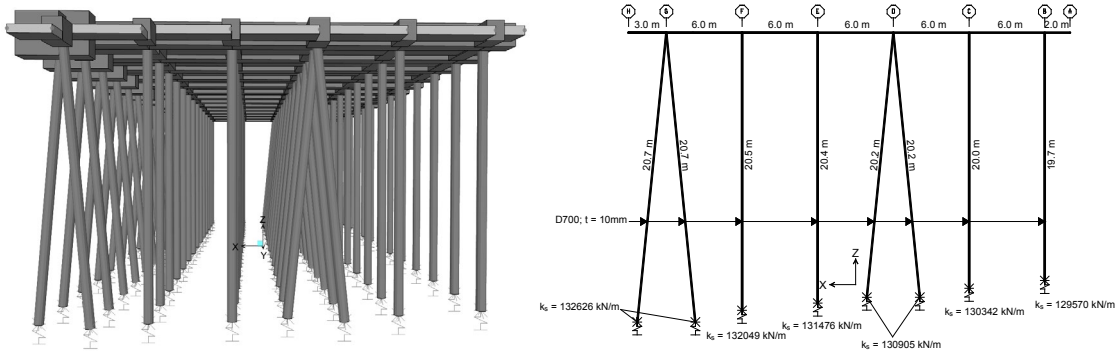

Figure 3. 3D structure analysis model & 2D cross frame for a wharf

The structure analysis for a number of different wharf structures in Vietnam, without or with earthquake load, were conducted by using their 3D structure models. Typically, the pile modelled in SAP2000 has a fixed support at the top of pile in connection with pile cap as well as the pile tip is assumed to have a vertical spring.

The computed results of displacements and stresses for wharf structure elements were compared between the cases without earthquake and with earthquake to evaluate the effects of earthquake action on the wharf structures quantitatively.

3.3 Input of earthquake load to the structure analysis model

The response spectrum method has been utilized to model the action of earthquake load on the wharf structure. According to [2], the design response spectrum function can be determined as follows

$$0 \le T \le T_B : \mathrm{S}_d(T) = a_g S\left[\frac{2}{3} + \frac{T}{T_B}\left(\frac{2.5}{q} - \frac{2}{3}\right)\right]$$

$$T_B \le T \le T_C : \mathrm{S}_d(T) = a_g S \frac{2.5}{q}$$

$$T_C \le T \le T_D : \mathrm{S}_d(T) = \max(a_g S \frac{2.5}{q}\frac{T_C}{T}, \beta a_g)$$

$$T_D \le T : \mathrm{S}_d(T) = \max(\beta a_g, a_g S \frac{2.5}{q}\frac{T_C T_D}{T^2})$$

in which

$S_d(T)$	design elastic response spectrum
T	vibration period of a linear single degree of freedom system
a_g	design ground acceleration on type A ground
T_B	lower limit of the period of the constant spectral acceleration branch
T_C	upper limit of the period of the constant spectral acceleration branch
T_D	value defining the beginning of the constant displacement response range of the spectrum

q behavior factor

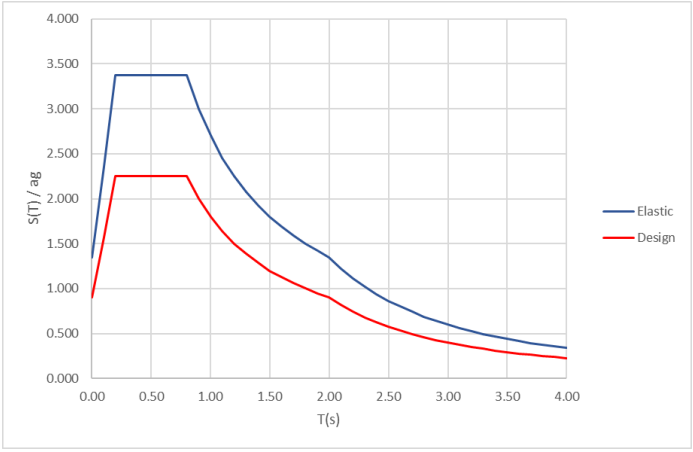

Figure 4. Elastic response spectra & Design response spectra

To avoid explicit inelastic structural analysis in design and the capacity of the structure to dissipate energy are taken into account by reducing the value of elastic response spectrum by introducing behavior factor q. Then, we obtained the design response spectrum which illustrated by the red line in Figure 4.

3.4 Analysis results for wharf structures under seismic condition

3.4.1 Maximum displacement of wharf

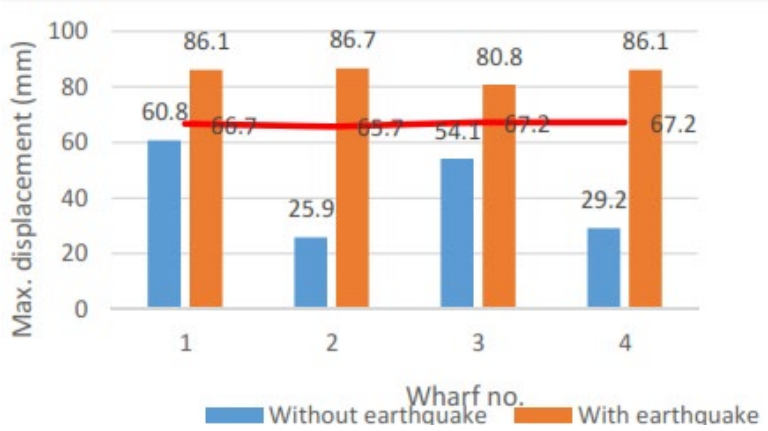

Figure 5. Maximum displacements of the wharves (without & with earthquake)

Under earthquake action, the lateral displacements of the wharves increase and are greater than those of non-earthquake case. The axial forces in the wharf piles are always smaller than those of non-earthquake case.

3.4.2 Maximum bending moments in the wharf piles

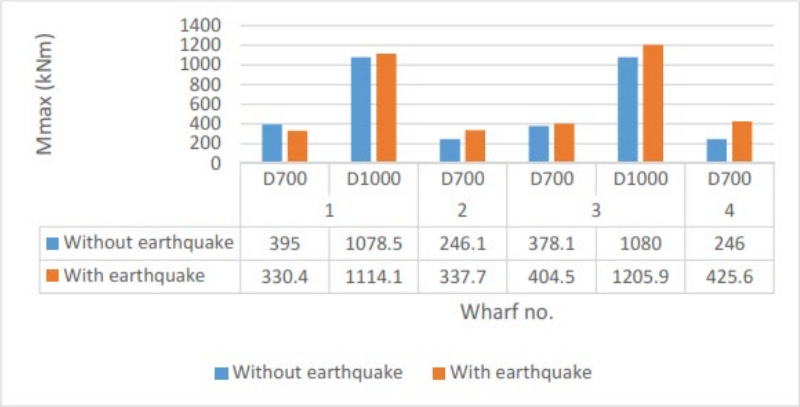

Figure 6. Maximum moments in the piles (without earthquake & with earthquake)

Under earthquake action, the bending moments in the wharf piles generally increase compared to the case without earthquake, in which the moment ratios between the two cases vary from minimum 3% to maximum 73%.

3.4.3 Computed stresses in the superstructure elements (beams, deck slab)

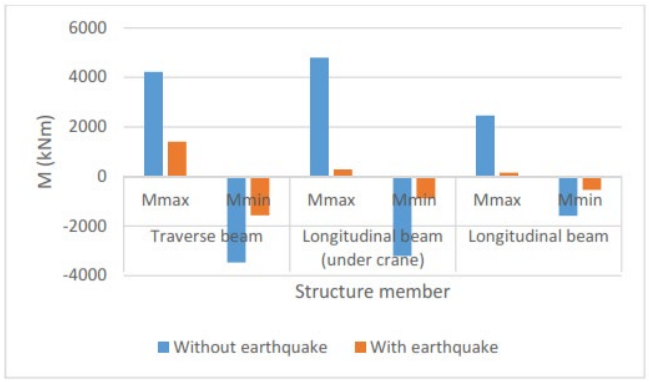

Figure 7. Comparisons of moments in the deck beams (without earthquake & with earthquake)

Because in seismic condition, due to the exciting force of earthquake is dominantly shear force, the stress in superstructure elements are usually smaller than that of non-seismic condition.

Table 1. Comparisons of moments in the deck slab (without earthquake & with earthquake)

Computed moments (kNm)	Without earthquake				With earthquake			
	M11		M22		M11		M22	
	M_{max}	M_{min}	M_{max}	M_{min}	M_{max}	M_{min}	M_{max}	M_{min}
	182	-254	351	-343	65	-61	44	-25

- M11, M22: moment in the deck slab in x, y direction in turn.

The above comparisons indicate that the earthquake does not induce significant effect on the superstructure of the wharves (beams, slab).

4. Conclusions

In case the earthquake action is considered, the structure analysis results for a number of wharves in Vietnam show that:

- The displacement of the pile heads (or the entire wharf superstructure) increases. It is therefore necessary to apply appropriate structure measures to limit the pile head displacement, in which the increase of the inclination of raking piles can be an effective solution.
- In the piles, the compression forces decrease and the tension forces may occur. Especially, the bending moments increase significantly.
- The stresses in the superstructure members (beams, slab) are much smaller than those of non-earthquake case. It is thus not necessary to take into account the seismic load in the design of wharf superstructure.

In conclusion, the load induced by earthquake should be considered in the design of piles of a wharf but it is not the case for wharf superstructure (beams, slab).

References

[1] C. A. Thoresen, Port Designer's Handbook, London, 2014, page 157.

[2] TCVN 9386-2012: Design of structures for earthquake resistances, 2012 (Vietnam Design Standard).

Self-degradation of Diesel Oil in Sediments of Sai Gon River

Dang Thuong Huyen*1), Tran Trung Huy 1), Phan Anh Tu 1), Nguyen Van Dong 1) and Do Hoang Le Dinh Loc 1)

1 Department of Earth Resources and Environment, Faculty of Geology and Petroleum Engineering, Ho Chi Minh City University of Technology, Vietnam

*E-mail:dthuyenus1982@gmail.com

Abstract: Deep Hoziron Oil Spill is the largest accident during the history of petroleum Engineering happened in 2010. Many oil spills have occurred around the world every year. Vietnam is on of the most country facing seriously with this type of accident causing a lot of environmental problems. The spilled oil includes crude oil or refined oil. The number of oil spills happened in Vietnam, including Sai Gon river where is to transport the oil from offshore to onshore. In this study, we intended to collect the sediment from the Sai Gon river and experience how the oil degradation naturally. The experiments were divided into two groups: 1) without additional Nitrogen (N), Phosphate (P) and Potassium (K); 2) additional NPK to the experience. We applied diesel oil (DO) and experience for 53 days. The results show that with addition NPK the concentrations of oil are degraded quicker than those of no addition of NPK. The decreasing concentrations of two groups are clear. We suggested that the bio-activities of local bacterias responded strongly with the additional DO in the experiences.

Keywords: Diesel oil, oil spill, remediation, sediment, Saigon river

Introduction

Oil spill accidents occur around the world every year. Deep Horizon accident is the biggest accident in 2010 during the history of petroleum engineering. As a country of exporting crude oil and consuming refined oil for economic development, Vietnam is one of the most country facing with this type of accident causing a lot of environmental problems, particularly in the rivers, wetlands or sea. Sai Gon river in Ho Chi Minh City (HCMC) is to transport the oil from offshore to onshore. Since 2001, there has been about 7 oil spills happened in the area (table 1). Many of them were spilled diesel oil into the river. There are a number of risks of leak of oil from the activities of maritime transport. Sediment of Saigon river is stressed of responsibility oil pollution.

In this study, we aim to conduct experiments to evaluate the capacity of self-degradation of oil in sediment of Sai Gon river

Table 1: Several oil spills in Vietnam

Oil Spill	Date of accident	Volume (type of oil)
Bach Ho reservoir	26/12/1992	300 – 700 tons (FO)

Neptune Aries Ship, Cat Lai, HCMC	03/10/1994	1.700 tons (DO)
Kasco Monrovia Ship, Cat Lai, HCMC	2005	518 tons (DO)
Duc Tri BWEG Ship, Binh Thuan	02/03/2008	1.700 tons
Gasoline storage in Hai Van pass	16/10/2008	3.000 m^3 (Jet)
Sao Mai, Vung Tau	27/04/2010	270 tons (DO)
Quy Nhơn coastal area	07/07/2013	50 tons (oil mixed with sand)

Material and Methods

Sediment sample was collected in Saigon river when tidal fell down and put into the plastic bucket made by polyvinylclorua (Figure 1). The water was collectd from the river and keep in the plastic bottle. The sample was brought back to the lab at Ho Chi Minh City University of Technology. Experience was taken in our laboratory.

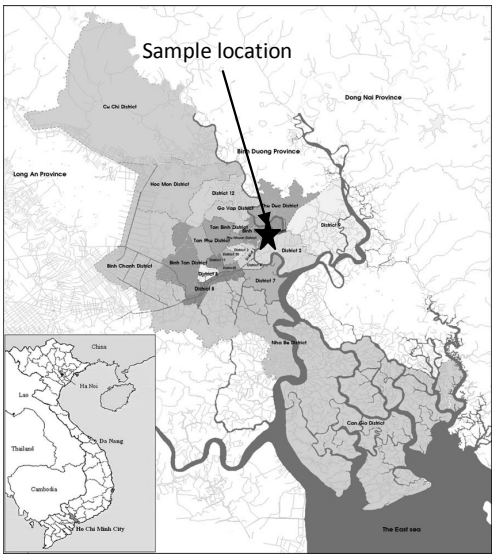

Figure 1. Location of sediment sampling

Figure 2 shows the flow chart of our experience. The experiences were done with two groups. Group 1 was with nutrient addition, group 2 was without nutrients. The sediment samples were mixed everyday and poured the water to make samples always saturated. Each experiemental group was done with different added DO.

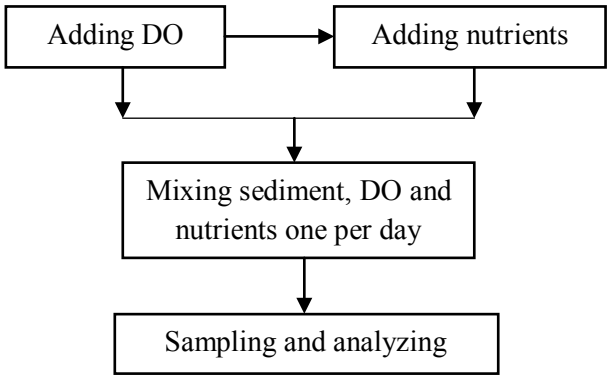

Figure 2. Flow chart of experience

Table 1 shows the detail of our experiements. Each group has been done the sample process just different DO concentrations and nutrients. Group 1 was added 10 ml of DO. Group 2 was added 200 ml of DO. DO was added to 10 kg of sediment for group 1 and 8kg of sediment for group 2 and mixed. After 15

minutes mixing, the mixed samples were divided into 2 buckets. Experiment 2 (exp2) and experiment 4 (epx4) were added nutrients as table below. Experiment 1 (exp1) and experiment 3 (exp3) was added only DO. Measured pH of sediment was 4.5; measured pH of water of Saigon river was 7. Nutrients were added to be sure that the ratio of N: P was 3: 1.

Table 1. Information of experiments

Information	Group 1		Group 2	
	Exp1	Exp2	Exp3	Exp4
Adding DO (ml)	500	500	2000	2000
Adding nutrients	0		0	
NH_4Cl (g)	-	261.32	-	150
N/NH_4 (g)	-	68.38	-	68.38
$KH_2PO_4.2H_2O$ (g)	-	100	-	57,4
P/KH_2PO_4	-	22.79	-	22.79

In group 1, samples were taken after 12 and 22 days. In group 2, samples were taken after 7, 14, 22, and 53 days. Samples were sent to the laboratory of Insitute of Resources and Environment for analysis with EPA 9071B on total oil in sediment.

Results and Conclusions

Figure 2 shows the results of our experiments of group 1. After adding DO, the total of oil was 1239 mg/kg. The concentration of oil decreases after 14 days to 215 mg/kg for experience 1 and 174 mg/kg for experience 2. After 22 days, samples were analyzed showing the lightly increase of total oil in the samples (525 mg/kg for exp1 and 348 for exp2).

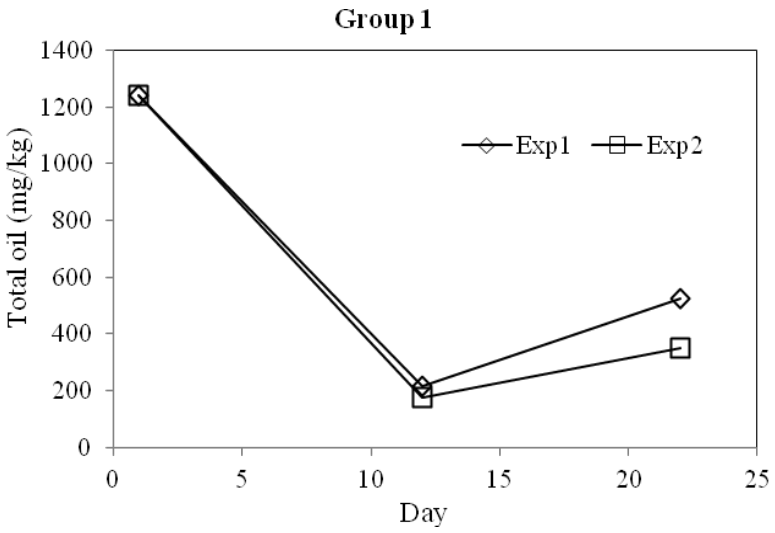

Figure 2. Results of group 1

Figure 3 shows the results of group 2 for experiments 3 and 4 by increasing the addition of DO. At the initial, the total oil was 8190 mg/kg for two experiments. In group 2, there is a decrease of total oil in the samples after 7 days (2557 mg/kg for exp3 and 809 mg/kg for exp4) and an increase after 14 days (4663 mg/kg for exp3 and 3464 mg/kg for exp4). The increase of total oil is still lower than the initial total oil. However, after 22 days, a decrease is clearer. The total oils are 2231 mg/kg for exp3 and 2165 mg/kg for exp4. On the day 53, total oil is much decreased, 1329 mg/kg for exp3 and 106 mg/kg for exp4.

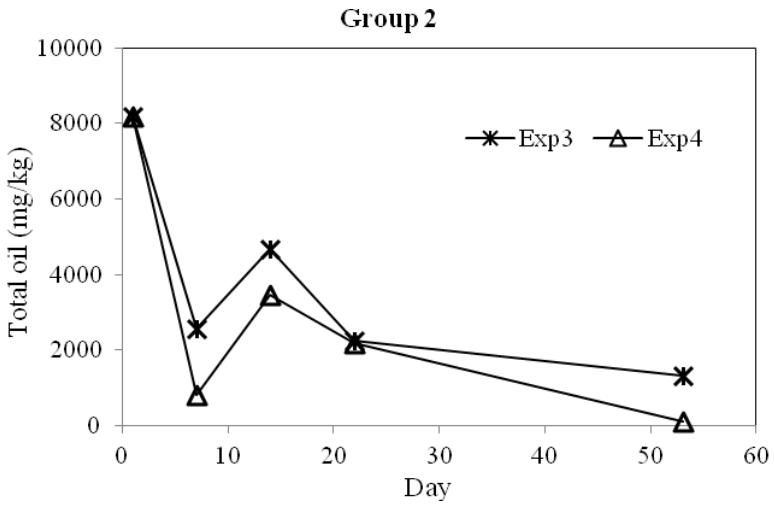

Figure 3. Results of group 2

In the four experiments, there was a decrease quickly after 7-14 days of total oil, then lightly increasing but still smaller than the initial total oil. It can be explained that the rapid development of local bacterial community consumes much DO while they receive their food. However, after quick growth up of bacteria, the supported energy was not enough causing death while the DO was still not decomposed to be the final stage. Then remain bacteria was again grown up to make complete decomposition. Therefore, after 22 days, the concentration of total oil decreased stably.

In both experimental groups, the addition of nutrients showed the good composition of DO of bacteria compared with the case of no added nutrients. The research also showed that sediment from Saigon river has a good responsibility to oil spill with the requirement of addition of nutrients.

Acknowledgment

This research is funded by Ho Chi Minh City University of Technology – VNU-HCM, under grant number T-ĐCDK-2017-94

APPLICATION OF REMOTE SENSING AND GIS FOR DERETECTION OF SHORELINE CHANGES IN PHAN THIET

[(1)]Mai Thi Yen Linh, [(2)]Nguyen Danh Thao

[(1)]Ho Chi Minh city University of Technology. Email: maithiyenlinh1601@gmail.com

[(2)]Ho Chi Minh city University of Technology. Email: ndthao@hcmut.edu.vn

Abstract: Vietnam, with 3260 km coastline and two vast low-lying deltas (the Red River Delta and Mekong Delta), suffers annually from the severe effects of natural disasters, and could be considered one of the most vulnerable countries against coastal disasters and climate change. The effects of natural disasters on Vietnamese settlements has become increasingly more severe in terms of magnitude, frequency and volatility, and there is the need to formulate a national strategy for natural disaster prevention, response and mitigation. The extraction of the Vietnam coastlines from ten Landsat satellite images, which was based on their availability to the author and their suitability to detect coastlines using remote sensing methodology, indicates spatial and temporal changes in 10 segments spreading 60 km length of Phan Thiet coastline. The study addresses the problem of paucity of coastal vulnerability research in Vietnam. This is contemporary research problem in low lying coastal areas throughout the world.

Keywords: shoreline change, Vietnam coastline, Phan Thiet coastline, remote sensing

Introduction

Lying in tropical monsoon climate regime, Vietnam is influenced by natural calamities as typhoon, monsoons, storm surge, sea level rise and El-Nino phenomena. Scientific research currently being undertaken in Vietnam indicates that significant impacts due to sea level rise may already be occurring. Even limited rise in sea level over coming decades could seriously affect human and nation, especially influence direct on people living near coastal area. According to Ministry of Natural Resources and Environment (2016), the recorded increments in sea level vary from 2.8 to 4.2 mm/yr at Vietnamese stations (Hon Dau, Da Nang, Qui Nhon, Vung Tau). The high value is observed in the north and in the south part of the country. It could be said that sea level rise in Vietnam is in comparision with the sea level rise in the region and in the world. In East Asia, Vietnam is the nation that would suffer the most significant impacts by sea level rise. Rise in sea level would inundate wetlands and lowlands, erode shorelines, exacerbate coastal flooding, increase the salinity of estuaries and aquifers and otherwise impair water quality and impact coastal ecosystem. Given the threats posed by relative SLR and a paucity of vulnerability assessment research for the coast of Vietnam, the purpose of this thesis is to assess the change of the densely settled areas of the Vietnam coastline to rising sea levels. An assessment of coastline change in Vietnam is required to identify the locations that have experienced erosion and accretion over an extended period of time in order to

identify coastal areas under threat.

Phan Thiet is one of the regions which have developed dramatically. Many resorts were built for tourism. Along with that, several artificial coastal structures such as groin, jetties were constructed for developing local economic targets. Consequently, the beach erosion has been happening. It is necessary to collect historic images for monitoring the shoreline evolution in this region. As a result, the study area in this paper is selected as Phan Thiet region. The coastline of Phan Thiet is about 60km. To facilitate the computational efforts, Phan Thiet coastline is divided into 10 segments as shown in Figure 1.

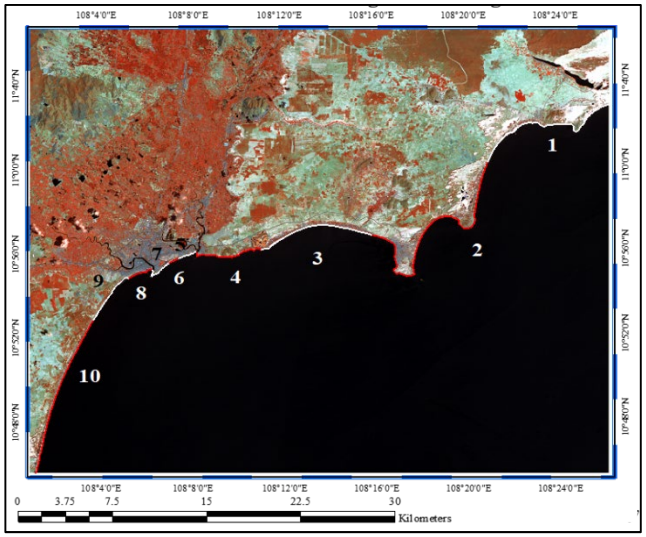

Figure 1. The Study Area

Methodology

There are two sequential stages to extract and measure of change of the coastline in this study. Firstly, remote sensing that exploits the differences in spectral reflectance signatures of water from non-water bodies are used as background in the extraction of coastlines from satellite images to delineate coastlines. Secondly, the Digital Shoreline Analysis System (DSAS) is applied to the quantitative assessment of erosion and accretion rates. The Figure 2 shows the methodology adopted to assess coastlines change using Landsat images.

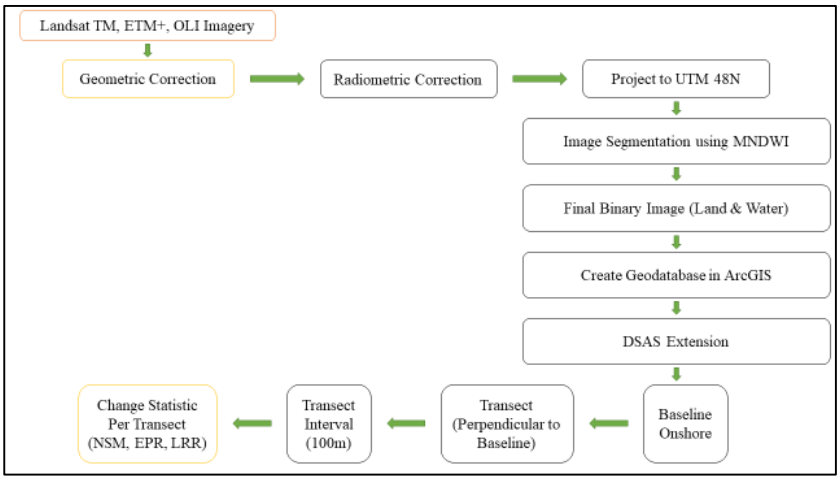

Figure 2. Assess Coastline Change Using Landsat Images

Four main steps are: (i) to acquiring satellite data; (ii) prepare data for analysis; (iii) extract coastline; and (iv) estimate rates of coastal change.

Acquiring satellite data

The image source is from University of Maryland, USA. All images which are orthorectified are captured at the same time 02:30 GMT over about 27 years from 1990 to 2017. The scenes for the study aera of Phan Thiet are listed in Table 1.

Table 1. List of Landsat scenes used for Phan Thiet shorelines

Date	Sensor
17/03/1990	Landsat 5 TM
02/05/1995	Landsat 5 TM
23/03/1998	Landsat 5 TM
16/04/2001	Landsat 5 TM
25/02/2003	Landsat 7 ETM+

Date	Sensor
26/03/2005	Landsat 5 TM
18/12/2009	Landsat 5 TM
07/02/2011	Landsat 5 TM
17/11/2015	Landsat 8 OLI
03/11/2017	Landsat 8 OLI

Prepare data for analysis

The images had been prepared for analysis through pre-processing procedures that involved three steps i.e. (i) resample for geometric correction, (ii) correct for radiometric distortions and (iii) project all geometrically and radiometrically corrected images to the UTM 48N coordinate system.

Extracting coastlines

The coastline extraction is used segmentation technique with background is the satellite images that were prepared for analysis. In the case of Vietnam, the reflectance values of band 4 for built-up land, soil and vegetation are much lower than for band5. This leads to the Modified Normalized Difference Water Index (MNDWI) proposed by Xu (2006) has been adopted in the study to delineate water from non-water features in the extraction of coastlines. The MNDWI have been applied in coastal extraction from satellite images by Ho et al. (2010), Xu-Kai et al. (2012), Deus and Gloaguen (2013), Mwakapuja et al.

(2013), Goncalves et al. (2014), Gomez et al. (2014).

Estimating Rates of Coastline Change

Coastline change rate is determined by the Digital Shoreline Analysis System (DSAS). Supporting to define the baseline for this study, there are four consideration were taken into account: (i) the 1995 coastline was chosen to be onshore or inward of the coastline of ten images; (ii) from the 1995 coastline, drawing the baseline to be broadly parallel; (iii) the baseline can't intersect with any of the 10 extracted coastlines; (iv) the transects from the baseline must not intersect. This leads to the baseline were establised to be 1500 m onshore of the 1995 coatsline. In order to minmize the effect of inter transect differences in identifying coastline change rate, the orthogonal transects to be baseline were seperated at 100 m intervals. From the menu of change statistics provided in DSAS, chosing the end point rate (EPR), the net shoreline movement (NSM) and the linear regession rate (LRR) to indentify coastline change rates.

The 60 km of the coatsline of the Study Area with 100 m transect intervals 731 transects showed in Table 2.

Table 2. Transect IDs Representing Coastal Communities

Transect ID	Segment	Name
1 – 130	1	Hoa Thang & Hong Phong
132 – 323	2	Mui Ne
323 – 420	3	Ham Tien
421 – 473	4	Phu Hai
474 – 489	5	Thanh Hai

Transect ID	Segment	Name
490 – 498	6	Phu Thuy
499 – 510	7	Hung Long
511 – 536	8	Lac Dao
537 – 585	9	Duc Long & Tien Duc
586 – 731	10	Tien Thanh

Results and discussion

Figure 3 show the graph for NSM, EPR, and LRR for Transects 1-731. EPR and NSM that compare the 1990 with the 2017 coastlines and LRR which takes into account changes in the 10 coastlines between 1990 and 2017 show broadly similar patterns. There are accretion in Hoa Thang – Hong Phong (1-130), accretion and erosion in Mui Ne (132-323), Ham Tien (323-430), Phu Hai (421-473), erosion in Thanh Hai (474-489), accretion in Phu Thuy (490-498), Hung Long (499-510), Lac Dao (511-536), accretion and erosion in Duc Long – Tien Duc (537-585), Tien Thanh (586-731). Expect for Hoa Thang – Hong Phong, Phu Thuy, Hung Long, Lac Dao, there is erosion in the other segments of the coastline. From the overall picture emerges in Figure 3, there is spatial variation regardless of the measure, the coastline change rate is quantified by EPR and LRR.

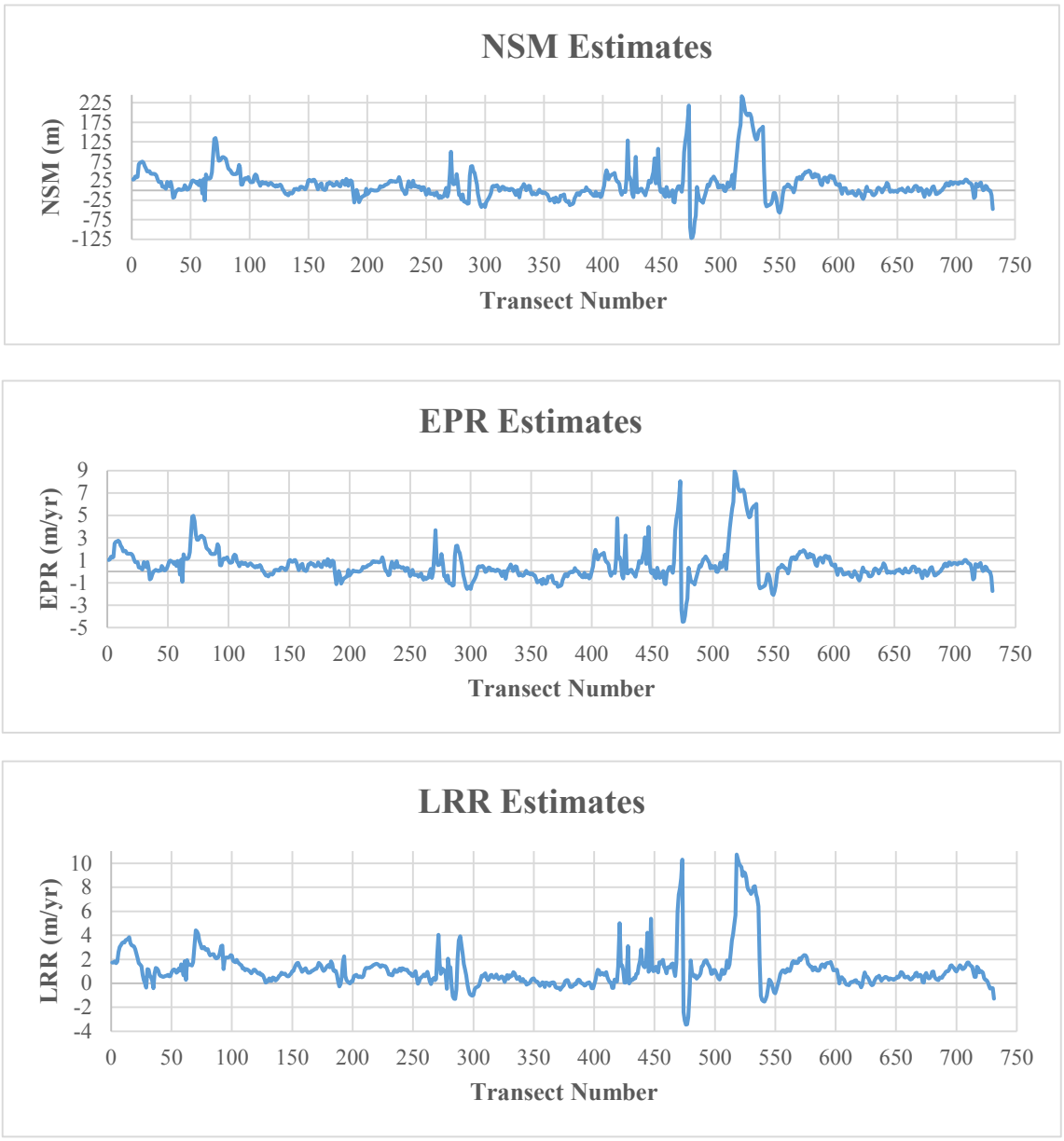

Figure 3. Estimates of a [NSM (m)], b [EPR (m/yr)], c [LRR (m/yr)]

There are complex change in Ham Tien and Tien Duc – Tien Thanh. The graph for NSM for Transects 339-399 in Ham Tien is shown in Figure 4. Within Transects (339-382), NSM that compare the 1990 with the 2017 coastlines. There is erosion in most of the transect (339-382) in Ham Tien. The average change statistics for the section of the coast are -13.06 m for NSM, -0.48 m/yr for EPR, and -0.02 m/yr for LRR.

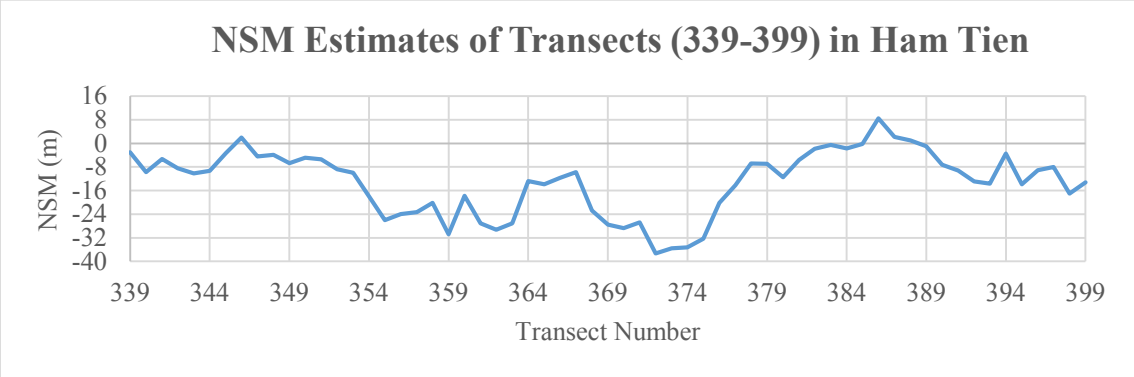

Figure 4. Estimate of NSM (m) for Transects (339-382) in Ham Tien

The graph for NSM for Transects 538-563 in Duc Long – Tien Duc is shown in Figure 5. Within Transects (538-563), NSM that compare the 1990 with the 1998 coastlines; the 1998 with the 2005 coastlines; the 2005 with the 2017 coastlines. In Transects (538-544), accretion from 1990 to 1998 followed by erosion from 1998 to 2017. In Transects (545-551), erosion from 1990 to 1998 is followed by accretion from 1998 to 2005 that is followed by erosion from 2005 to 2017. In Transects (552-563), accretion from 1990 to 2005 is followed by erosion from 2005 to 2017. The average change statistics for the section of the coast are -16.55 m for NSM, -0.61 m/yr for EPR, and -0.1 m/yr for LRR.

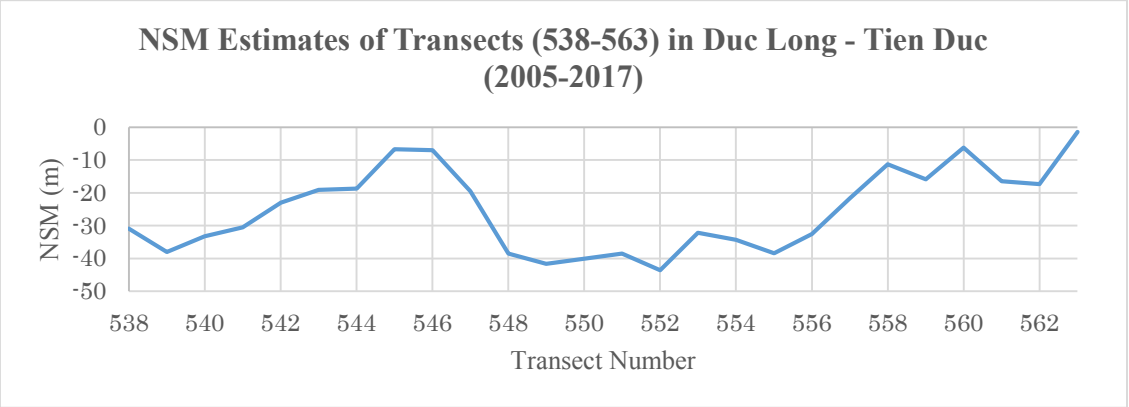

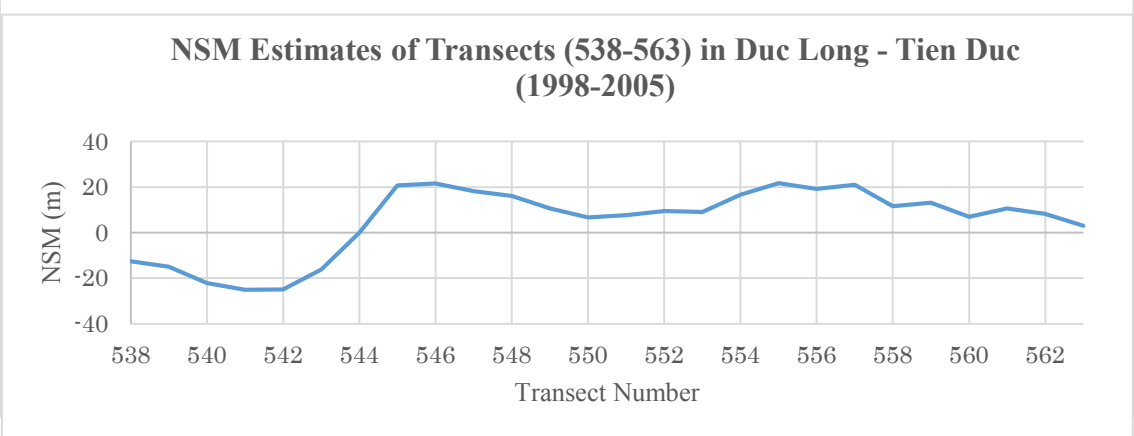

Figure 5. Estimate of NSM (m) for Transects (538-563) in Duc Long-Tien Duc

Conclusions

The integration between remote sensing and GIS technology is a useful tool for coastal engineers and managers who need an overview of the long-term shoreline changes in the concerned area. The state of the art technique does not only reduce investment budgets, but also decrease time and facilitate human work-forces. The paper showed that Phan Thiet shoreline could be determined rapidly by the improved band ratio although tidal adjustments were neglected. The shoreline change rates could be calculated by several statistical methods which were built in the extension of GIS tool. Quantitatively, the shoreline of Phan Thiet bay on average advances 0.57 m/yr over 27 years from 1990 to 2017.

The assessment of coastline change and the results on spatial and temporal variability of the coastline of the Study Area suggest that the low lying coastal areas of Vietnam with soft sandy beaches, extensive mudflats would be vulnerable to sea level rise in the 21st century. The existing threat posed by coastal erosion is likely to be reinforced by exposure to future sea level rise. The estimates of erosion and accretion of coastline segments in this chapter provide planners with additional estimates of erosion that identify the locations of areas of greatest concern or the hot spots that are under the threat of erosion. Prioritization of repair and reconstruction of the sea defenses should follow. Further, the disaggregated estimates of erosion and accretion are an essential input in determining the physical coastal vulnerability of the Study Area.

References

Deus, R.. and Gloaguen. R., 2013. ". Remote Sensing Analysis of Lake Dynamics in Semi- arid Regions: Implications for Water Resource Management". *Lake Manyara, East Africa Rift, Northern Tanzania. Water 5*, 698-727.

Gómez, C.; Wulder, M.A.; Dawson, A.G.; Ritchie, W., and Green, D.R., 2014. "Shoreline Change and Coastal Vulnerability Characterization with Landsat Imagery: A Case Study in the Outer Hebrides, Scotland". *Scottish Geographical Journal*, 130(4), 279-299, DOI: 10.1080/14702541.2014.923579.

Gonçalves, G.; Duro, N.; Sousa, E.; Pinto, L., and Figueiredo, I., 2014. "Detecting changes on coastal primary sand dunes using multi-temporal Landsat imagery". *SPIE Remote Sensing 2014*, Amesterdam, Netherlands, 22-25 September. doi: 10.1117/12.2067189.

Ho, L.T.K.; Umitsu, M., and Yamaguchi, Y., 2010. "Flood hazard mapping by satellite images and SRTM DEM in the VU GIA – THU BON alluvial plain, Central Vietnam". *International Archives of the Photogrammetry, Remote Sensing and Spatial Information Science, Volume XXXVIII, Part 8, Kyoto Japan*.

Mwakapuja, F.; Liwa, E., and Kashaigili, J., 2013. "Usage of indices for extraction of built-up areas and vegetation features from Landsat TM image: A case of Dar Es Salaam and Kisarawe Peri-Urban areas, Tanzania". *International Journal of Agriculture and Forestry*, 3(7), 273-283.

Xu, H., 2006. "Modification of Normalized Difference Water Index (MNDWI) to enhance open water features in remotely sensed imagery". *International Journal of Remote Sensing*, 27(4) 3025-3033.

Xu-kai, Z.; Xia, Z.; Qiong-qiong, L., and Ali, M.H., 2012. "Automated Detection of Coastline Using

Landsat TM Based on Water Index and Edge Detection Method". *Second International Workshop on Earth Observation and Remote Sensing Applications (EORSA)*: 153-156.

Hydrodynamic Analysis for Hull Shape Improvement of an Amazonian School Boat Utilizing a CFD Tool

Toshi-Ichi Tachibana [1], Harlysson W. S. Maia [2], Fernando C. da Cruz [2], Vitor H. M. Cardoso [2], Breno F. da Silva [2], Yuri V. R. Guedes [2]

[1] Department of Naval Architecture and Ocean Engineering/
Polytechnic School of the USP (University of São Paulo)/
São Paulo/ São Paulo/ Brazil

[2] Faculty of Marine Engineering and Naval Architecture/
Institute of Technology/ UFPA (Federal University of Pará)/
Belém/ Pará/ Brazil

Abstract: The objective of this work is to present a numerical simulation and hydrodynamic analysis based on CFD of an Amazonian school boat prototype, in order to propose a hull form modification for resistance reduction. This boat design was funded by the FNDE (National Fund for Development of Education), in order to provide a faster and more efficient transportation of students who lives in riverside regions to the schools. However, in full-scale trials, it was noted that the prototype has not achieved the design speed, along with the generation of a large amplitude wave train, implying a high fuel consumption. Therefore, a methodology for numerical modeling and simulation is presented, along with a hull form modification and further results comparison for the same speed range, where a maximum reduction of 41,04% is achieved.
Keywords: Simulation; CFD; Hydrodynamics; Resistance; Amazonia.

1 Introduction

This work was conceived with the objective of producing a consistent solution to the problem of hydrodynamic efficiency of the hull shape of a riverboat. The studied hull model has specific problems to reach the design speed (11 knots). Based on this, the main objective of this work is to increase the hydrodynamic efficiency of this hull within a range of operating speeds.

In general, the problem is related to the shape of the bow and the keel region. These regions hinder the flow of the incident fluid, the generation of hydrodynamic lift for entering into the planing regime and still facilitate the generation of bow waves within the displacement regime. In this case, the elaboration of evaluation criteria to identify discontinuities in the hull is necessary, as the design velocity is not reached. Thus, the proposed approach is the application of tools in computational platform, interconnected to the real-scale tests of the boat.

The speed of service and the wave train profile of the current hull form were determined by sea trials. Based on the geometric characteristics and initial conditions of the sea trial, it was possible to define the computational model of the hull geometry as well as the fluid domain, along with turbulence conditions and the phase model. Under these conditions

two numerical hull models were created, one representing the current model and another with proposed geometric variations of the first.

2 School Transportation in the Amazon Region

The proposed hull model has a shape with displacement characteristics, emphasizing that the hull structure is composed entirely of naval steel with sufficient tensile strength to maintain the structural integrity with respect to the forces from the external environment of the vessel, as shown in Figs. 2 and 3.

Judging the inconsistencies with the hull shape criteria as well as the conditions to reach the design speed of the vessel, it becomes clear the need to remodel the hydro-dynamic behavior of the hull, keeping the design guidelines fixed and the main dimensions unchanged.

For the computational analysis method, it is necessary to validate the shape of the model through Computational Fluid Dynamics (CFD). The following table 1 gives the main characteristics of the vessel to be studied in this work.

Table 1. Main characteristics of the school boat.

Characteristic	Dimension
Length Overall (LOA)	7.80 m
Length between Perpendiculars (LPP)	7.52 m
Moulded Breadth	2,55 m
Moulded Depth	1,40 m
Design Draught	0,67 m
Design Speed	20 km/h
Capacity	20 passengers + 1 crewman

3 Literature Review

With the development of Computer Aided Design (CAD) and Computational Fluid Dynamics (CFD) tools, several processes for measuring and analyzing issues regarding the area of naval hydrodynamics can be studied with greater accuracy. Theoretical models used as base for this work are presented below.

3.1 Experimental Method on Ship Hydrodynamics

According to Tachibana (2017), from the assumption that the flow around the hull of a ship is three-dimensional, the process can be analyzed from the individualization of each resistance component. By this means, an adequacy is identified in the area of flows around hull forms, within the area of ship hydrodynamics.

Most of the "pure" resistance components and the existing intersections do not have satisfactory experimental means of verification, being subjected to imprecise numerical

measurement and extrapolation processes, with a tradition in experimental hydrodynamics within the area of determination of resistance components.

3.2 Resistance to Forward Motion

The movement of a vessel through a fluid (water), at constant speed, generates two types of forces against the hull, normal and tangential. The force against the movement of the vessel is called resistance to forward motion.

The interaction between fluid and structure results in generation and destruction of waves, and this demanded energy composes the wave resistance. A schematic diagram with detailed components of the resistance to forward motion is presented on figure 1, based on Tachibana (2017).

Due to the no-slip condition of viscous fluids on solid surfaces, when the vessel moves through a fluid at rest, the particles close to the hull tend to adhere to the surface, acquiring the speed of the vessel. The integral of the friction components on the wetted surface of the hull results in the frictional resistance.

Figure 1. Schematic diagram of the components of the resistance to forward motion.

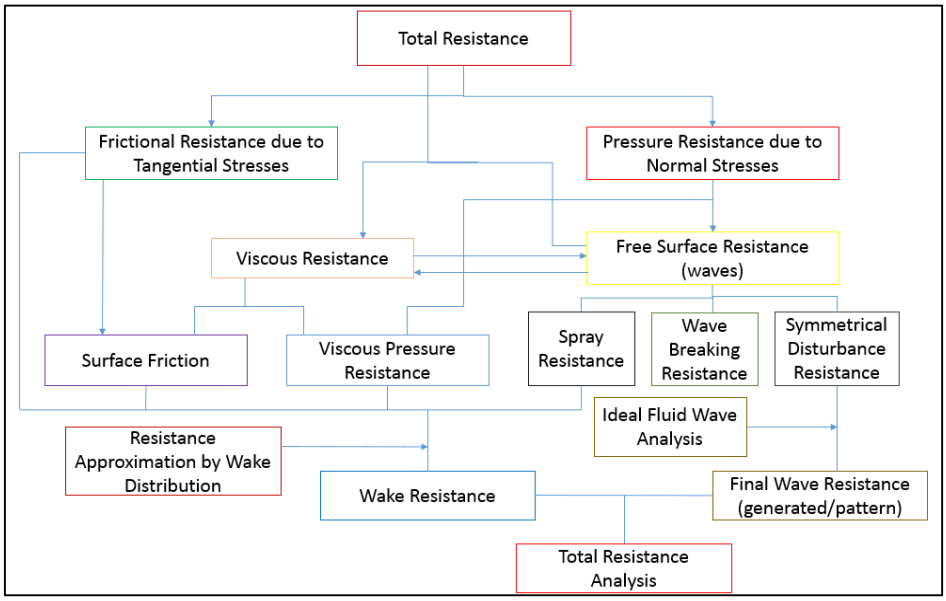

3.3 CFD Analysis of Vessels

According to Iervolino (2015), the Computational Fluid Dynamics is characterized by a numerical simulation of any physical or chemical process where a fluid flow happens. The application of boundary conditions on several finite element models can be recorded on the time and space domain, based on the behavior of several parameters of the flow itself in each of these elements.

Within this procedure, the separation of the model into three main stages is highlighted: Pre-processing, solution and post-processing. In the pre-processing stage we define the

flow model and the boundary conditions of the problem. In the solution step, the resolution procedures are used to determine the desired results. Finally, the post-processing phase allows the analysis of the results with illustrative graphics.

4 Methodology

4.1 Computational Modeling of the School Boat Hull

The full scale model of the boat used on the sea trials is illustrated on the figure 2 below. The three-dimensional model was generated from the lines plan provided by the manufacturer.

Figure 2. Longitudinal view of the school boat.

The profile view of the school boat hull and the model with the proposed shape modifications are illustrated on figure 3.

Figure 3. Profile view of the unchanged hull with side keel (above) and the modified hull (below).

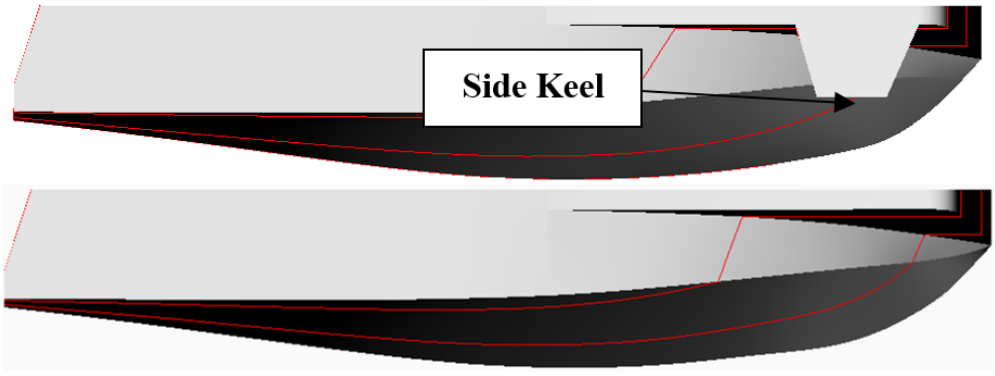

The modified hull shape was generated based on the original hull, by removing the side keels at the bow and modifying the flat bottom area to a V-shaped keel, in order to attenuate the flow lines by the hull.

A view of the transverse sections of the bow, displaying the proposed shape modi-

fications is illustrated on figure 4.

Figure 4. View of the transverse sections of the bow. On the left side, the modified hull shape, and on the right side, the unchanged hull of the school boat.

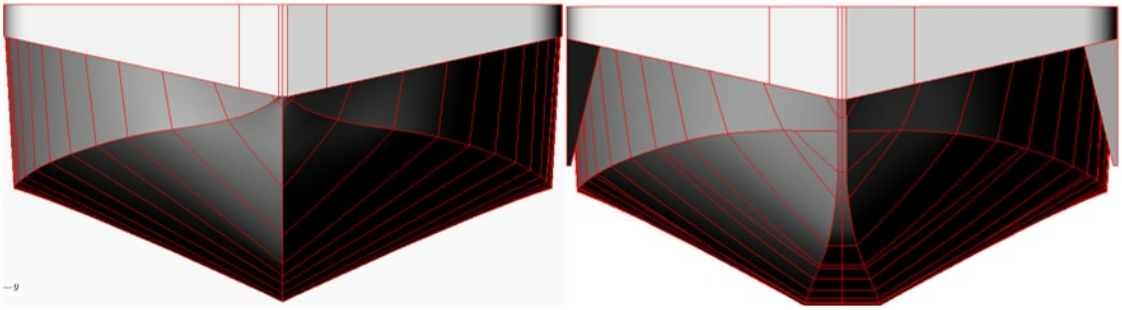

On figure 5 below, the three-dimensional hull models are illustrated, as exported from the 3D CAD software Rhinoceros 5.0.

Figure 5. Three-dimensional hull model with the proposed modifications, with a V-shaped bottom keel on the left side, and the unchanged school boat hull on the right side.

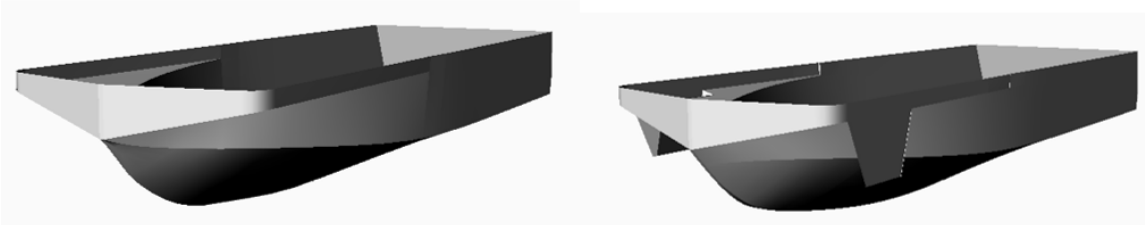

With the three-dimensional hull models modeled, the next phase is to define the fluid control volume that the water and air will occupy around the boat in the simulation. The dimensions of the fluid control volume are illustrated on figure 6, related to the Length Overall of the boat, defined as L.

For the criterion analysis, is is important to analyse the wave resistance generated in the case, using a resistance model that simulates the interaction of the hull discontinuities effects on the generation of the wave train, taking into account the vorticity formation in abrupt shape changes in the hull.

Figure 6. Dimensions of the fluid control volume surrounding the boat hull, related to the Length Overall of the boat, L. The control volume is a box with dimensions 4L x 2L x 2L (port).

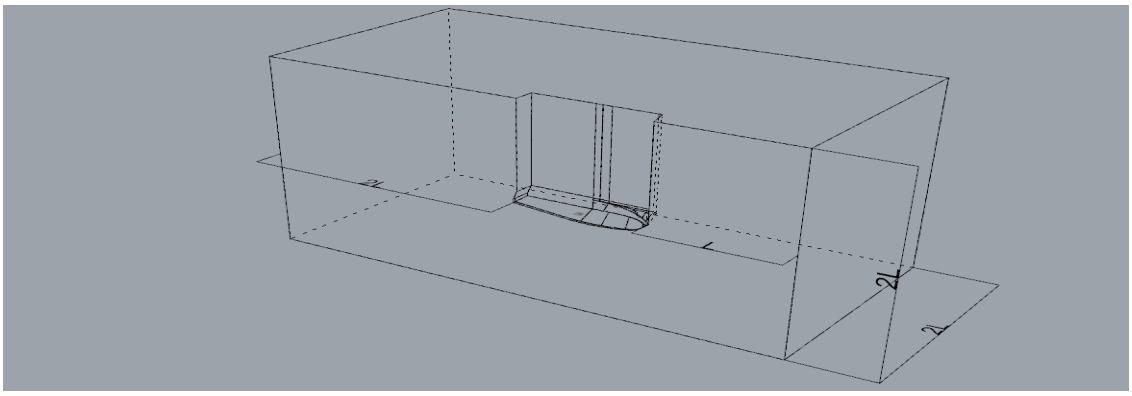

4.2 Physical Model Considerations

For the analysis of the wave formation, a transient analysis is used, as the hull geometry is complex and the calculation model used in the permanent analysis generates numerical inconsistencies that must be taken into account. The section that represents the hull is symmetrical in shape with the plane of symmetry, so, only the port side will be simulated.

Into the case conditions of operation, the following physical parameters are defined: the gravitational acceleration: $g_z = -9{,}81\ m/s^2$, the density of operation: $\rho_{op} = 1{,}225\ kg/m^3$, the pressure of operation: $p_{op} = 101325\ Pa$ and the reference position of pressure: $z_{ref} = L$, where L is the Length Overall of the hull. For the multiphase model, the Volume of Fluid method is used, considering the flow along the control volume an Open Channel Flow type, and the Implicit Body Force model for forces delimitation.

The turbulence model used is the SST K- ω and the Flat method is used for the phase initiation.

5 Results

The definition of the parts of the control volume is adjusted to the model of calculation used by the software Ansys Fluent. The surfaces of the control volume were named according to the regions of analysis. The water inlet represents a cross section of the control volume, namely the entrance of the fluid flow (air + water) for the analysis. The water outlet corresponds to a cross section of the control volume where the fluid flow (air + water) exits the channel in the analysis. The symmetry section delimits a symmetry plane for half of the control volume. The walls that surrounds the control volume are defined by a no-slip condition, thus, the model has reliability to measure the degree of resistance.

On figure 7 it is possible to check the details of the mesh used for the computational simulation in Fluent.

Figure 7. Indication of the mesh elements present in the fluid control volume around the hull, with the legend indicating the orthogonal quality of the mesh.

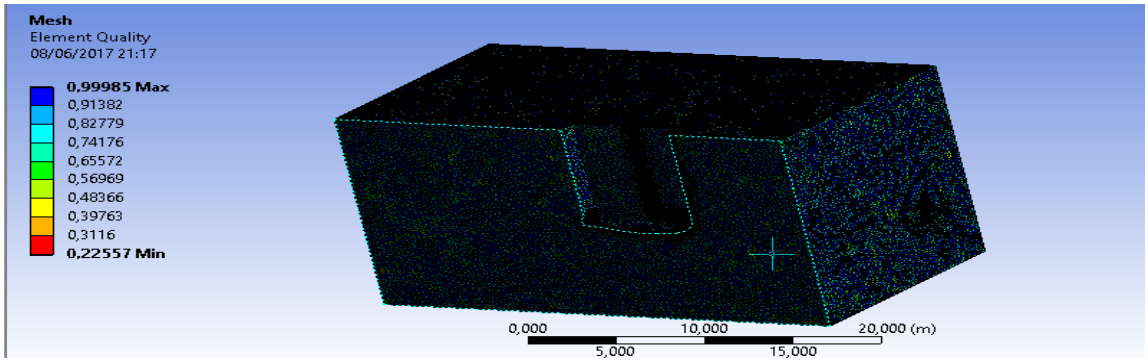

The orthogonal quality of the mesh can be verified, highlighted in the legend. No refinement tool was used around the hull. The mesh was generated with a minimum element size in the order of 5 cm. It was generated a total of 452.461 nodes and a total number of 2.577.166 elements.

According to the values indicated on figure 7, it can be verified that about 2.096.942 elements presented a orthogonal quality of over 0,75, and 1.510.942 elements presented a orthogonal quality of over 0,85. The quality of the mesh did not reach higher values because the model was based on tetrahedral elements with a random method for filling the control volume.

The angle of curvature used corresponds to 18 °, with a minimum gap size of 1,5 cm and a maximum element size of 30 cm. A growth rate of 1,4 was used for the elements of the hull region and for the outermost regions of the control volume.

Figure 8. Free surface wave profile at 20 km/h.

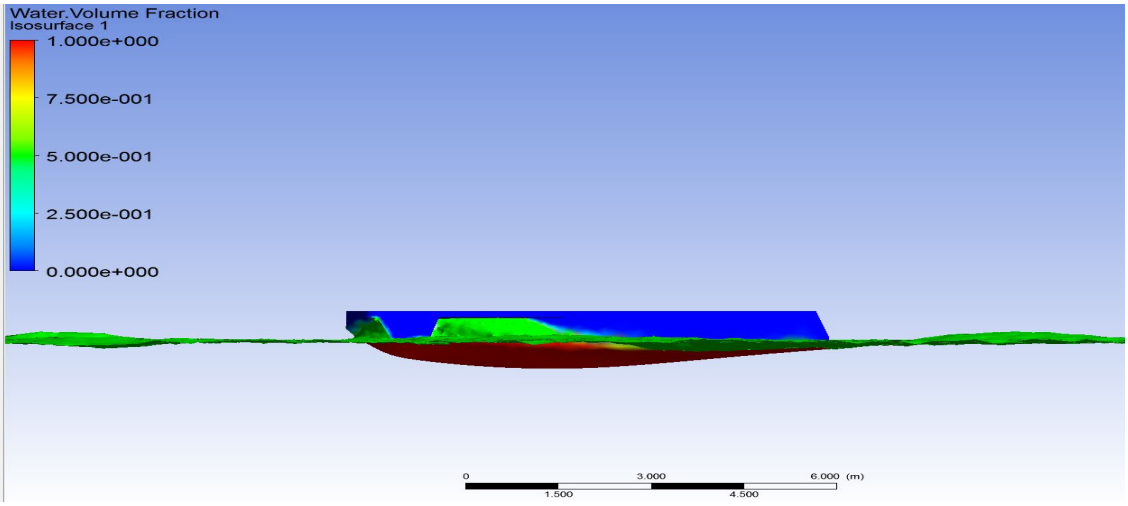

For the calculation of 1.500 iterations of the computational model, it was defined a total of 30 iterations per timestep, resulting in 50 timesteps for each velocity. The timestep duration was defined as 0,02 s. The restriction degree used for the residual convergence was in the order of 10^{-5}. Figure 8 illustrates the longitudinal profile of the school boat with the free surface wave profile for a velocity of 20 km/h. The wave elevation in the region of the side keel is illustrated on figure 9. The irregularities in the surface of the hull can be noticed, due to the mesh quality used in this region.

Figure 9. Wave elevation at the bow region.

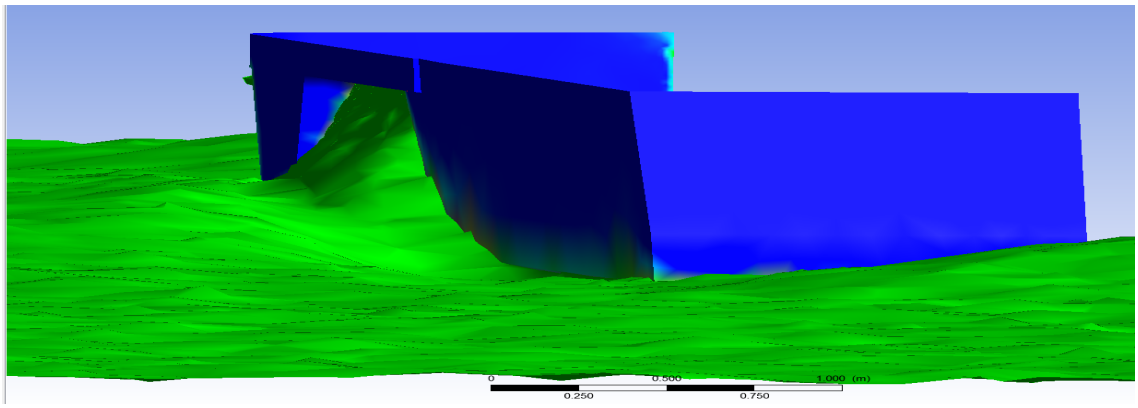

Based on the results of the three analysis (sea trials and both numerical hull models), the methodology was validated, and based on the proposed hull shape modifications, a maximum reduction of the total resistance of about 41% for a velocity of 25 km/h was reached. Figure 10 illustrates the progression of the total resistance for the range of velocities simulated for both hulls, the school boat and the model with the proposed modifications.

Figure 10. Total Resistance values in relation to the Froude Number for both hull models. Blue dots: Original hull of the school boat. Orange dots: Modified hull shape.

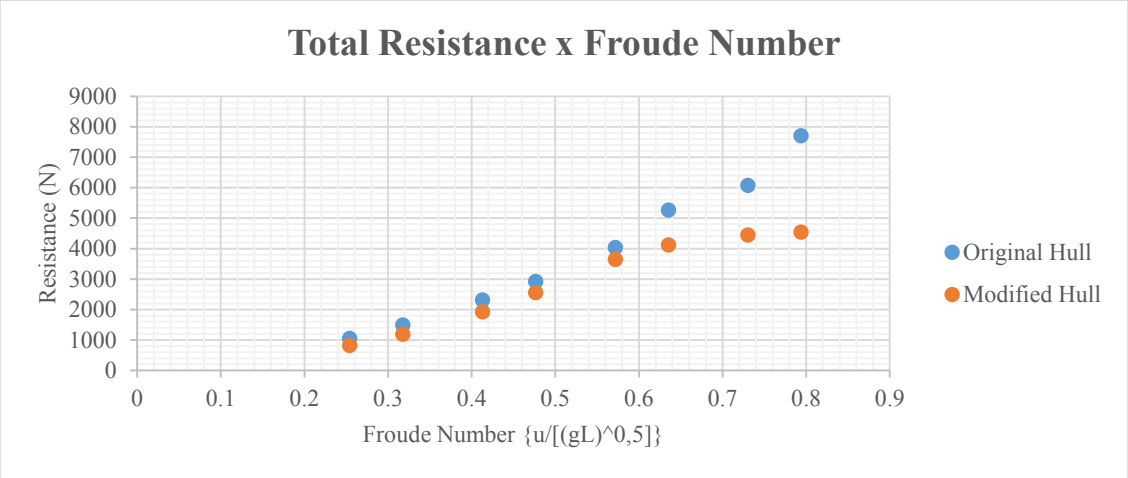

The figure 11 illustrates the percentage reduction of resistance for each velocity in the simulated range, varying from 8 km/h to 25 km/h.

Figure 11. Percentage of resistance reduction for each velocity.

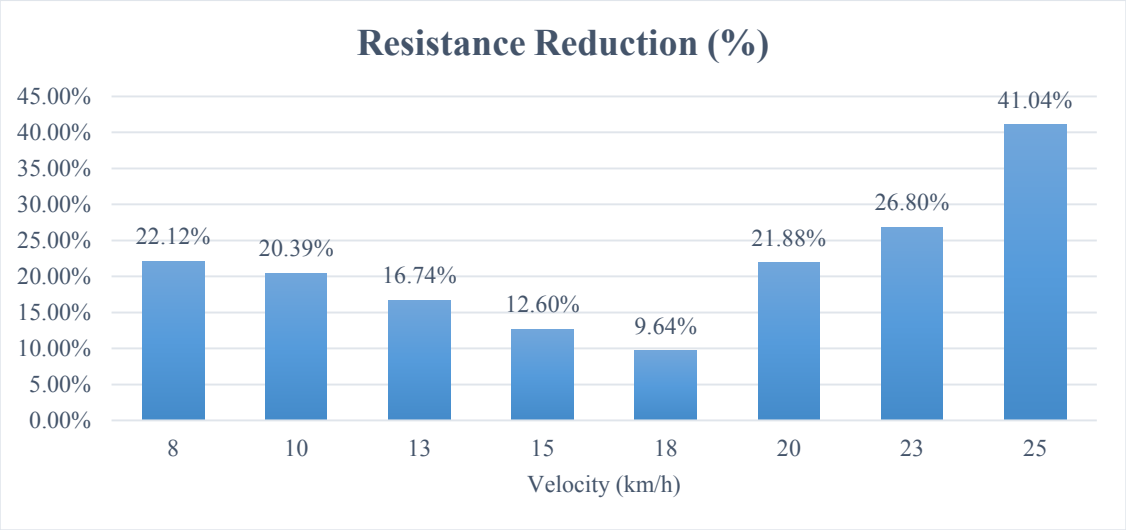

The largest reduction rate was identified on the velocity of 25 km/h, as seen on figure 11 above. For this velocity, the corresponding value for the Froude number is equal to 0,794. Relating the Froude number value with the large resistance reduction achieved, a change on the planing mode of the proposed hull is identified. The absolute resistance values are presented on table 2.

Table 2. Total Resistance values obtained in CFD simulation.

Velocity	Froude # ($V/\sqrt{gL}$)	Total Resistance/ Modified Hull	Total Resistance/ Original Hull
8 Km/h	0,254	822,38 N	1055,94 N
10 Km/h	0,318	1190,79 N	1495,69 N
13 Km/h	0,413	1926,57 N	2313,86 N
15 Km/h	0,476	2551,10 N	2919,01 N
18 Km/h	0,572	3651,21 N	4040,74 N
20 Km/h	0,635	4117,62 N	5271,12 N
23 Km/h	0,730	4450,65 N	6079,81 N
25 Km/h	0,794	4545,24 N	7709,15 N

6 Conclusions

With the results obtained in this work, a great capacity of variation of the total resistance of the school boat's original hull was identified for subtle changes in the hull

shape. The calculated resistance for the model was based on the viscous pressure and wave resistance components of the vessel.

Therefore, the proposed objective of the work was achieved, with a large reduction of the total resistance to forward motion in the range of velocities analyzed. With the present study, a proposal for geometric modification after a hydrodynamic analysis resulted in a maximum reduction of 41,04%. For future studies, a parametric optimization can be done in order to propose further modifications on the bow frames of the boat, related to the wave resistance.

In this way, an even more significant reduction of the resistance can be achieved for the proposed speed range, in order to make the operation of the school boat economically feasible. Thus, students residing in more isolated areas of the Amazon basin can be benefited with a quality school transport.

We would like also to thank the entities CAPES and FAPESPA for their contribution with research grants to the students, being of great importance to direct the academic work within the area of academic articles publication.

References

Bertram, V. 2000. “Pratical Ship Hydrodinamics”. 1st edn. Butterworth-Heinemann, England.

Coelho, D. F. 2016. “Evaluation of the Hydrodynamic Behaviour of a School Boat Using CFD”. pp. 72. Federal University of Pará – UFPA. Belém-PA, Brazil.

Graefe, A. V. et al. 2015. “Comparison of Aqwa, Gl Rankine, Moses, Octopus, Pdstrip and Wamit with Model Test Results for Cargo Ships Wave-Induced Motions in Shallow Water”. In: ASME 2015 34th International Conference on Ocean, Offshore and Arctic and Artic Engineering OMAE2015, Canada.

Grinberg, M., Padovezi, C., Tachibana, T. 2017. “Utilization of Model Testing in Reduced Scale for Definition of Optimized Ship Shapes”. In: XXII COPINAVAL – IPIN, pp. 28. Buenos Aires, Argentina .

Iervolino, L. A. 2015. “Study of the Resistance to Forward Motion of a Planing Vessel of 20 feet: Computational Approach Based on CFD”. Undergraduate Thesis – pp. 88. Federal University of Santa Catarina - UFSC. Joinville - SC, Brazil.

Issues on MaaS for sustainable mobility in port cities

Fumihiko Nakamura
Professor, Vice President
Yokohama National University
nakamura-fumihiko-xb@ynu.ac.jp

1. Introduction

A lot of port cities all over the world both in developed countries and in developing countries have been facing various types of traffic problems these years. Not only as one of the important nodes for freight transport network, but also as a focal point of passenger movement, port city should keep on tackling with the problems.

In this short paper, the author focuses on passenger transportation and its mobility, especially on new approaches in order to accomplish sustainable mobility. Among a lot of new keywords, the author has a strong concern about MaaS, or Mobility as a Service, which has become popular among the transportation and/or Intelligent Technology experts these few months. The author assumes that the deployment of MaaS would be so significant as to contribute to the sustainable and balanced mobility if it successfully stimulates travelers to have their behavioral changes such as modal shift, timing change and so on.

2. Emergence of MaaS

MaaS is normally recognized as an application mainly for smartphones, providing travel information on various types of transportation mode in a city or a region across the operators, as well as comparison, booking, payment functions are available.

The root of MaaS must be a big and unique project in Helsinki, Finland, where citizen could subscribe the service and get reasonable monthly payment system. This case should be appreciated as it clearly shows the policy direction of the comprehensive transport in the city, which is directed to less dependence on private

cars because of their risks on global warming, traffic accidents and social exclusion. The application shows its users how it costs when a user chooses a private car as her/his travel option in terms of cost and damage to the environment.

Referring to the recent articles on MaaS, there should be some sorts of misunderstanding or insufficient understanding about the root of MaaS. As mentioned in the previous section, the author's assumption is on some possibility to have implication between travel behavior change and MaaS. Travel behavioral change could be described as a part of TDM, Travel Demand Management strategies. Relations between TDM and MaaS, could be conceptually shown in Figure 1.

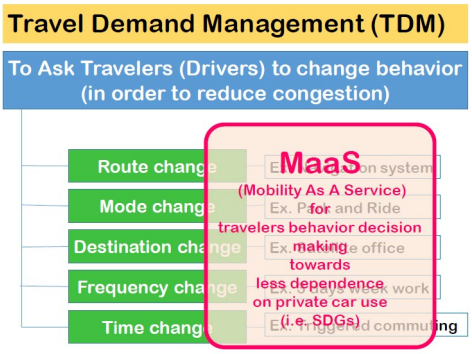

Figure 1. TDM and MaaS

As one of the ideas to solve some sorts of misunderstanding problems, some recent articles propose the several different levels of MaaS, which is conceptually described in Figure 2, where the author strongly recommends that the expected types of MaaS application would be between Level 2 and 4.

LEVEL	INTEGRATION	CONTENTS	EXAMPLES
0	None	By each operator	Many cases already
1	information provision	all operators Join	Trip planner app. in many cities
2	Booking and Payment	By each trip event	Hanover model
3	Service	Subscription and Contract	Helsinki model SHIFT (LOS)
4	Policy	P-P partnership	EMMA (Montpellier)

Figure 2. Different levels of MaaS

Private-Public partnership shown in the Level 4 in the Figure 2 should be ideal in the field of urban transportation. In most cases transport operators are in the private sector while the planning and management is done by the public. Private sectors should be provided some incentives to work with the public to support the public policies. In many cities, especially in developing countries, private bus operators are facing with traffic jams and expect the powerful approach by the public to reduce car traffic congestion.

3. Issues on MaaS

The author has been facing other two problems when discussing MaaS and related issues. One is the target field of the transportation demand. As shown in Figure 3, the goals of the transport policies are different among the types. As a result, expected roles of MaaS could be different. In case of port cities, some MaaS discussion could be just about city center traffic problems, while, on the other hand some MaaS argument could be mainly about intercity transport issues including some competition between water transport, air and trains.

Demand	Target policies	Target demand
City Center	Walkable Less car usage	Walk Bikes. Bike-sharing Public Transportation
Suburban	Better feeder accesses Giving-up Second-cars Less car usage	Public Transportation Park and Ride Demand-Responsive Transport Shares for feeders
Rural	More trips by elderly More efficient service	Demand Responsive Transport Shares
Intercity	Less car usage Less GHG Better feeder accesses	Each mode with access modes Possibly accompanied by hotel booking car rental booking

Figure 3. Maas for the different transportation demand

(based on some materials by Katsutoshi Ohta at FPPMET, Japan)

Another concern by the author would be the role of stakeholders. Especially venders for applications should seek just their profit regardless of policy contribution such as reduction of greenhouse gases, social exclusion problems and traffic accident problems. Recently in Japan, a car manufacturer and a regional railway operator started internal project team on MaaS, whose interest must be some sorts of business opportunities and profits, which should not be criticized of

course. Even though, the role of the travelers and operators should be identified somehow. Figure 4 shows one example of this approach. According to some recent movement on MaaS, provision of greener ways to travelers as well as faster and cheaper ones would be recognized as a very cool and smart MaaS apprication.

Actors	Benefits	Risks
Travelers	Easy access to info. Easy process for choice Get wider choices ex. Faster Cheaper More comfortable	Social exclusion of anyone who cannot use smartphones Service down in case of MaaS server down or Electricity blackout
Operators	Save cost for information provision marketing Opportunity to get more passengers	Lose revenue by some modal shift from public transport to ride-shares Disclosure of information to rival companies
Policy Makers	Reduce GHG emissions by decrease SOV veh-miles Synergy possibility with Autonomous Vehicles and Sharing Mobility services	Lower efficiency due to less competitiveness Increase of GHG due to more supply of shares

Figure 4. Roles by actors for MaaS (Level 3 and 4)

(based on some materials by Katsutoshi Ohta at FPPMET, Japan)

4. Conclusion

In this paper, the author summarizes the issues on MaaS, considering the implication on passenger mobility issues observed in a lot of port cities, where residents, workers, visitors, long distance travelers are mingled in a complex way. As the density of the cities is normally high, it must be impossible to rely on personalized modes for these demand. Travel behavioral changes including modal shift to public transportation modes should be considered. In this context it is no doubt for MaaS to show some potential. By considering the difference of actors such as, travelers, transport operators, MaaS service providers, policy makers (government, municipalities), Roles could be identified as in service of each mode with necessary infrastructure, service of information management, policy setting and linkages, share of technical levels. In terms of acceptability, there would be some concern such as travelers use it well but change behavior?, private operators become sensitive, nervous or aggressive and the government could control MaaS. At the same time, feasibility of open architecture of necessary data, and poor services due to less competitiveness or risk of monopoly would be problems for the next stage.

The Crisis of the World Trading System

How can we fix it?

Ichiro Araki
Graduate School of International Social Sciences
Yokohama National University
79-4 Tokiwadai, Hodogaya-ku, Yokohama, 240-8501 Japan
araki@ynu.ac.jp

Abstract
Until a few years ago, the study of international trade law was often regarded as a boring subject, with too much technicalities and details. With the recent change of the US trade policy, the subject has suddenly become interesting – not necessarily in a positive way. The paper explores the history of the multilateral trading system and the central role the United States played in the development of the system. Then, it will investigate the root cause of the current crisis and contemplates the possible way out of the crisis.

Keywords: WTO, Trade Policy, United States

Biography
Ichiro Araki
The University of Tokyo, Faculty of Law
The University of California (Berkeley) School of Law
Saitama University (now National Graduate Institute of Policy Studies)
Bachelor of Law (Tokyo) 1983
Master of Laws (California) 1988
Master of Policy Science (Saitama) 1994

Developing International Collaboration Potential for Port-City Air Quality Management

Heekwan Lee, Ph.D., Hyoji Im, Ph.D.

School of Construction and Environmental Engineering, Incheon National University, South Korea

Email: airgroup@inu.ac.kr

Bang Quoc Ho, Vu Hoang Ngoc Khue, Thanh Nguyet

Institute of Environment & Resources (IER), Vietnam National University, Ho Chi Minh City (VNU-HCM), Vietnam

Abstract

The worldwide air pollution issues nowadays have pretty much common aspects from their beginning including emission source inventory to the end including applicable technologies and policies as potential solution to manage and improve them. This trend has also a good deal of benefit and potential for worldwide cities either maintaining city-level air quality well or still struggling with unhealthy air quality, which could be a strong motivation for cities in different status to exchange and collaborate together ultimately. The air quality in a port area, i.e. port-city air quality, would be a good example for some cities suffering from out-of-control air quality and other cities enjoying well-managed air quality. In addition to the public concern for city air quality, port-city air quality has been becoming further complicated and aggravated due to steadily increasing marine logistics as well as complex coastal meteorology.

Surely there have been a lot of studies and projects to challenge this port-city air quality and support many other efforts for their improvement. As well-known, the fundamental of air quality management is strongly based on a good emission inventory system, e.g. EMEP/EEA by EU, NEI by USEPA, CAPSS by Korean MOE, etc. Current inventory systems are very useful for national-level air quality management plan by utilizing national energy consumption statistics mainly including fossil fuel sources. These existing inventory systems however are not well-fitted or applicable to the case of mobile emission sector, as the nature of mobile air emission is mostly made away from the fuel source, e.g. a car driving around and a gas station. The accuracy measure of emission inventory in a port city would be even further degraded because of international shipping with different national flags.

In this study, two research groups from Incheon National University from South Korea and Vietnam National University will be sharing their related research experience on this interesting topic and developing next level of knowledge sharing and research collaboration, while inviting more potential research groups to join.

Keywords: Port-city, Marine transportation, Air pollution, Emission inventory, Auto-identified system (AIS)

Biography